## Title

Optimal Dynamic Inversion: Towards Safety, Reliability and Performance with Application to the Active Magnetic Bearing System



## Author

rouhani, shahin

## Publication Date

2021

Peer reviewed|Thesis/dissertation

UNIVERSITY OF CALIFORNIA

Los Angeles

# Optimal Dynamic Inversion: Towards Safety, Reliability and Performance with Application to the Active Magnetic Bearing System

A dissertation submitted in partial satisfaction
of the requirements for the degree
Doctor of Philosophy in Mechanical Engineering

by

Shahin Rouhani

2021

ABSTRACT OF THE DISSERTATION

Optimal Dynamic Inversion: Towards Safety, Reliability and Performance with Application to the Active Magnetic Bearing System

by

Shahin Rouhani
Doctor of Philosophy in Mechanical Engineering
University of California, Los Angeles, 2021
Professor Tsu-Chin Tsao, Chair

Rotating machinery is commonly used in mechanical systems, including machining tools, aircraft gas turbine engines, and other industrial applications. However, the synchronous vibration due to the rotor mass unbalance is the common disturbance source encountered in rotor operations. Unbalance occurs when the rotor's inertia axis does not match its axis of geometry. Given the cost and difficulty of the perfect balancing and the current trend for high-speed operations, which is directly correlated with the greater centrifugal unbalance forces, vibration control is essential in improving achieving longer bearing, spindle, and tool life in high-speed machining. As opposed to conventional ball bearings, Active Magnetic Bearings (AMBs) provide both the contact-less support and the possibility for applying real-time force to regulate the rotor-dynamic behaviors. This additional control facility allows the rotor to spin around its principal axis of inertia if a sufficient air gap exists between the rotor and housing. Consequently, by annihilating the rotor's centrifugal force, the rotor vibration dramatically decreases and no reaction forces are transmitted to the housing.

Beyond the functionality of AMB in reducing the rotor vibration, the aspects of safety and reliability have become important in all rotor operations. The AMB is a highly nonlinear and open-loop unstable system, and therefore it is common that the control system includes different controllers, tailored for different regimes of the operating conditions. However,

the stability of the entire control system depends on the flawless operation of its sensors and actuators. Otherwise, the malfunctioning of any system components may disturb the stability of the supported rotor resulting in damage to the whole system. Hence, to ensure the safe operation and reliable performance of AMB, an online Fault Detection and Isolation (FDI) scheme is necessary to identify the faulty components and safeguard the system to remain in a safe region when faults are detected.

Given the inherited cost and complexity of adding redundant physical components, this dissertation presents a novel model-based FDI scheme for the AMB based on analytical redundancy by integrating two linear estimators called the Game-Theoretic Detection Filter (GTDF) and the Unknown Input Observer (UIO). Optimal inversion filters for both estimation and compensation are also introduced for the unified framework of the integrated fault detection, estimation, and Disturbance Observer-Based Control (DOBC) that safely switches between controllers when faults are detected. By extending and exploiting the Youla parameterization of stabilizing controllers, where the robust feedback control, the fault detection, and DOBC are realized by a bank of full-order state observers running in parallel, the controller in each regime always stabilizes the AMB. Lastly, a novel multi-variable Adaptive Feedforward Control (AFC) scheme featured by optimal delay-inversion-based compensation is proposed and implemented for its premium on stability and its simplicity in selecting the delay length as the single design parameter for the multi-variable controller to suppress the synchronous vibrations during varying and constant speed operations.

The dissertation of Shahin Rouhani is approved.

Jason L. Speyer

Tetsuya Iwasaki

James S. Gibson

Tsu-Chin Tsao, Committee Chair

University of California, Los Angeles

2021

*To my family ...*

*for their unconditional love*

TABLE OF CONTENTS

LIST OF FIGURES

LIST OF TABLES

# ACKNOWLEDGMENTS

I would like to express my deepest gratitude to my advisor Professor T-C Tsao for his guidance and support through my years at UCLA. His excitement, patience and positive outlook was major factor in getting me through many highs and lows of the grad-school. He took in a guy who came to his office babbling about equations into a researcher developing ideas for real engineering applications by pushing me to play with mechatronic systems in our lab despite my initial reluctance. At the same time, he was instrumental in obtaining a position for me at Jet Propulsion Laboratory. Finally, I should mention all those late-night Zoom meetings during the Covid days helped me publish my first journal paper. For that, I am always grateful.

I would like to thank all my other committee members, Professors Iwasaki, Speyer, and Gibson. I would like to thank Professor Speyer for the many hours I spent in his office having heated discussions about fault detection algorithms, which turned to be the first topic presented in this dissertation, and some off-topic conversations about politics and the economy. His remarkable knowledge and extreme patience in addressing my questions were precious for me to expand my skills in the field of Estimation and Control. Also, I would like to thank Professor Gibson for his generous support and all the discussions we had about adaptive filtering and MPC. His humble personality and down-to-earth attitude have been a great source of help in dealing with failed research attempts and personal difficulties.

During my research at Mechatronics and Control Laboratory at UCLA, I was fortunate to interact with not only the smartest people in the field of controls and mechatronics but also some of the nicest. A special thanks go to Dr. Sandeep Rai for helping me get started in the lab and running experiments on the magnetic bearing system. I would also like to thank my other lab mates. To Dr. James Simonelli, thank you for helping me with running experiments after Sandeep's graduation. To Dr. Cheng-Wei Chen, Dr. Martin Lee, and Dr. Matt Gerber, thank you for being great role models as the senior members and sharing your wisdom and knowledge. To Jack, Edwin, Han, Omar, Aziz, and Paul, thank you for making

the first floor of Boelter Hall a perfect place to work.

During my years at JPL, I met and worked with some great individuals. I thank Dr. Herrick Chang who was first my mentor during the summer internship and then became my valuable co-worker. By introducing the FPGA-Based-GNC, he provided me the opportunity to be part of the development of the Coronagraph Instrument. I also want to thank my group supervisor Dr. David Bayard and my project manager Dr. Nanaz Fathpour who had faith in my ability to work on developing a concept that had not been exercised previously in our section. I also valued many technical discussions with Dr. Joel Shiels on digital filtering and signal processing. Lastly, I want to express my sincere gratitude to Dr. Milan Mandic, who for a time lived a professional life identical to my own and truly understood what I was expecting. His mentoring provided me invaluable insight into the critical thinking that helped me with this dissertation, and our daily long conversations made me confident that I am capable of solving challenging problems in the industry. For that, I am always grateful.

I have been very fortunate to have supportive individuals by my side during this journey. To Behrouz, I decided to become a mechanical engineer after talking to you at age of five, and I always admire your intelligence and empathy. To Shahrouz, although we selected different paths for our professional life, your hard-working and generous personality has been always inspirational for me. To the other Behrouz, you have become my best friend since I moved here, and we shared so many great memories from late-night parties to many road trips. To Sahba, you convinced me to study for the Ph.D. Preliminary exam despite my original plan to only pursue a master's degree. Student life would have simply been boring without the unique stories we made together, which is better to be left unfolded as you suggested in your dissertation. To Donya, I was so lucky to meet you along the way, and thank you for being the best study partner on Sundays.

Last and foremost, I want to express my deepest gratitude to my family for going through many ups and downs as immigrants to make this doctorate degree happen. To my parents, you sacrificed everything; leaving your hometown, living as a refugee in Turkey, and working a tremendous number of hours with the minimum wage here in the U.S. to make sure that

we can make ends meet. For that, I am always grateful. To my sisters Tanin and Tanaz, thank you for cheering me up whenever I was overwhelmed with too much workload and frustrated with student life.

# VITA

| | |
|---|---|
| 2016 | B.S. (Mechanical Engineering), University of California - Los Angeles (UCLA), Los Angeles, California. |
| 2018 | M.S. (Mechanical Engineering), University of California - Los Angeles (UCLA), Los Angeles, California. |
| 2019–2021 | Guidance/ Control Engineer, NASA Jet Propulsion Laboratory (JPL), Pasadena, California. |
| 2017–2021 | Teaching Assistant, Mechanical and Aerospace Engineering Department, University of California - Los Angeles (UCLA), Los Angeles, California. |
| 2017–2021 | Graduate Research Assistant, Mechanical and Aerospace Engineering Department, University of California - Los Angeles (UCLA), Los Angeles, California. |
| 2019 | Guidance/ Control Intern, NASA Jet Propulsion Laboratory (JPL), Pasadena, California. |

# PUBLICATIONS

Shahin Rouhani, Sandeep Rai, Tsu-Chin Tsao. "MIMO Adaptive Feedforward Control and Experiment on Synchronous Vibration Suppression of Active Magentic Bearing Systems." Automatica, Submitted.

Shahin Rouhani, Tsu-Chin Tsao, and Jason L Speyer. "Integrated MIMO fault detection and disturbance observer-based control." Mechatronics, 73:102482, 2021.

Shahin Rouhani, Sandeep Rai, and Tsu-Chin Tsao. "Inversion Based Adaptive Feedforward Control for Multivariable Systems." IFAC-PapersOnLine, 53(2):3791–3796, 2020.

Shahin Rouhani, Tsu-Chin Tsao, and Jason L Speyer. "Multivariable Disturbance Observer Based Control with the Experiment on an Active Magnetic Bearing Spindle." IFAC-PapersOnLine, 52(15):388–393, 2019.

Shahin Rouhani, Tsu-Chin Tsao, and Jason L Speyer. "Robust Disturbance Estimation-An Integrated Game Theoretic and Unknown Input Observer Approach." In 2019 American Control Conference (ACC), pp. 5077–5082. IEEE, 2019.

# CHAPTER 1

# Introduction

Active Magnetic Bearings (AMBs) consist of a series of electromagnets arranged in a ring to create a contact-free rotor bearing, and they have found numerous industrial applications, including vacuum operation, energy storage systems, and flywheels [SM09]. The Active Magnetic Bearing Spindle (AMBS) refers to a machine tool in which AMBs support the spindle holding the cutting tool. With the emergence of high-speed machining, AMBS has received attention among researchers because of its potential benefits in mitigating wears, eliminating thermal expansions given its friction-less rotation, and creating high bandwidth and dynamic stiffness [CK07a]. High-speed machining allows for faster processing time, and a better surface finish [Kin13]. In addition to high-speed advantages, unique properties of AMBS have been researched for other machining applications, including indirectly measuring the cutting force using the control commands[ACL04], and preventing chatter instability by applying model-based robust control [CK07b].

Despite its numerous capabilities, AMBS is a challenging mechatronics system given its open-loop unstable, nonlinear and coupled-axis multi-input-multi-output (MIMO) dynamics nature that require careful modeling, identification, and control to realize its potential benefits. Most control approaches to AMBS address ensuring stability or compensating unbalanced spindle motion, which may require the control system with different controllers, tailored for different regimes of operating conditions. In this case, monitoring is necessary to determine the active controllers in different regimes. Furthermore, fault detection is necessary to safeguard the system to remain in a stable regime when faults are detected.

## 1.1 Safety and Reliability

Safety and reliability are somehow overlapping terms as presented in [Sch05]. Safety refers to the quality of a system to impose no danger to humans or environments during the failures. In contrast, reliability ensures the system remains operational [Sch05]. To ensure both safety and reliability of AMBS, the improvement of fault tolerance is necessary. The main objective for fault-tolerant control is to allow the continued safe operation of the spindle during levitation or rotation in the presence of a fault so that it can subsequently be run down safely and the machine shut down for repair. Both selections of bearing/sensor configurations and component redundancies can maximize the fault tolerance and have been investigated by researchers. For example, magnetic bearings with redundant poles were reconfigured following the functional loss of one or more coils [Che00, MM95]. However, changing locations of actuators and sensors, or adding the additional actuator is usually impractical given the almost fixed original design. Furthermore, introducing extra sensors imposes additional costs even there exists no space limitation.

As described in [CKS04], system faults to the AMBS can be classified either *internal* or *external*. External disturbances acting on the system can model the external faults, while internal faults cannot be considered as external disturbances as they affect the system dynamics. Robust control design by considering faults or system disturbances, or adaptive control algorithms may improve the operation, but they are usually not needed for internal faults. Previous control systems designs for external faults have included robust $H_\infty$ and $\mu$-synthesis [NSL15]. In contrast, faults that are internal to AMBS require reconfiguration of the control system. The re-configurable control has the greatest potential for dealing with a wide range of fault conditions and particularly those that involve the functional loss of a control actuator or sensor. The successful implementation and integration of control systems for internal faults remain an important research topic.

## 1.2 Performance

The undesired synchronous vibration due to rotor mass imbalance is the main disturbance source in all rotating machinery including AMBS. The most effective way in reducing the spindle's synchronous vibration is to align its geometric and inertia axis. However, it is impossible to perfectly align the inertia and geometric axes even with utilizing balancing devices. AMBs provide the possibility of changing the dynamic behaviors of the AMBS and controlling the spindle's imbalance response by applying the electromagnetic force in real-time. Furthermore, the AMB's control facility allows the spindle to spin about its center of inertia given a sufficient gap between the spindle and housing, which is called automation balancing, or to spin about its geometric axis, which is called imbalance compensation. Automation balancing eventually annihilates the spindle's radial motion and reduces the rotor vibration significantly. Consequently, the automation balancing is applicable for the case required high speed and smooth running. Correspondingly, the imbalance compensation attenuates the rotor synchronous vibration and improves the rotating precision sharply, so it is suitable for precision machining.

Unbalance control in AMBS has been popular among researchers. For the imbalance compensation at the fixed rotational speed, a Kalman filter with an optimal state feedback regulator has been utilized to improve rotor positioning accuracy and compensate unbalance forces and vibrations [SHW11]. For time-varying speed and decoupled AMBs, an oscillator for disturbance rejection based on the Internal Model Principle (IMC) has been designed using SISO design techniques in [KT16]. Furthermore, another method has utilized the gain-scheduling approach to generate the control signal [KCL15]. For coupled AMBs, a repetitive controller was implemented in [RCS16] to target multiple Fourier harmonics of the fixed rotational speed. For the automation balancing at the fixed rotational speed, notch filters of the rotor speed were placed in the feedback control loop to suppress the control forces [KHF95, LP08]. The main drawback of this approach is that it may perturb the feedback control loop too much which can result in instability, especially for varying rotor speeds. To relax the stability condition, gain scheduled controllers and notch filters were implemented

on decoupled MIMO AMBs [MNH96, CLW16].

## 1.3 Dissertation Overview and Summary of Contributions

A comprehensive summary and overview of the seven chapters in this dissertation are outlined as below:

- The experimental set-up used as the test-bed in this dissertation is discussed in Chapter 2.

- In Chapter 3, a new method of fault estimation in discrete-time LTI systems using game-theoretic detection filters (GTDFs) is proposed. First, the direct unknown input observer (UIO) design is reviewed, and its application in fault estimation is discussed. Motivated by the UIO design limitations, the GTDF is introduced which decouples the multi-variable faults into a scalar target fault and remaining nuisance disturbances for a virtual plant model. The estimation of the target fault is then obtained by the UIO design for the virtual plant. This method can be used to estimate all faults in the system individually. Simulation and experimental results from the AMBS are presented to demonstrate the robustness of the proposed approach with respect to noises and uncertainties, and comparison to the direct UIO approach.

- In Chapter 4, a new method of disturbance observer-based control (DOBC) for MIMO highly-coupled unstable systems is proposed. In contrast to the current input–output approach for stable SISO systems, the Youla parameterization of stabilizing controllers by full order state observer (FOSO) feedback control is shown more appropriate for general MIMO systems, while retaining the intuitive aspects of DOBC design. A general MIMO DOBC expanded from this single FOSO stabilizing control is proposed, where a parallel number of FOSOs for fault detection, state estimation, and disturbance observer are integrated to achieve the relevant operational requirements and performance. Within this integrated control system, this chapter propose a MIMO

disturbance observer design method by a GTDF design. The DOBC design features GTDF disturbance decoupling followed by H-infinity model matching to establish the desired bandwidth for each channel of the decoupled disturbance observer. The proposed DOBC is applied to the AMBS, and experimental results are presented to demonstrate the design method and control performance.

- In Chapter 5, a novel multi-variable adaptive feedforward control (AFC) scheme is created. The proposed AFC is featured by delay-inversion-based compensations, decoupling for multi-variable systems, and the stability and convergence analyses that reveal new insights added to the existing literature. Using complex exponential than real sinusoidal representations, the well-established results on the AFC's linear time-invariant equivalence and stability conditions are re-derived without invoking the averaging or transformations techniques in the existing analyses. Furthermore, the gradient of quadratic objective functions can readily be derived, giving the Hermitian of the plant's frequency response, and used to construct the steepest decent AFC (GAFC) by frequency-dependent phase compensations. The GAFC method cannot achieve uniform convergence rate for multi-tone time-varying frequencies and multiple channels by a fixed adaptation gain for the implementation simplicity. Toward implementation simplicity, inversion-based AFC (IAFC) scheme based on delay-inversion of the MIMO plant and its phase compensations by simple time shifts in AFC signals is proposed.

- In Chapter 6, the IAFC synthesis is applied to the AMBS for automation balancing motivated by suppressing the synchronous vibrations in AMBs during ramping and constant speed operations. Both stability and convergence analyses are presented to show the superior performance of the proposed synthesis in comparison to the existing GAFC. The experimental results are presented to demonstrate the IAFC's effectiveness in suppressing synchronous vibrations, particularly during speed ramping.

**Notation**.

- $z^{-1}$ denotes the delay operator, i.e., for a signal $x$, $z^{-1}x(t) = x(t-1)$ and conversely $zx(t) = x(t+1)$. Hence, $z$ is the complex variable associated to the z-transform.
- $RH_\infty$ denotes the set containing all the LTI systems that are rational and stable as defined in [ZDG96].
- The upper index $^{(l)}$ is used to denotes the index number in a vector. This does not denote an exponent.
- The upper index $^{(T)}$ is used to denote the transpose of a matrix or vector.
- The upper index $^{(*)}$ is used to denote the complex conjugate of a complex matrix or vector.
- The upper index $^{(H)}$ is used to denote the complex conjugate transpose of a complex matrix or vector. Notice that for a real matrix or vector $^{(T)}$ and $^{(H)}$ are equivalent.
- $\delta$ is one step difference operator for discrete-time signals, i.e., for a signal $x$, $\delta x(t) = x(t+1) - x(t)$ is the forward difference, and $\delta x(t) = x(t) - x(t-1)$ is the backward difference. For continuous-time signals, it is the differential operator.
- $\|.\|_2$ denotes the standard $H_2$ norm of a LTI system.
- $\|.\|_\infty$ denotes the standard $H_\infty$ norm of a LTI system.
- $\dagger$ denotes the pseudo inverse of the matrix.
- $I_n$ is the $n \times n$ identity matrix.
- *det* is used to denote the determinant of a matrix.
- $\mathcal{R}$ denotes the set of real numbers. $\mathcal{C}$ denotes the set of complex numbers.

# CHAPTER 2

# System Description and Experimental Set-Up

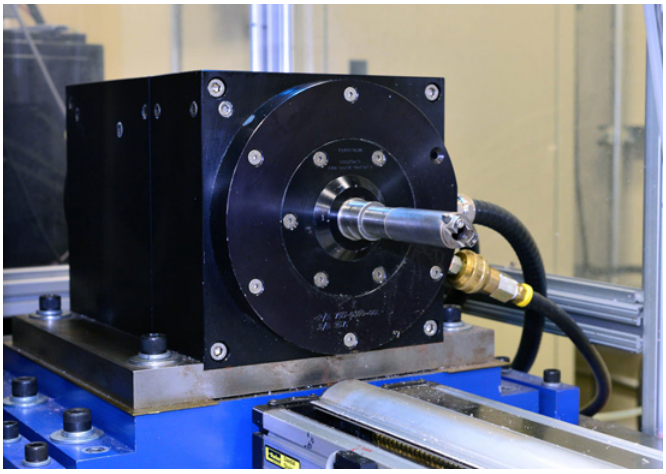

**Figure 2.1:** Picture of the AMBS considered in this thesis.

The Active Magnetic Bearing Spindle (AMBS) (Figure 2.1) used as the test bed for this thesis includes two radial AMBs and one thrust (axial) AMB. The front AMBs are capable of loading up to 1400 N, while the rear is rated for 600 N. There is also an induction motor that enables spinning the spindle up to 50,000 RPM at 10 kW. Five degrees of freedom are available for control, including two translational degrees $v$ and $w$ at each radial bearing, as well as the axial translation $z$. Four eddy current sensors are located at two ends of the rotor to measure its geometric center position with respect to the housing in $x$ and $y$ directions. The power amplifier is a PWM type that regulates the current into the coils. Then, the nonlinear electromagnetic forces caused by the coils' currents levitate the rotor. Control architecture was implemented at 10 kHz sampling rate for all system identification and control tasks using LabVIEW Real-Time target installed on a computer with an interfacing National Instrument R-series card (NI PCI7852R) used for the analog and digital signal

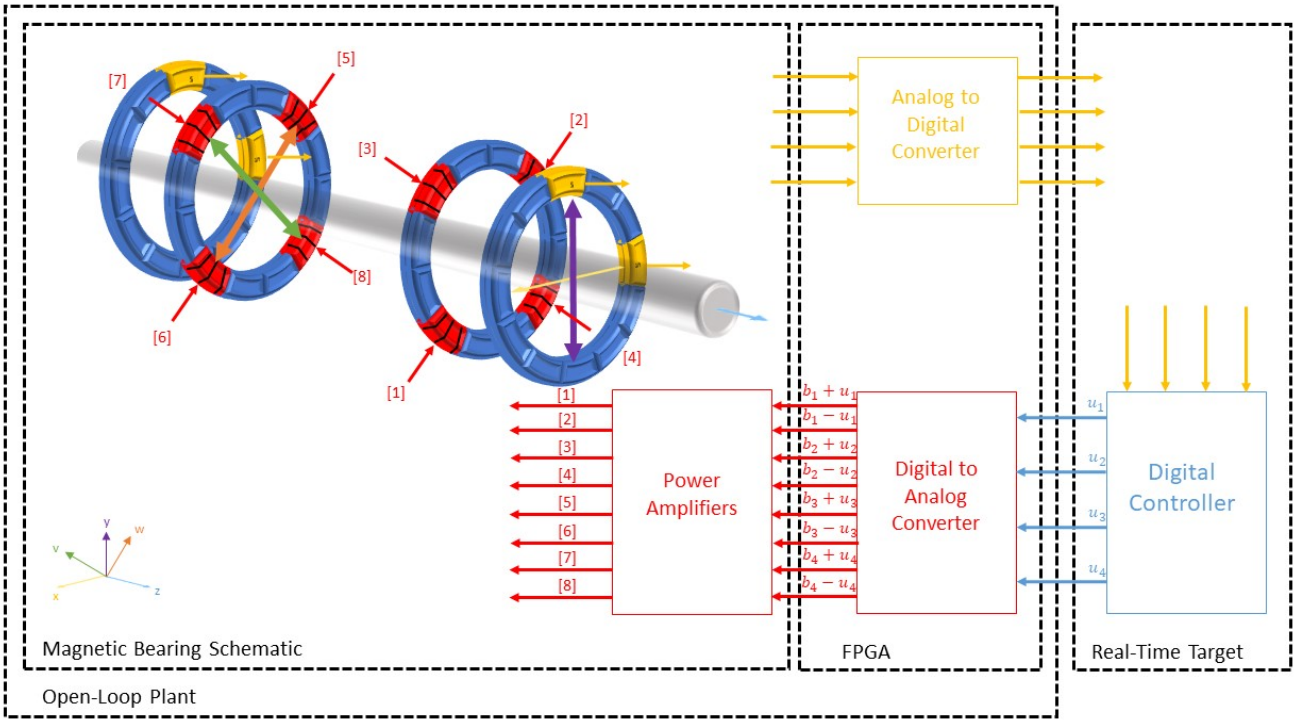


**Figure 2.2:** Schematic of AMBS System. The AC induction motor and thrust AMBs are omitted for brevity.

conversion and processing via a Field Programmable Gate Array (FPGA). The sinusoidal regressor signals are synchronized to the spindle rotations by an attached rotary encoder, which has 2000 counts per revolution. The FPGA samples and updates the encoder at 40MHz rate. The encoder resolution and the FPGA update rate make accurate and precise regressor signal synchronized with the spindle rotation. A schematic of the overall is shown in Figure 2.2.

## 2.1 System Identification and Baseline Stabilizing Control Design

The effort of system identification and control design was based on the four electromagnetic forces by the two radial AMBs in $v$ and $w$ directions, and the rotor's position at its each end in $x$ and $y$ directions measured by the four eddy current sensors. The $z$ axis was assumed

to be decoupled from the radial motion $v$ and $w$, and therefore was regulated by a SISO PID controller. There were several challenges in the identification of the AMBS used in this dissertation. First, since the axes of the sensors are not co-located with electromagnetic forces from the actuators, the system had strong off-diagonal coupling effects. Furthermore, the non-linearity in electromagnetic forces with respect to the coils' currents and the gap between rotor and housing requires adding bias currents to the opposing coils to render the system more linear.

With an initial stabilizing PID controller, a time-domain identification method using Pseudo-Random Binary Sequence (PRBS) input data and Autoregressive Exogenous Input (ARX) modeling was utilized to identify a model for $4 \times 4$ MIMO open-loop plant $P(z)$. The 20th-order identified model, with the state space representation $P_n(z) = (A, B, C, D)$, indicates the system is truly MIMO with strong coupling effect as shown in Figure 2.3. Consecutively, a model-based Linear-Quadratic-Gaussian with Integral action (LQGi) controller was designed to stabilize the open loop plant and attenuate low frequency disturbances. After levitation, the rotor has a radial distance of around 200 $\mu m$ from the housing. Maintaining this radial distance requires a more conservative controller for the initial lift up of the rotor to prevent hitting the housing and the resulting instability. The details of modeling and control design of this system are reported in [RCS16].

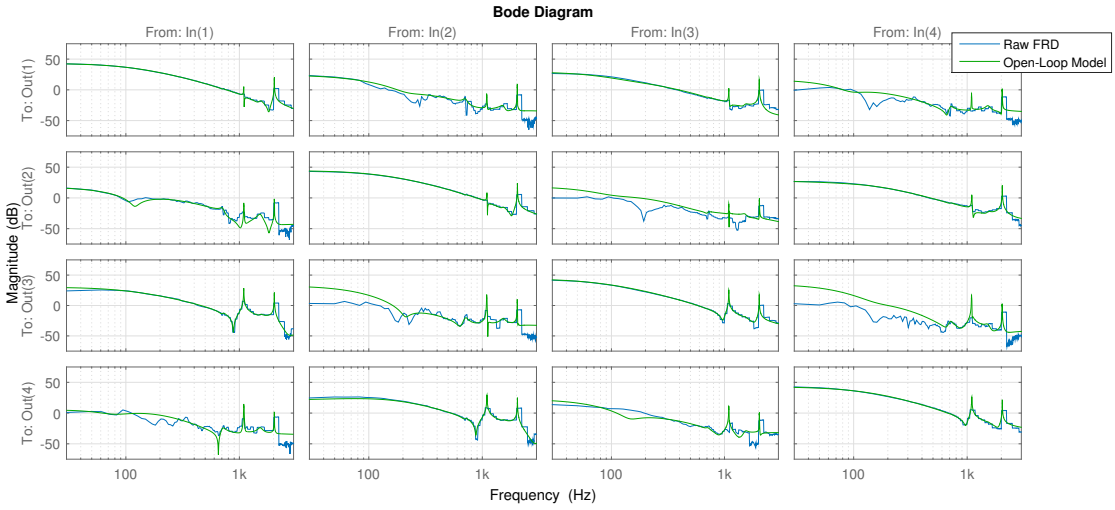


**Figure 2.3:** Bode magnitude plot of open-loop plant model VS raw Frequency Response Data (FRD) obtained from sine sweep experiments. Two flexible modes are identified at 1.1 and 2 kHz which also appear in the coupling terms.

# CHAPTER 3

# Robust Fault Detection, Isolation and Estimation- An Integrated Game Theoretic and Unknown Input Observer Approach

The problem of estimating unknown inputs is motivated in control applications where it is either too expensive or perhaps not possible to measure some of the system's input. If the unknown inputs represent the disturbances or effect of uncertainties, the knowledge of them will be useful for robust control [Gao14, Che04, ONO87, Han09]. Additionally, when the unknown inputs represent the effect of failure in actuators, sensors, or other plant components, an estimate of the unknown input can be a great value for fault detection and isolation (FDI). A robust FDI scheme is necessary for monitoring complex systems when they are subject to uncertainties or unknown disturbances.

Studies on unknown input estimation can be classified into two main groups. The first group is an open-loop estimation based on the inversion of the system dynamics [KC03, Hub13], and it has been popular in some control approaches for SISO stable systems, disturbance observer control [YCS09, YS14]. However, the estimation error transient dynamics cannot be assigned, and it can not be directly applied to unstable and non-minimum phase systems. In contrast, the second group is a closed-loop estimation based on the state-space approach, similar to Luenberger observer. A few techniques in state-space domain proposed a combined state/disturbance estimator [CT98, SO02, FB06]. Moreover, some techniques used a state function instead of full states in their estimators [XS03].

Among model-based FDI methods, observers play key roles by utilizing input and out-

put data to monitor the consistency between the model and actual process's output, which leads to a decision. To attenuate possible uncertainties and disturbances from diagnosis decisions, various optimization techniques have been developed to make the observer residual sensitive to faults and insensitive to disturbances [PC00]. Other attenuation methods have involved geometrically decoupling the process disturbances for FDI [DI01]. Among various decoupling FDI schemes, the unknown input observer (UIO) has been studied extensively to decouple disturbances from state estimations [CPZ96]. The UIO-based fault/disturbance estimation and reconstruction were addressed in [IJG07, ZJS10]. However, the UIO designs were constrained by some existence criteria, including rank conditions imposed on unknown inputs/faults. Consequently, there is a motivation to use the existing decomposition techniques in handling systems when disturbances cannot be completely decoupled. For state and fault estimations, a UIO was designed in [GLC15] for an augmented system forming from augmenting the system states and the concerned faults by attenuating the disturbances that cannot be decoupled using the linear-matrix-inequality (LMI) technique. However, only simulations results were provided.

This chapter reviews the direct UIO design used in state estimations for linear time-invariant systems and addresses the problems associated with the design process, including imposed rank conditions on the unknown inputs and robustness. Furthermore, it proposes a new approach to deal with the fault estimation problem for discrete-time unstable MIMO linear systems to overcome the difficulties in the direct UIO for the fault estimation. This method does not use the plant's states estimation nor the states' functions estimations. The proposed technique decouples faults into the scalar target fault and the remaining nuisance faults by designing observers using the game-theoretic method which is constructed by using optimization theory. By decoupling, the rank condition imposed on unknown inputs is relaxed. Furthermore, by including the measurement noise in the design process, the plant uncertainty will be considered. Finally, unknown input estimation for the open-loop unstable MIMO AMBS is investigated using both direct UIO and the proposed detection filter techniques.

## 3.1 DIRECT UNKNOWN INPUT OBSERVER (UIO) TECHNIQUE

Consider a dynamic system in the form of

$$\begin{aligned} x(t+1) &= Ax(t) + Bu(t) + Ef(t) \\ y(t) &= Cx(t) \end{aligned} \tag{3.1}$$

where $x(t) \in \mathcal{R}^n$ represents state vector, $u(t) \in \mathcal{R}^q$ and $y(t) \in \mathcal{R}^p$ stand for control input vector and measurement output vector, and $f(t) \in \mathcal{R}^m$ is the unknown input or fault to be estimated. $A$, $B$, $C$, $E$ are constant matrices with appropriate dimensions.

An observer is defined as a UIO for the above plant, if its state estimation error approaches zero asymptotically regardless of the presence of unknown inputs. Following [CP12], the structure of the full-order UIO for the above plant is described as:

$$\begin{aligned} z(t+1) &= Fz(t) + TBu(t) + Ky(t) \\ \hat{x}(t) &= z(t) + Gy(t) \end{aligned} \tag{3.2}$$

where $\hat{x} \in \mathcal{R}^n$ is the estimated state vector and $z \in \mathcal{R}^n$ is the state of this full order observer. Furthermore, $F, K, T, G$ are matrices to be designed such that the state estimation error approaches zero asymptotically. The error dynamic is governed by the following

$$\begin{aligned} e(t+1) = &(A - GCA - K_1C)e(t) \\ &+ [F - (A - GCA - K_1C)]z(t) \\ &+ [K_2 - (A - GCA - K_1C)G]y(t) \\ &+ [T - (I - GC)]Bu(t) + (GC - I)Ef(t) \end{aligned} \tag{3.3}$$

where $e(t) = x(t) - \hat{x}(t)$ is the state estimation error and $K = K_1 + K_2$. The state estimation error will be

$$e(k+1) = Fe(k) \tag{3.4}$$

if the following conditions hold.

$$\begin{aligned} 0 &= (GC - I)E && (3.5)\\ T &= I - GC && (3.6)\\ F &= A - GCA - K_1C && (3.7)\\ K_2 &= FG && (3.8) \end{aligned}$$

Therefore, if all eigenvalues of $F$ are stable, $e(t)$ will approach zero asymptotically. The necessary and sufficient conditions for existence of the UIO in (3.2) are

$$\text{(i) } rank(CE) = rank(E)$$

$$\text{(ii) } (C, A_1) \text{ is a detectable pair.} \quad (3.9)$$

where $A_1 = A - E[(CE)^T(CE)]^{-1}(CE)^TCA$. If conditions in (3.9) hold, observer matrices can be designed as following

$$\begin{aligned} G &= E[(CE)^T(CE)]^{-1}(CE)^T && (3.10)\\ T &= I - GC && (3.11)\\ A_1 &= TA && (3.12)\\ F &= A_1 - K_1C && (3.13) \end{aligned}$$

where $K_1$ is any matrix that stabilize $F$, and it may be selected by using pole placement or LQR techniques. Following [SS15], once the observer is designed, a step delay of the disturbance estimate can be found by using

$$\hat{f}(t-1) = (CE)^{\dagger}[y(t) - CA\hat{x}(t-1) - CBu(t-1)] \quad (3.14)$$

where $\hat{f}$ is the estimate of the fault vector.

## 3.2 GAME THEORETIC DETECTION FILTER (GTDF) TECHNIQUE

The UIO design in (3.2) ignores the effect of uncertainties and disturbances in fault estimation. Furthermore, the design constraints require satisfying both rank and detectablity condition. To relax the rank condition in (3.9), we seek to estimate the vector fault as separate scalar faults by designing a distinct UIO for each fault.

To achieve decoupling faults, we employ fault detection filters to detect and isolate faults by placing the reachable subspace of each scalar fault into non-overlapping invariant subspaces called detection spaces [Bea71, Jon73, WS87]. In this chapter, a bank of detection filters is constructed to detect and isolate each target scalar fault $f_i$ as a single fault while blocking the nuisance fault $\bar{f}_i = \begin{bmatrix} f_1 & \cdots & f_{i-1} & f_{i+1} & \cdots & f_m \end{bmatrix}^T$. Each detection filter is a Luenberger observer in the form $(i = 1, 2, ..., m)$:

$$\begin{aligned} \hat{x}_i(t+1) &= (A - L_i C)\hat{x}_i(t) + Bu(t) + L_i y(t) \\ y(t) &= Cx(t) + w(t) \end{aligned} \tag{3.15}$$

and the state estimation error dynamics:

$$e_i(t+1) = (A - L_i C)e_i(t) + E_i f_i(t) + \bar{E}_i \bar{f}_i(t) - L_i w(t) \tag{3.16}$$

$$r_i(t) = H_i C e_i(t) + H_i w(t) \tag{3.17}$$

where $\hat{x}_i \in \mathcal{R}^n$ is the state estimate, $e_i = x - \hat{x}_i$ is the estimation error, $f_i \in \mathcal{R}$ is the scalar target fault to be estimated, $\bar{f}_i \in \mathcal{R}^{m-1}$ is the nuisance fault, $w \in \mathcal{R}^p$ represents the combined effects of uncertainties and disturbances, and $r \in \mathcal{R}^p$ is the residual. Furthermore, $H_i$ and $L_i$ are the residual projector and observer gain respectively with proper dimension. The detection problem is to choose the residual projector $H_i$ and the observer gain $L_i$ such that the residual $r_i$ is nonzero if and only if the scalar target disturbance $f_i$ is nonzero.

### 3.2.1 Residual Projector Design

A vector space geometrical method outlined below [MS14, RTS19] can be used to find $H_i$. For the nuisance fault, the estimation error $e_i$ lies in

$$\text{Im}W_i = \text{Im}\begin{bmatrix}\bar{E}_i & (A-L_iC)\bar{E}_i & \cdots & (A-L_iC)^{n-1}\bar{E}_i\end{bmatrix} \tag{3.18}$$

and the output estimation error, $y - C\hat{x}_i$, lies in $CW_i$, where Im denotes the range space of a matrix. Let $\text{Im}W_i^*$ be the smallest reachable, observable subspace associated with $\bar{E}_i$ defined in (4.11), which is called the detection subspace. To block the nuisance fault, the output estimation error is projected by $H_i$ to the complement of $CW_i^*$:

$$H_i = I - CW_i^*[(CW_i^*)^T(CW_i^*)]^{-1}(CW_i^*)^T \tag{3.19}$$

Numerical computation of the above geometric method must take care of vector space numerical conditioning issues, particularly for high dimensional cases. The numerical procedure to find the detection subspace $\text{Im}W^*$ is outlined to obtain $W_i^*$ robustly. For simplicity, the subscript $i$ is dropped. By definition of $\text{Im}W^*$:

$$\text{Im}W^* \cap \text{Ker}C = \emptyset \tag{3.20}$$

where Ker denotes the null space of a matrix. Furthermore, if $n \geq p \geq m$, (3.20) is equivalent to $\begin{bmatrix}W & N_c\end{bmatrix}$ is full-column rank, meaning the smallest singular value is non-zero. Here, $N_c$ denotes the basis matrix for the null space of $C$.

First, it is observed from (3.18), $\text{Im}W = \text{Im}\bar{E}$ if the eigenvectors of $A - LC$ span $\text{Im}\bar{E}$. If $W$ satisfies (3.20), $W^* = W$. Otherwise, to extract the unobservable subspace from the non-empty intersections, $\text{Im}W^*$ is decomposed into two parts, one intersects with the null space of $C$, and the other does not:

$$\text{Im}W^* = \text{Im}\bar{E} = \text{Im}\begin{bmatrix}\hat{E} & \tilde{E}\end{bmatrix} \tag{3.21}$$

where $C\hat{E} = 0$. By this, (3.18) becomes

$$\text{Im}W = \text{Im}\,[\hat{E} \quad \tilde{E} \quad A\hat{E} \quad (A-LC)\tilde{E} \quad \cdots] \tag{3.22}$$

Furthermore,

$$\mathrm{Im}W^* = \begin{bmatrix} \tilde{E} & A\hat{E} \end{bmatrix} \tag{3.23}$$

if the eigenvectors of $A - LC$ span $\mathrm{Im}\begin{bmatrix} \hat{E} & \tilde{E} & A\hat{E} \end{bmatrix}$. By this construction, the unobservable subspace of $\mathrm{Im}W^*$ is reduced, and this process is iterated until (3.20) holds.

Numerical computation of $W^*$ in (3.19) must take care of vector numerical conditioning particular for high dimensional cases. In numerical evaluation, the singular values must be greater than a small positive threshold value to qualify as 'non-zero' [GR71, GK65].

**Algorithm 1** Numerical Iteration

$W^* \leftarrow$ normalized basis matrix for $\mathrm{Im}\bar{E}$
$n_w \leftarrow$ number of columns in $W^*$
$N_c \leftarrow$ normalized basis matrix for $\mathrm{Ker}C$
$K = \begin{bmatrix} W^* & N_c \end{bmatrix}$
$n_k \leftarrow$ number of columns in $K$
$\sigma_{n_k} \leftarrow$ smallest singular value of $K$
$N_k \leftarrow$ normalized basis matrix for $\mathrm{Ker}K$
$thr \leftarrow$ threshold for non-zero singular values
**while** $\sigma_{n_k} < thr$ **do**
    $\hat{E} = W^* N_k$(extract first $n_w$ rows)
    $E = (W^{*T} W^*)^{-1} W^{*T} \hat{E}$
    $\bar{E} \leftarrow$ normalized basis matrix for the complementary subspace of $\mathrm{Im}E$
    $\tilde{E} = W^* \bar{E}$
    $W^* \leftarrow$ normalized basis matrix for $\begin{bmatrix} \tilde{E} & A\hat{E} \end{bmatrix}$
    $K = \begin{bmatrix} W^* & N_c \end{bmatrix}$
**end while**

### 3.2.2 Observer Gain Design

The geometric method for deriving the residual projector $H_i$ in the previous subsection can also be applied to find the observer gain $L_i$ [Mas86, MVW89, WS87]. However, this method,

based on vector space decomposition and projections, does not account for sensitivity to model uncertainty and noise. To increase the flexibility of the detection filter, the observer is approximated as a state estimation problem with disturbance attenuation bound [CS98, MS00], where the transmission from the nuisance fault, uncertainties and initial condition error to the projected estimation error $H_i C e_i$ is bounded:

$$\frac{\sum_{t=0}^{N-1} ||H_i C e_i(t+1)||_Q^2}{||e_i(0)||_{P_0}^2 + \sum_{t=0}^{N-1}(||\bar{f}_i(t)||_N^2 + ||w(t)||_{V^{-1}}^2)} \leq \gamma \tag{3.24}$$

where $N, V, P_0, Q$ are weighting matrices, and $\gamma$ is the disturbance attenuation bound and specifies the degree in which the nuisance fault is blocked. Smaller $\gamma$ makes the residual to be less sensitive to the nuisance fault. Therefore, the detection filter can block the nuisance fault approximately or completely. This problem may be formulated a discrete time minimax problem, and solving the game leads to a Riccati based filter [MS00]:

$$\begin{aligned} M(t+1) = \hat{A}^T M(t)\hat{A} + 2C^T(\gamma V^{-1} - H_i Q H_i)C \\ - \hat{A}^T M(t)\hat{A}\bar{E}_i[2\gamma N + \bar{E}_i^T \hat{A}^T M(t)\hat{A}\bar{E}_i]^{-1}\bar{E}_i^T \hat{A}^T M(t)\hat{A} \end{aligned} \tag{3.25}$$

where $\hat{A}A = I$, and $M(t)$ propagates according to (3.25). The sufficient condition for (3.25) to converge is that $C^T(\gamma V^{-1} - H_i Q H_i)C$ be positive semi-definite. Since it is desired to find a constant $L_i$ for constructing a linear-time-invariant (LTI) UIO for fault estimation, the infinite horizon steady state solution $M$ can be readily solved as an algebraic Riccati equation. Once $M$ is obtained, the observer gain has the following form

$$L_i = 2\gamma M^{-1} C^T V^{-1} \tag{3.26}$$

For the limiting case, $\gamma = 0$, a reduced-order Riccati and detection filter can be found [MS00]. The reduced-order detection filter completely blocks the nuisance fault. However, this reduced-order filter is more sensitive to the model uncertainties. Since the game-theoretic detection filter (GTDF) discussed here only detects one fault, a bank of GTDFs are required to target all faults in a system.

## 3.3 Target Fault Estimation

As discussed in the previous section, by letting $\gamma \to 0$ for each GTDF, the nuisance fault and measurement noises can be blocked completely. Therefor, the error dynamics for each of detection filters can be rewritten as

$$\begin{aligned} \bar{x}(t+1) &= \bar{A}\bar{x}(t) + E_i f_i(t) \\ \bar{y}(t) &= \bar{C}\bar{x}(t) \end{aligned} \tag{3.27}$$

where $\bar{x} = e_i, \bar{A} = (A - L_i C)$ and $\bar{C} = H_i C$. This can be considered as a virtual plant with the target fault as a scalar unknown input and no known input. Then, the target fault can be approximated by constructing UIO for the virtual plant as following:

$$\begin{aligned} z(t+1) &= Fz(t) + K\bar{y}(t) \\ \hat{\bar{x}}(t) &= z(t) + G\bar{y}(t) \end{aligned} \tag{3.28}$$

where $\hat{\bar{x}} \in \mathcal{R}^n$ is the estimated state vector for the virtual plant and $z \in \mathcal{R}^n$ is the state of this full order observer. $F, K, G$ are matrices to be designed for achieving unknown input decoupling. The error dynamic is governed by the following

$$\begin{aligned} \bar{e}(t+1) = &(\bar{A} - G\bar{C}\bar{A} - K_1\bar{C})\bar{e}(t) \\ &+ [F - (\bar{A} - G\bar{C}\bar{A} - K_1\bar{C})]z(t) \\ &+ [K_2 - (\bar{A} - G\bar{C}\bar{A} - K_1\bar{C})G]\bar{y}(t) + (G\bar{C} - I)E_i f_i(t) \end{aligned} \tag{3.29}$$

where $\bar{e} = \bar{x} - \hat{\bar{x}}$ is the state estimation error vector, and $K = K_1 + K_2$. Since the unknown input is scalar for the virtual plant, the rank condition in (3.9) holds. Therefore, the necessary and sufficient condition for existence of the UIO for the virtual plant is

$$(\bar{C}, \bar{A}_1) \text{ is a detectable pair.} \tag{3.30}$$

where $\bar{A}_1 = \bar{A} - E_i[(\bar{C}E_i)^T(\bar{C}E_i)]^{-1}(\bar{C}E_i)^T(\bar{C}\bar{A})$. $F, G, K$ may be designed as described in Section 3.1. Once the observer is designed, a step delay of the scalar target disturbance estimate can be found by using

$$\hat{f}_i(t-1) = (\bar{C}E_i)^{\dagger}[r_i(t) - \bar{C}\bar{A}\hat{\bar{x}}(t-1)] \tag{3.31}$$

where $\hat{f}_i \in \mathcal{R}$ is the estimate of scalar target disturbance. There is a SISO transfer function, $\boldsymbol{G_i}$, such that,

$$\hat{f}_i(t-1) = \boldsymbol{G_i} f_i(t) \tag{3.32}$$

where,

$$\begin{aligned} \boldsymbol{G_i}(z) = & (\bar{C}E_i)^\dagger \bar{C}(zI - \bar{A})^{-1}E_i \\ & - (\bar{C}E_i)^\dagger z^{-1}[\bar{C}\bar{A}(zI - F)^{-1}K + \bar{C}\bar{A}G] \\ & \times [\bar{C}(zI - \bar{A})^{-1}E_i] \end{aligned} \tag{3.33}$$

When $\gamma = 0$, $\boldsymbol{G_i}$ should have a DC gain close to 0 dB. However, since the reduced order detection filer is sensitive to the model uncertainties, $\gamma$ is usually selected to be a positive number. Therefore, the dynamics from the virtual plant is influenced by the nuisance fault although the detection filter decouples the disturbances. In order to relax the effect of $\gamma$ into the estimator, a scalar factor, $\lambda_i$, is added to the estimator equation to normalize the DC gain of $\boldsymbol{G_i}$

$$\hat{f}_i(t-1) = \lambda_i(\bar{C}E_i)^\dagger[r_i(t) - \bar{C}\bar{A}\hat{\bar{x}}(t-1)] \tag{3.34}$$

where $\lambda_i$ is the normalization factor.

## 3.4 Implementation on AMBS

In order to investigate the effectiveness of proposed integrated approach in comparison with existing direct UIO method, two distinct fault scenarios are tested, where in both cases actuators are assumed to be faulty. The fault demonstration on the actuator is modeled by injecting artificial known inputs into the corresponding input channel, which is unknown for estimators. Therefore, $E$ are selected from columns of $B$ for each FDI scenario.

### 3.4.1 Case 1: Faults in Two Actuators

In the first case, actuator faults were assumed to exist in two channels. To model the faults, two multi-tone sinusoidal signals were injected into first two input channels, which were

unknown to estimators. Given, the satisfaction of (3.9), there exists a direct UIO design to estimate both faults simultaneously. Furthermore, it can be verified that a UIO exists for each virtual plant obtained from GTDFs. The superior performance of the direct UIO approach in estimating both faults simultaneously is shown in a simulation, where no uncertainties or noises are considered as show in Figure 3.1. However, the direct UIO approach suffers hugely from robustness when adding a zero mean noise with 0.05 standard deviation, and simulating the algorithm with a 100th order model instead of the 20th order model used in its design compared to the robust GTDF estimator as shown in Figure 3.2

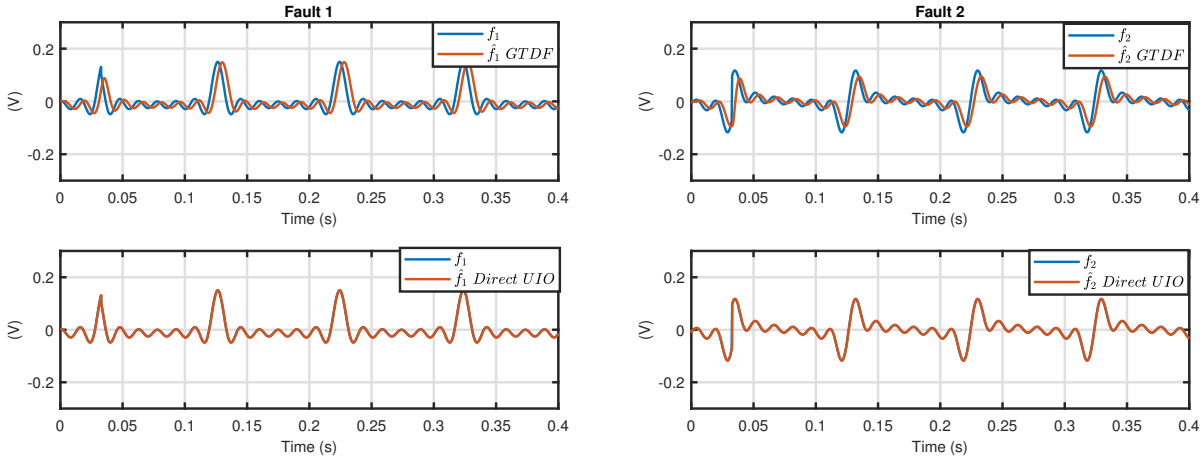


**(a)** **(b)**

**Figure 3.1:** Simulation comparison showing perfect fault estimation in the direct UIO method in comparison with the existing lag in the GTDF estimator in the absence of uncertainties and measurement noises. (a) Fault 1 (b) Fault 2

Given lack of robustness in the direct UIO approach, only the proposed integrated GTDF and UIO method is implemented. The effectiveness of proposed method is proved while each estimator detected, isolated and estimated the target fault in the experiment as shown in Figure 3.3. It can be shown the existence of faults in other actuators does not effect the fault estimation from the estimator designed for the specific fault.

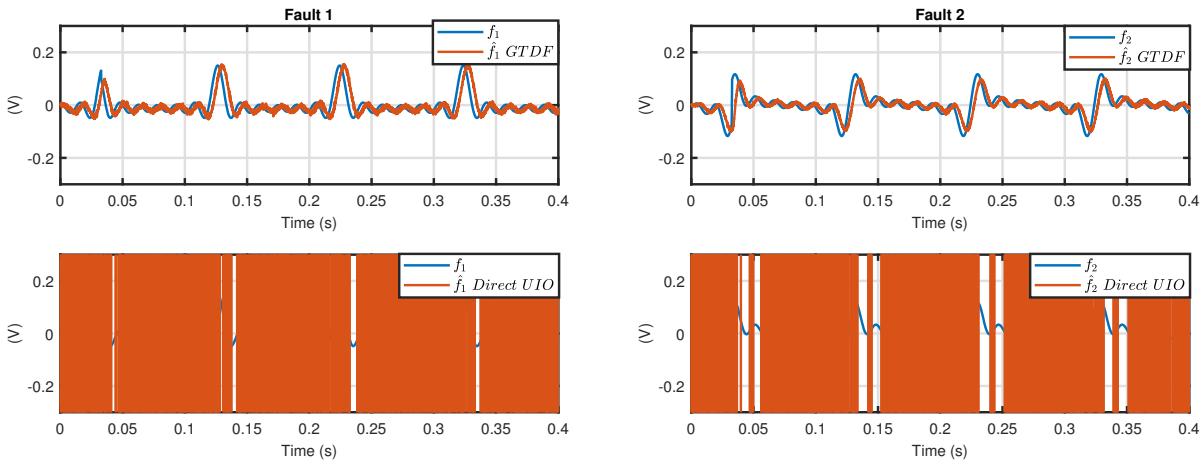


**(a)** **(b)**

**Figure 3.2:** Simulation comparison showing robust fault estimation in the GTDF method in comparison with the poor performance in the UIO estimator, where uncertainties and measurement are added into the model. (a) Fault 1 (b) Fault 2

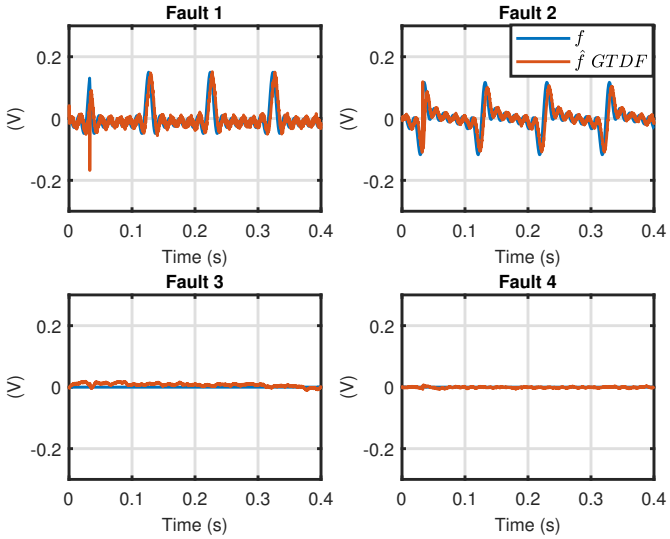


**Figure 3.3:** Experimental results showing the effectiveness of proposed integrated scheme in estimating the target fault only.

### 3.4.2 Case 2: Faults in All Actuators

In the next case, actuator faults were assumed to exist in all channels. To model the faults, four multi-tone sinusoidal signals were injected into all input channels. It can be shown that for AMBS the detectablity condition in (3.9) is not satisfied given existence of faults in all actuators. Consequently, there exists no direct UIO design to estimate all faults simultaneously, and the direct UIO design cannot be applied for fault estimations. However, it can be verified that a UIO exists for each virtual plant obtained from GTDFs given existence of faults in all actuators. The effectiveness of proposed integrated GTDF and UIO approach can be verified in experiment as shown in Figure 3.4.

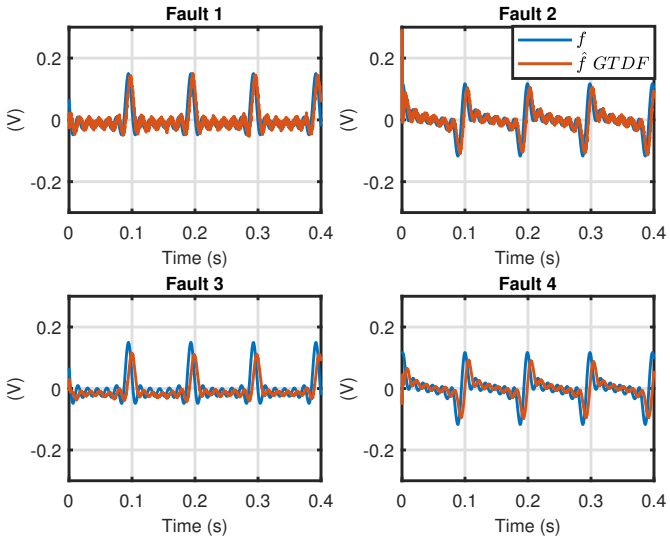


**Figure 3.4:** Experimental results showing the effectiveness of proposed integrated scheme in estimating the target fault only.

## 3.5 Summary

In this chapter, a novel fault estimation method for discrete-time LTI systems has been proposed. This method has been utilized to handle MIMO unstable systems subjected to multiple faults. The robustness is ensured by decoupling multi-variable faults into scalar

target fault and remaining nuisance faults for a virtual plant model using game-theoretic detection filters. The superior performance of the proposed method compared to the direct UIO design has been shown in both simulation and experimental results for the unstable MIMO AMBS system.

# CHAPTER 4

# Integrated MIMO Fault Detection and Disturbance Observer Based Control

Disturbance rejection is a common objective in control system design. If the disturbances can be determined at the plant input, feedforward control can be applied to cancel the disturbances. For unmeasurable disturbances, feedback control reduces the sensitivity of the regulated signal, typically measured output to the disturbances. An intuitive feedback control design method is to explicitly estimate the disturbances from the output measurements and compensate for the disturbances by control inputs to the plant as an emulation of the feedforward action. This feedforward compensation motivated approach, termed as Internal Model Control (IMC) [GM82, SO14] or more recently Disturbance Observer-Based Control (DOBC) [CYG15, LYC16], involves three design issues, which are disturbance estimation, system inversion, and closed-loop stability.

A Majority of the DOBC literature addresses SISO linear stable systems [YK94, BT99, FT10, Hub13, LKJ16], consisting of an input disturbance observer constructed by filtering the output measurement by the nominal plant inverse. Then, a low-pass 'Q-filter' is introduced as a trade-off between performance and uncertainties by limiting the bandwidth of the disturbance compensation [KC03, YCS09]. The Q-filter design may involve considerable tuning to satisfy multiple design criteria [UKH93, Han09]. Furthermore, the inversion of the stable plant must be stable and causal, thus preventing direct pole-zero cancellation for non-minimum phase systems [JSS10, WS15]. Because of its simplicity in designing feedback control, DOBC has been popular and celebrated by many applications, such as motor drives [KIO91], robotic manipulators [YS14], automobiles [BOA02], networks [NO08] and

spacecrafts [LLW18].

There is a little DOBC literature that addresses MIMO systems. In [NH09], DOBC is designed for diagonal channels separately where the cross channel dynamics are ignored. However, this simplification is not valid for MIMO systems with noticeable coupling effects. Another method minimizes the $H_\infty$ norm of closed-loop dynamics which can be applied for MIMO systems [ZZT17]. However, this method does not address unstable plants or the trade-off between performance and uncertainty, and the typically high-order numerical result may not be practical for real-time implementation.

For a MIMO unstable nonlinear system, such as an active magnetic bearing spindle (AMBS), it is common that the control system includes different controllers, tailored for different regimes of the operating conditions. In this case, monitoring is necessary to determine the active controllers in different regimes. Furthermore, fault detection is necessary to safeguard the system to remain in a safe stable regime when faults are detected. A scenario of the AMBS control system is that a stabilizing controller robust to all operating regimes is added on with a high-performance disturbance rejection controllers, which are effective for specific operating regimes but lack robustness and risk failures in other operating regimes. Continuous monitoring by fault detection filters is required to switch with smooth transitions of the add-on controllers. Motivated by this scenario we propose an integrated fault detection, state estimation, and DOBC. We exploit and extend the Youla parameterization of stabilizing controllers, where the robust feedback control, the DOBC, and the fault detection are realized by a bank of full-order state observers running in parallel. With this unified framework, the controller in each regime always stabilizes the nominal plant.

In the previous chapter, a bank of full-order UIO was presented for FDI and fault estimation with preliminary experimental results. Inversion filters for both estimation and compensation are introduced for the unified framework of the integrated estimation, detection, and control in this chapter. Furthermore, comprehensive analysis and discussions on the stability and performance of the MIMO DOBC, the fault detection filter design, smooth transitions of controller switching, and new elucidating experimental results are presented

here.

## 4.1 Conventional DOBC

The structure of DOBC is illustrated in Figure 4.1, where $P(z)$ represents the real physical plant, $P_n(z)$ is the nominal model used for the controller design, $Q(z)$ is the stable filter, $C(z)$ is the baseline controller, $r_e$ is the reference signal, $u_0$ is the feedback controller output, $d$ is the external disturbance, $u$ is the control input, $w$ is the measurement noise, $y$ is the measurement output, and $\hat{d}$ is the estimate of the disturbance. The intuitive idea of the conventional DOBC is to use the inverse of the plant model to construct the plant's input, $u$. Then, by utilizing $Q(z)$ the actual disturbance over specified frequency ranges can be estimated.

In the absence of disturbances and uncertainties, the inner loop with the disturbance estimation and compensation is not activated. In this case, the baseline controller $C(z)$ should be designed based on tracking performance and stability conditions. Once the baseline controller is designed, the inner loop with the DOBC can be designed to reject disturbances and handle uncertainties. Therefore, tracking and disturbance rejection are separately designed by the baseline controller and the DOBC.

There are three considerations in conventional DOBC design, which are stability, causality, and robustness. Stability requires $P_n(z)$ to be non-minimum phase or an alternative method to find $P_n^{-1}(z)$ such that $P_n^{-1}(z)P_n(z) \approx 1$. For the strictly proper plant, $Q(z)$ should be designed such that $Q(z)P_n^{-1}(z)$ is proper. Finally, the robust design of $Q(z)$ requires considering uncertainties in plant model.

## 4.2 FOSO Based MIMO DOBC

A method using FOSO to construct a model matching inversion filter for DOBC with the selected frequency-domain bandwidth is proposed in this article. To start with, the MIMO

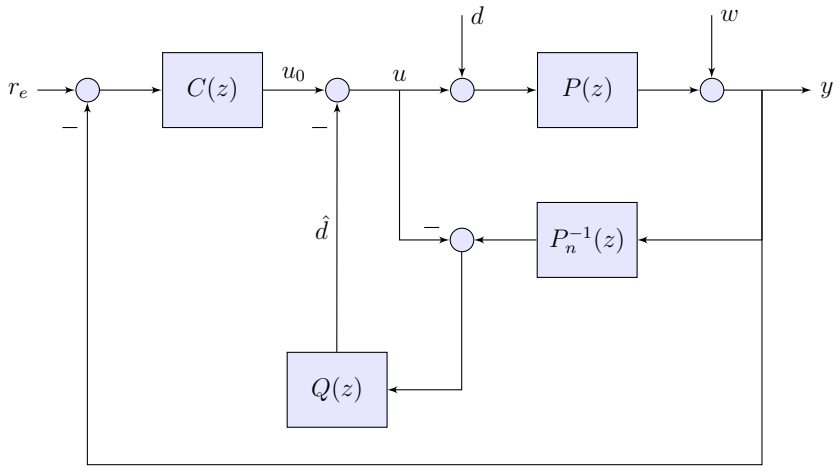


**Figure 4.1:** Conceptual diagram of conventional DOBC

DOBC problem is cast in the state space representation of the Youla parameterization [YJB76] of all stabilizing controllers. Then, a bank of FOSOs with corresponding inversion filters are proposed for disturbance estimation and compensation. This is followed by a comprehensive analysis and discussion of its stability and performance.

### 4.2.1 Youla Parametrization of FOSO Feedback Control

The MIMO DOBC problem in this paper is based on the following state space model of the plant $P_n(z)$

$$x(t+1) = Ax(t) + B(u(t) + d(t)) \tag{4.1}$$

$$y(t) = Cx(t) + w(t) \tag{4.2}$$

where $t(= 0, 1, 2, ...)$ is the sample time or sample number, $x \in \mathcal{R}^n$ is the state vector, and $u \in \mathcal{R}^q$ and $y \in \mathcal{R}^p$ are the control input and measured output vectors. Respectively, $d \in \mathcal{R}^q$ is the unknown input or disturbance vector, and $w \in \mathcal{R}^p$ represents the combined effects of sensor noise and model uncertainties.

The controller architecture shown in Figure 4.2 includes a FOSO feedback control used as a baseline stabilizing controller while describing all add-on controllers that will maintain the stability of the closed-loop plant. The state observer is a full order Luenberger observer

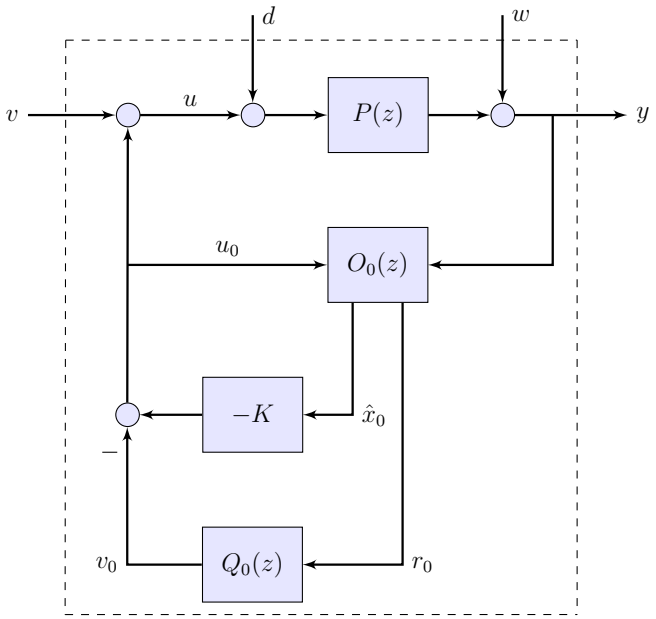


**Figure 4.2:** Youla parameterization of FOSO feedback control

$O_0(z)$ in the form

$$\hat{x}_0(t+1) = (A - L_0C)\hat{x}_0(t) + Bu_0(t) + L_0y(t) \tag{4.3}$$

$$r_0(t) = y(t) - C\hat{x}_0(t) \tag{4.4}$$

$$u_0(t) = -K\hat{x}_0(t) - v_0(t) \tag{4.5}$$

where $\hat{x}_0 \in \mathcal{R}^n$ is the state estimate, $r_0 \in \mathcal{R}^p$ is the residual output, and $u_0 \in \mathcal{R}^q$ is the control input to $O_0(z)$. The state observer and feedback gains $L_0$, $K$ with appropriate dimensions are designed such that $A - L_0C$ and $A - BK$ are stable. From Youla parameterization, the stability of the closed-loop system is guaranteed if $Q_0(z)$ is a stable filter. Therefore, $Q_0(z)$ can be designed for loop shaping or other performance motivations.

With the parameterization of stabilizing controllers, the MIMO DOBC is merely selecting the stable filter $Q_0(z)$ by designing $Q_0(z)$ to invert a virtual model obtained from the error dynamics by subtracting (4.3) from (4.1):

$$e_0(t+1) = (A - L_0C)e_0(t) + Bd(t) - L_0w(t) \tag{4.6}$$

$$r_0(t) = Ce_0(t) + w(t) \tag{4.7}$$

where $e_0 \in \mathcal{R}^n$ represents error in state estimation. The closed-loop system with inputs $[w, d, v]$, outputs $[u, y]$ and states $[x, x_0, e_0]$ is:

$$G_0(z) =$$

$$\left[\begin{array}{ccc|ccc} A-BK & -BC_0 & BK-BD_0C & -BD_0 & B & B \\ 0 & A_0 & B_0C & B_0 & 0 & 0 \\ 0 & 0 & A-L_0C & -L_0 & B & B \\ \hline C & 0 & 0 & I & 0 & 0 \\ -K & -C_0 & K-D_0C & -D_0 & 0 & I \end{array}\right] \tag{4.8}$$

with state space representation of $Q_0(z) = (A_0, B_0, C_0, D_0)$.

For DOBC, the disturbance vector can be estimated by inverting the dynamics $E_0(z)$ obtained from (4.6) and (4.7) with input $d$ and output $r_0$. Exact inversion is often impossible for non-minimum phase or strictly proper systems; hence, $H_2$ or $H_\infty$ model matching can be applied to find $Q_0(z)$:

$$Q_0(z) = \underset{Q_0(z) \in RH_\infty}{\arg\min} \; \|(M(z) - Q_0(z)E_0(z))W(z)\|_{(\infty,2)} \tag{4.9}$$

where $M(z)$ is a low-pass filter which specifies the bandwidth of the estimation, and $W(z)$ is a weighting filter for relative strengths in different frequencies and channels. Furthermore, $RH_\infty$ is the set of proper stable real-rational transfer functions. Clearly, $Q_0(z)$ as a stable inversion of the virtual plant $E_0(z)$ is a stabilizing controller, and is analogous to $Q(z)P_n^{-1}(z)$ in Figure 4.1.

### 4.2.2 Proposed Decoupling DOBC

Numerical methods for solving the MIMO inversion in (4.9) often render high-order approximate solutions, which may not be conducive to real-time implementation. Furthermore, the disturbance's relative strengths in different channels may change during operations, requiring a fixed optimal filter with compromised performance with equal weighting or a more complex adaptive optimal filter adapting in real-time to the changing disturbance characteristics. In

this paper, we seek to estimate and compensate for the vector disturbance as separate scalar disturbance channels.

To achieve disturbance decoupling, we employ fault detection filters, which can be used for the disturbance detection and isolation by placing the reachable subspace of each scalar disturbance into non-overlapping invariant subspaces called detection spaces [Bea71, Jon73, WS87]. In this paper, a bank of detection filters is constructed to detect and isolate each target scalar disturbance $d_i$ as a single fault while blocking the nuisance disturbance $\bar{d}_i = \begin{bmatrix} d_1 & \cdots & d_{i-1} & d_{i+1} & \cdots & d_q \end{bmatrix}^T$. Each detection filter $O_i(z)$ is a Luenberger observer in the form $(i = 1, 2, ..., q)$:

$$\hat{x}_i(t+1) = (A - L_i C)\hat{x}_i(t) + Bu(t) + L_i y(t) \tag{4.10}$$

and the state estimation error dynamics:

$$e_i(t+1) = (A - L_i C)e_i(t) + B_i d_i(t) + \bar{B}_i \bar{d}_i(t) - L_i w(t) \tag{4.11}$$

$$r_i(t) = H_i C e_i(t) + H_i w(t) \tag{4.12}$$

where $\hat{x}_i \in \mathcal{R}^n$ is the state estimate, $e_i = x - \hat{x}_i$ is the estimation error, $d_i \in \mathcal{R}$ is the scalar target disturbance, $\bar{d}_i \in \mathcal{R}^{q-1}$ is the nuisance disturbance, $r_i \in \mathcal{R}^p$ is the residual, and $H_i$ and $L_i$ are the residual projector and observer gain respectively with appropriate dimensions. The detection problem is to choose the residual projector $H_i$ and the observer gain $L_i$ such that the residual $r_i$ is nonzero if and only if the scalar target disturbance $d_i$ is nonzero. The construction of $H_i$ and $L_i$ to achieve this will be given in Section 4.3.

For the SIMO virtual model, $E_i(z)$ from the scalar disturbance input $d_i$ to the residual output vector $r_i$, a MISO inversion filter $F_i(z)$ is obtained to estimate the scalar disturbance $d_i$:

$$F_i(z) = \underset{F_i(z) \in RH_\infty}{\arg\min} \; \|(m(z) - F_i(z)E_i(z))w(z)\|_{(\infty,2)} \tag{4.13}$$

where $m(z)$ and $w(z)$ signify scalar transfer functions. Then, a MISO inversion filter $F_i(z)$ is obtained for each $E_i(z)$ to estimate the scalar disturbance $d_i$. Figure 4.3 shows this

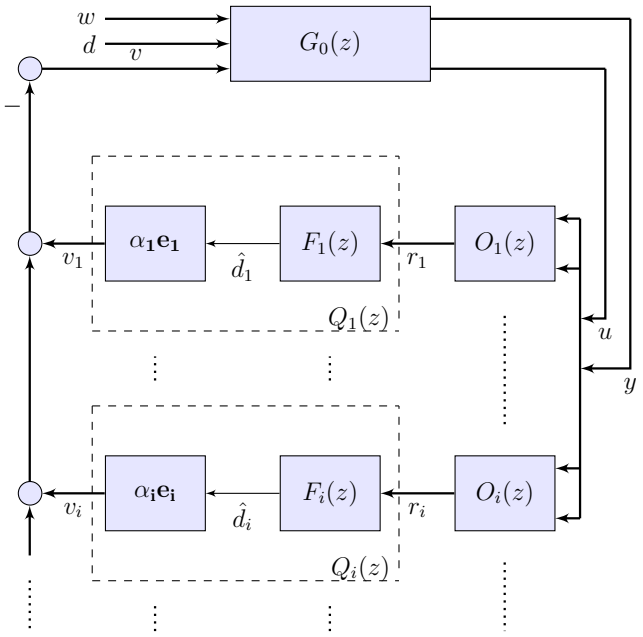


**Figure 4.3:** Youla parameterization of FOSO feedback control with the detection filter-based DOBC

expanded Youla parameterization of the FOSO feedback control with the additions of the detection filter-based DOBC where $0 \leqslant \alpha_i \leqslant 1$ is used for DOBC activation, deactivation and transition, which will be discussed in Section 4.3, $\mathbf{e_i} = \begin{bmatrix} 0_1 & \cdots & 0_{i-1} & 1_i & 0_{i+1} & \cdots & 0_q \end{bmatrix}^T$, $Q_i(z) = \alpha_i \mathbf{e_i} F_i(z)$ and $v_i = \alpha_i \mathbf{e_i} \hat{d}_i$.

### 4.2.3 Performance Analysis of the Proposed Decoupling DOBC

In this section, the performance of the disturbance estimator and DOBC is analyzed, where transfer functions from $d$ to $\hat{d}_i$ and $d$ to $y$ are derived. To investigate the performance of each disturbance estimator, the estimation transfer function with inputs $[w, d, v]$ and output $\hat{d}_i$ is obtained as following given the state space realization of $F_i(z) = (A_{f,i}, B_{f,i}, C_{f,i}, D_{f,i})$

and using (4.11) and (4.12).

$$G_i(z) = \begin{bmatrix} G_{\hat{d}_i w}(z) & G_{\hat{d}_i d}(z) & G_{\hat{d}_i v}(z) \end{bmatrix}$$

$$= \left[\begin{array}{cc|ccc} A_{f,i} & B_{f,i}H_iC & B_{f,i}H_i & 0 & 0 \\ 0 & A - L_iC & -L_i & B & 0 \\ \hline C_{f,i} & D_{f,i}H_iC & D_{f,i}H_i & 0 & 0 \end{array}\right] \tag{4.14}$$

It is shown from (4.14) that the performance of each estimator is independent of both the baseline FOSO feedback controller and $Q_0(z)$ design, and activation or deactivation of the DOBC. This is a form of the separation principle, where each disturbance estimator can be designed separately and independent from other estimators and the feedback controller.

Furthermore, the transfer function from $d$ to $y$ can be obtained in steady states for a fixed $\alpha_i$. Using (4.14), the following equality is obtained:

$$V(z) = -\sum_{i=1}^{q} \alpha_i \mathbf{e_i} [G_{\hat{d}_i w}(z) W(z) + G_{\hat{d}_i d}(z) D(z)] \tag{4.15}$$

where $V(z), W(z), D(Z)$ are unilateral Z-transform of discrete time signals $v(t), w(t), d(t)$. Using (4.15) in (4.8), the transfer function for the proposed decoupling DOBC is obtained as following.

$$G_{yd}(z) = G_{0yd}(z) - G_{0yv}(z) \sum_{i=1}^{q} \alpha_i \mathbf{e_i} G_{\hat{d}_i d}(z) \tag{4.16}$$

Furthermore, it can be seen from (4.8) $G_{0yd}(z) = G_{0yv}(z)$. Then, (4.16) is simplified to:

$$G_{yd}(z) = G_{0yd}(z)[I_{q\times q} - \sum_{i=1}^{q} \alpha_i \mathbf{e_i} G_{\hat{d}_i d}(z)] \tag{4.17}$$

It is clearly shown in (4.17) that $G_{0yd}(z)$, the baseline controller's performance, can be improved multiplicatively in steady states for $\alpha_i = 1$ by the DOBC if $\sum_{i=1}^{q} \mathbf{e_i} G_{\hat{d}_i d}(z)$ is designed such that it is close to but not necessarily exactly diagonal and that the diagonal elements are close to one in adequate frequency range.

## 4.3 Integrated DOBC and Fault Detection

To isolate the scalar disturbance as outlined in the previous section, each residual projector $H_i$ and the observer's gain $L_i$ must be designed so that the residual $r_i$ passes the scalar disturbances $d_i$ and blocks the nuisance disturbance $\bar{d}_i$. The GTDF design discussed in the previous chapter can be employed here to isolate the target disturbance followed by the proposed integrated disturbance estimation, detection, and compensation for MIMO systems.

While the numerical iteration in the previous chapter may be found useful to obtain the residual projector $H_i$, the observer gain $L_i$ can be obtained by solving the disturbance attenuation problem:

$$\frac{\sum_{t=0}^{N-1} ||H_i C e_i(t+1)||_Q^2}{||e_i(0)||_{P_0}^2 + \sum_{t=0}^{N-1}(||\bar{d}_i(t)||_N^2 + ||w(t)||_{V^{-1}}^2)} \leq \gamma \tag{4.18}$$

where $N, V, P_0, Q$ are weighting matrices, and $\gamma$ is the disturbance attenuation bound and specifies the degree in which the nuisance disturbance is blocked. This problem may be formulated as a discrete time minimax problem, and solving the game leads to a Riccati based filter [MS00]:

$$\begin{aligned} M(t+1) = \hat{A}^T M(t)\hat{A} + 2C^T(\gamma V^{-1} - H_i Q H_i)C \\ - \hat{A}^T M(t)\hat{A}\bar{B}_i[2\gamma N + \bar{B}_i^T \hat{A}^T M(t)\hat{A}\bar{B}_i]^{-1}\bar{B}_i^T \hat{A}^T M(t)\hat{A} \end{aligned} \tag{4.19}$$

where $\hat{A}A = I$, and $M(t)$ propagates according to (4.19). The sufficient condition for (4.19) to converge is that $C^T(\gamma V^{-1} - H_i Q H_i)C$ be positive semi-definite. Since it is desired to find a constant $L_i$ for constructing a fixed $F_i(z)$, the infinite horizon steady state solution $M$ can be readily solved as an algebraic Riccati equation. Once $M$ is obtained, the observer gain has the following form

$$L_i = 2\gamma M^{-1} C^T V^{-1} \tag{4.20}$$

The essential feature of the detection filters is to analyze the projected residual generated by all GTDFs in the presence of uncertainty and determine if input channels are corrupted by input disturbances or faults. This requires higher-level decision making and creation

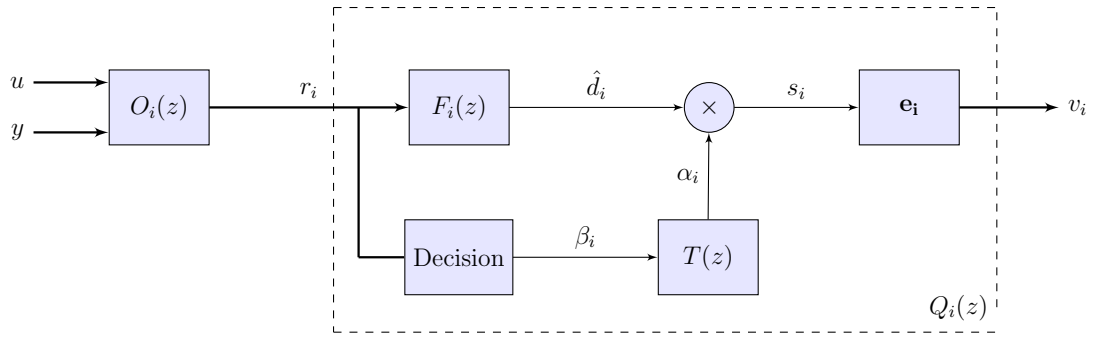


**Figure 4.4:** Proposed integrated DOBC and fault detection

of thresholds. Nominally the projected residual obtained from each GTDF is zero in the absence of the target disturbance and non-zero otherwise. However, when driven by sensor noise and nonlinearities, the projected residual fails to go to zero even in the absence of the target disturbance. Since the combined effects of sensor noise and nonlinearities is different on each element of the projected residual vector, a threshold is set on the matrix norm of the projected residual for each GTDF. Figure 4.4 shows the proposed integrated DOBC and fault detection. The projected residual enters the Decision block:

$$\beta_i(t) = \begin{cases} 1 & \text{if } ||r_i(t)||_{R_i} - \epsilon_i \geq 0; \\ 0 & \text{if } ||r_i(t)||_{R_i} - \epsilon_i < 0. \end{cases}$$

where $R_i$ is the weighting matrix, and $\epsilon_i$ is the threshold on the projected residual matrix norm. Furthermore, to alleviate excessive transient excursions in the switching between LTI controllers, the binary value coming out of the Decision block is smoothened by a moving average filter $T(z)$:

$$T(z) = \frac{1}{k}\frac{1 - z^{-k}}{1 - z^{-1}} \tag{4.21}$$

where window size $k$ makes the binary gain $\beta_i$ linearly increase to one once the target disturbance is detected, such that the disturbance estimate $\hat{d}_i$ is gain scheduled between 0 and 1 to enter the control as $s_i$.

It should be noted that the closed-loop system is LTI stable for any fixed $\alpha_i$ value, thanks to the specific control system architecture. This feature is in contrast to the 'bumpless transfer' of two controllers in other control system architectures, where the frozen gain

stability may not be enforced. Furthermore, this integrated DOBC and fault detection can easily include more fault detection filters, which are not directly aimed for the disturbance estimation and compensation. These additional fault detectors can be used to monitor the system health and provide additional decision logic for switching, with the transitional interpolations, among the finite set of stabilizing LTI controllers. For example, internal state variables may be estimated and monitored for the system's faults and decision logic can be made accordingly to ensure safe operations.

## 4.4 Implementation on AMBS

In this section, the proposed integrated DOBC and fault detection is applied to an open-loop unstable MIMO AMBS. Furthermore, the experimental set-up and GTDF design process are discussed followed by the illustration of the experimental results.

### 4.4.1 MIMO DOBC Design and Performance

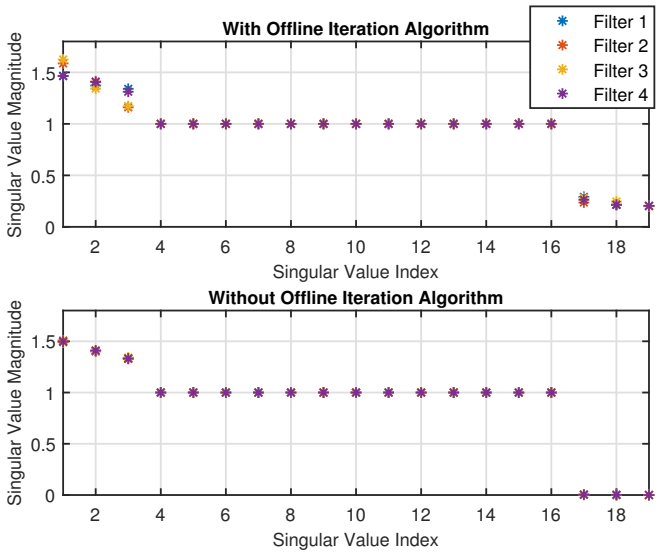


**Figure 4.5:** Singular value analysis for detection spaces

To justify the GTDF based integrated DOBC method, first a single FOSO based DOBC is investigated by designing $Q_0(z)$ using (4.9) with $M(z) = m(z)I_q$ and $W(z) = w(z)I_q$, where

$m(z)$ and $w(z)$ are chosen to be low-pass and high-pass filters respectively. The resulting numerical solution for the approximated optimal $Q_0(z)$ is shown to be a 140th order four by four filter in its minimal realization, which is not practical for implementation given hardware constraints. In contrast, for the GTDF based DOBC, the optimal $Q_i(z)$ obtained from (4.13) using same $m(z)$ and $w(z)$ for each detection filter has 40th order adding to the four 20th full-order observers.

For the numerical computation of the residual projector $H_i$ and the observer gain $L_i$, the design for $H_i$ involves obtaining the basis matrix $W_i^*$ for the detection subspace in which the nuisance disturbance resides. Since it is desired for the detection subspace to be observable for blocking the nuisance disturbance, $\begin{bmatrix} W_i^* & N_c \end{bmatrix}$ should be full-column rank and have non-zero singular values, where $N_c$ denotes the basis matrix for the null space of $C$. Figure 4.5 shows that near zero singular values in the direct computation are increased by the iterative algorithm in the Appendix.

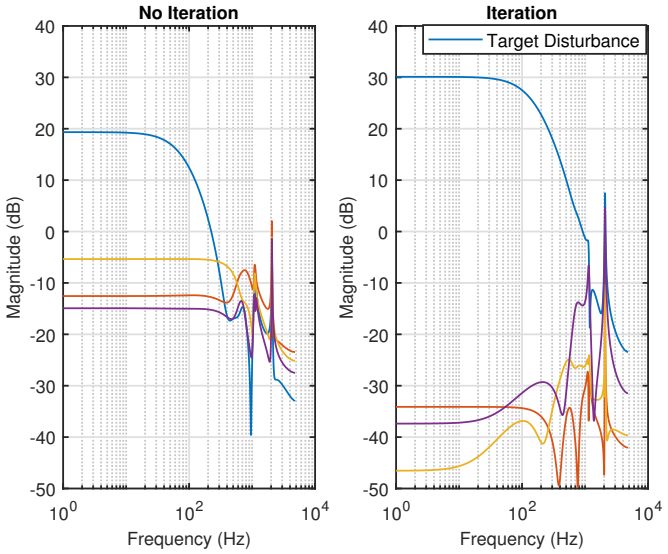


**Figure 4.6:** Singular values of one GDTF using different $W_i^*$

The computation of the $W_i^*$ has significant impact on the performance of the subsequent GTDF. Figure 4.6 shows the singular values plot of the transfer function from $d$ to $r_i$ for one GTDF (others behave similarly) using (4.11) and (4.12). It is illustrated that given the same tuning parameters ($Q = 10^{-5}$, $\gamma = 10^{-5}$, $V = 0.7I$, and $N = I$) for designing $L_i$, applying

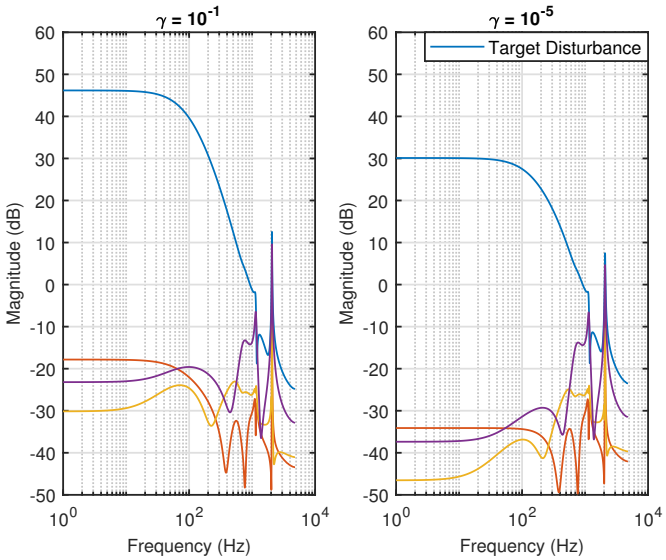


**Figure 4.7:** Singular values of one GTDF using different $\gamma$

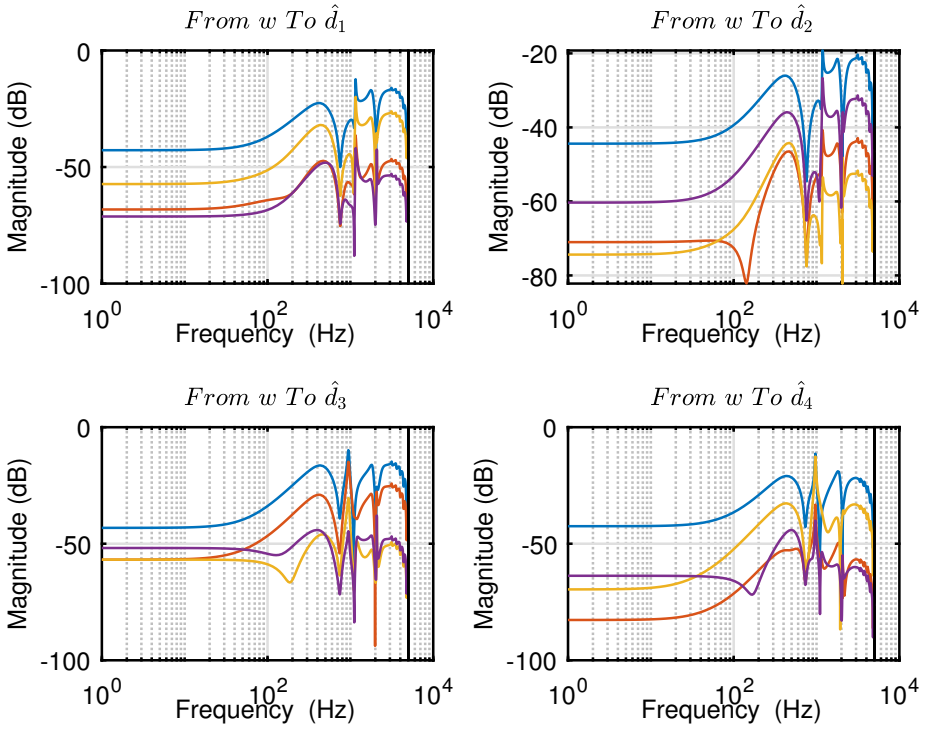


**Figure 4.8:** Sensitivity plots of each GTDF estimator to $w$

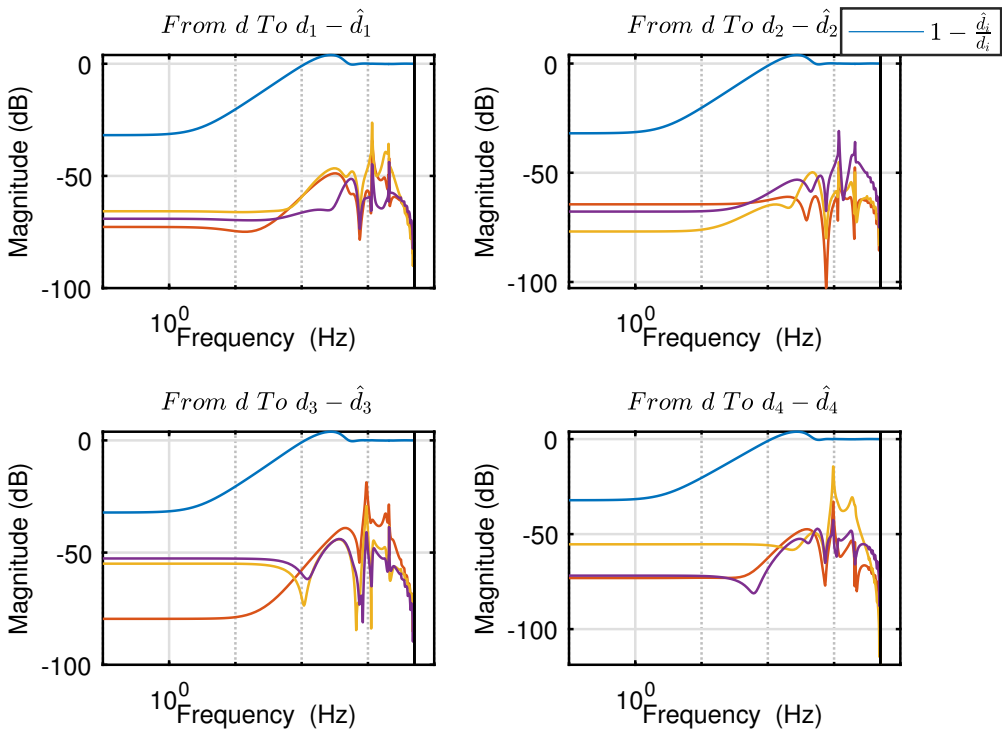


**Figure 4.9:** Magnitude bode plots of disturbance estimation error

the iterative algorithm in finding the detection space increases both the magnitude ratio and the bandwidth of the decoupling effect between the target and nuisance disturbance.

To illustrate the effect of the attenuation bound $\gamma$ in the GTDF design in (4.18), Figure 4.7 shows that increasing the attenuation bound $\gamma$ decreases the bandwidth for the target disturbance estimation with other parameters remaining the same. The subsequent inversion filter design is based on $\gamma = 10^{-5}$, where every GTDF estimator has a bandwidth of 100 Hz while maintaining above 50 dB decoupling between the target and nuisance disturbance.

To illustrate the effectiveness of the GTDF estimator in accounting for sensitivity to the combined effects of sensor noise and model uncertainties $w$, Figure 4.8 shows that every GTDF estimator maintains more than 40 dB in blocking them.

Lastly, Figure 4.9 summarizes the closed-loop performance of the activated GTDF based DOBC. It is shown that the estimation error respect to the nuisance disturbance is less than

-50 dB in the estimation bandwidth, and sufficiently small in the rest of the frequency range. Furthermore, the estimation error respect to the target disturbance is less than 0 dB in the estimation bandwidth. Using (4.17), it can be seen that the baseline controller's performance is improved multiplicatively in the estimation bandwidth by the GTDF DOBC.

## 4.5 Experimental Results

In all experiments, the rotor is lifted off the housing at the beginning of levitation by the baseline LQGi controller, and then known sinusoidal disturbances are injected into the input channels. The integral action in the LQGi compensates for constant disturbances due to gravity, so the DOBC here does not target them despite their presence in the estimators. Two sets of experiments are presented to verify the effectiveness of the activated GTDF based DOBC in improving the baseline controller's performance multiplicatively. Furthermore, two representative experiments were performed in each set to compare the performance of the baseline LQGi controller alone and the LQGi controller combined with the integrated DOBC and fault detection. In the absence of disturbances, the first $7.24s$ were identical for both experiments in each set.

In the first set of experiments shown in Figure 4.10, known 20 Hz sinusoidal disturbances entered Channel 1 and 2 at the same time. In the experiment with integrated DOBC and fault detection skim, once disturbances entered input channels, they were detected by the corresponding fault detection filters, and the integrated DOBC and fault detection skim gained schedule their estimates for disturbance compensation. Furthermore, since Channel 4 was not perturbed by the external disturbance, its corresponding DOBC was not activated. For Channel 3, the fault detection filter detected the external disturbance during the transient, although no external disturbance entered the input channel, which was due to the possible error in the linear approximation of the nonlinear plant. Furthermore, although only two input channels were perturbed by the known sinusoidal disturbances, all output channels show the effect of disturbances, which was due to the high coupling effect in the AMBS.

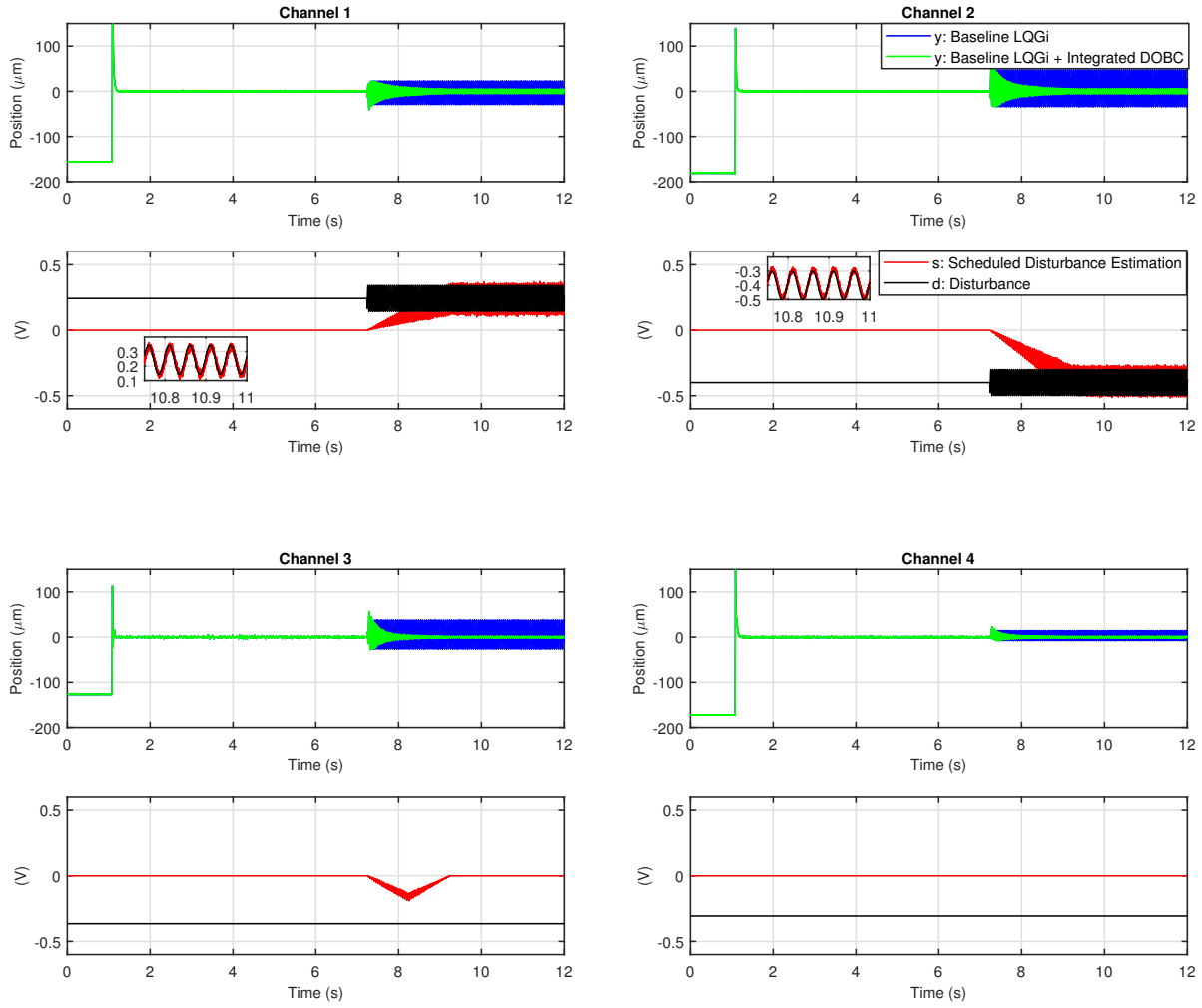


**Figure 4.10:** Experimental performance comparisons showing improved disturbance rejection achieved by integrated DOBC and fault detection skim. The rotor was lifted off the housing at $t = 1.08s$, and 20 Hz sinusoidal disturbances entered Channel 1 and 2 at $t = 7.24s$. The rotor's position from each sensor $y$ is in micro-meter, and the input disturbance $d$ and the gain scheduled disturbance estimation $s$ are in volt.

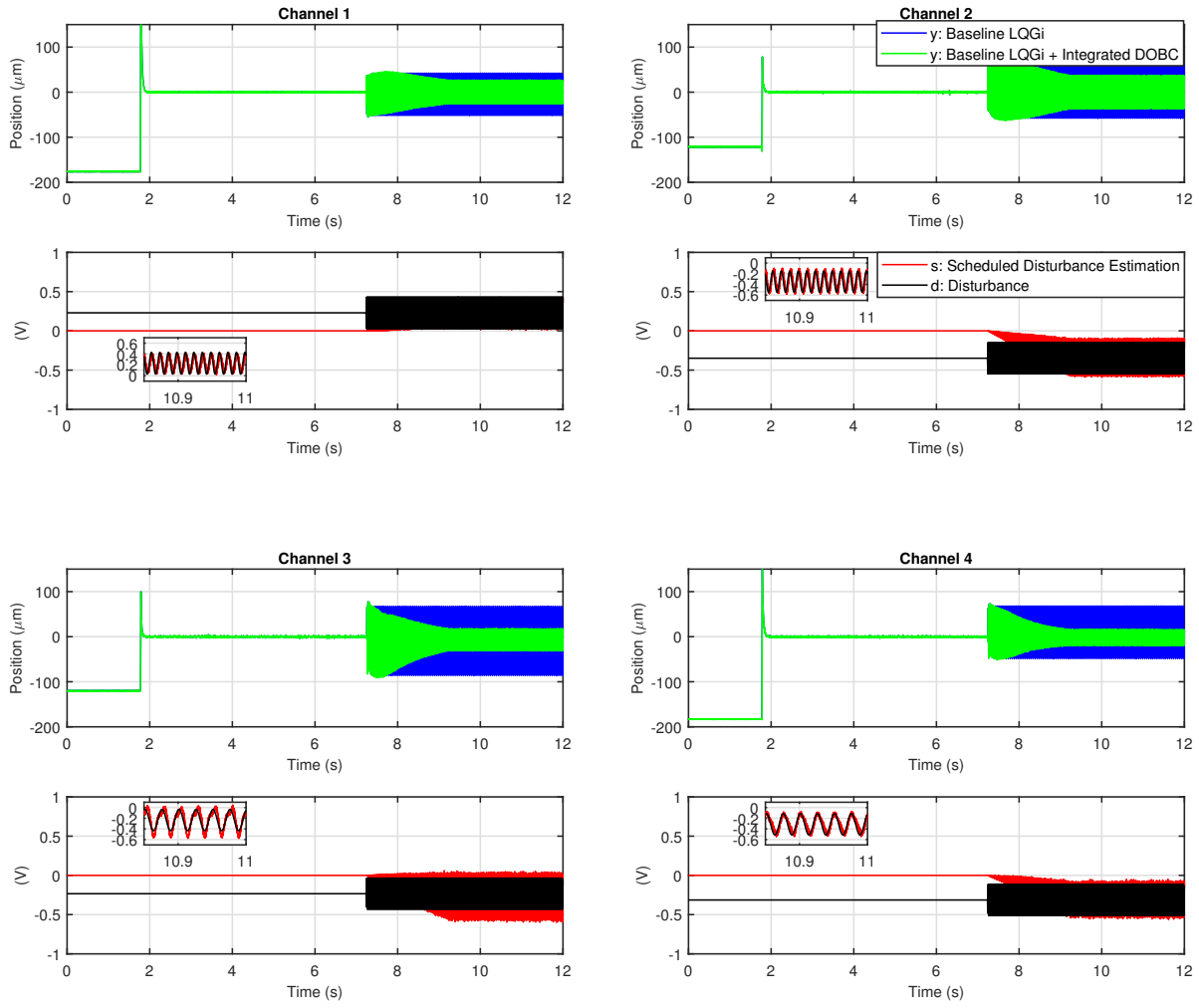


**Figure 4.11:** Experimental performance comparisons showing improved disturbance rejection achieved by integrated DOBC and fault detection skim. The rotor was lifted off the housing at $t = 1.78s$. Then, 80 Hz sinusoidal disturbances entered Channel 1 and 2, and 40 Hz sinusoidal disturbances entered Channel 3 and 4 respectively at $t = 7.24s$. The rotor's position from each sensor $y$ is in micro-meter, and the input disturbance $d$ and the gain scheduled disturbance estimation $s$ are in volt.

In the second set of experiments shown in Figure 4.11, 80 Hz sinusoidal disturbances entered Channel 1 and 2, and 40 Hz sinusoidal disturbances entered Channel 3 and 4 respectively at the same time. In the experiment with integrated DOBC and fault detection skim, all disturbances were detected by the corresponding fault detection filters once they entered the input channels, and the integrated DOBC and fault detection was activated in each channel automatically for gain scheduling the disturbance estimate for the compensation.

## 4.6 Summary

In summary, the DOBC based on the Youla parameterization of stabilizing controller with a FOSO feedback control is more general than the common input–output approach since it alludes to the MIMO DOBC. Furthermore, the extension of the Youla parameterization, which further includes multiple observers, has facilitated the observer design for the separate purposes of fault detection, state estimation, and disturbance estimation. This integrated control system, as an extension of the Youla parameterization, has been proven stable since the observer residuals are used for the disturbance observer feedback compensation. For the disturbance observer design, the exploitation of the game-theoretic approach, originally used in fault detection to create decoupled disturbance observer has been shown useful for rendering lower-order compensators than the full order observer approach. The application to the AMBS demonstrates the several features of the proposed method and its practical usefulness and effectiveness in monitoring and control of the MIMO unstable open-loop system.

# CHAPTER 5

# Adaptive Feedforward Control (AFC)

In the previous chapter, the DOBC based on Youla parameterization of stabilizing controller with a FOSO feedback control was presented to attenuate broadband and stochastic disturbances. Furthermore, the integrated control system was proven to be stable since the observer residuals are used for the disturbance compensation. In this chapter, the problem of eliminating narrow-band disturbances is investigated.

Several methods are available for the rejection of sinusoidal disturbances, and their extension can apply to the case with multiple sinusoidal components. For fixed disturbance frequencies, the internal model principle (IMP) is the most common approach. The IMP design includes a model of the disturbance in the feedback path, and the feedback controller is designed to stabilize the plant together with the internal model [FW76]. However, since the disturbance rejection requirement is incorporated into the feedback controller design, the implementation needs a complex gain scheduling of controller parameters as a function of disturbance frequencies. Furthermore, closed-loop stability will be difficult to maintain given a time-varying disturbance, as the internal model is updated.

Sinusoidal internal models in the form of peak filter were developed to simultaneously satisfy both stability and performance, and they were implemented for various applications including, AMB rotor systems [KHF95, LP08]. In [HBG96], a generalized multi-variable notch filter was cascaded with a stabilized plant for automation balancing while maintaining the closed-loop stability. However, the parameters of generalized notch filters strongly depend on the inverse sensitivity matrix evaluated at rotor speed which requires extensive memory for varying rotational speed. In [SBL94] a digitized realization of the notch fil-

ter based on an iterative algorithm was used to obtain the Fourier coefficient of vibration. In [CLW16] multiple phase-shift notch filters were implemented where phases were gain-scheduled according to the rotation speed.

Repetitive control is another IMP type controller widely used for Harmonic rejection [RCS16]. Integer delays are used to generate the internal model at disturbance frequencies as well as all its harmonics to the Nyquist frequency in the prototype repetitive controller [TTC89]. However, the closed-loop sensitivity reduction in so many narrow bands causes amplification in the spectrum at other frequencies according to the waterbed effect. In [TT94], the higher harmonic effects are reduced to increase the robustness by integrating a low-pass filter although it limits the control gain. Furthermore, repetitive control is cumbersome for disturbances with non-harmonic makeup, and it has a limited set of allowable disturbance periods, speeds, rejection since the delay length is required to be integer values. Even with fractional delay solutions in [YH01, THD07], the performance of the IMP was sacrificed.

Adaptive feedforward control (AFC) is another approach for rejection of sinusoidal disturbances based on a different concept [BSK94, BKU99]. With this approach, a feedforward control that cancels the disturbance effect is constructed by the periodic regressor signal. The regressor signal is modeled as a linear combination of finite or infinite basis functions with unknown coefficients, and an adaptive algorithm estimates these unknown coefficients. Unlike the IMP, AFC does not alter the loop gain, and its design is independent of rejecting disturbances with other frequencies, low-frequency attenuation. However, stability of original AFC is ensured for single-input-single-output (SISO) strictly positive real (SPR) systems [SB89]. For non-SPR systems, averaging theory proves that the adaptation gains must be sufficiently small to ensure stability [RK85, Bod88b]. Therefore, AFC reduces the table look-up burden for variable disturbance frequencies based on external models than internal models so that the stabilizing feedback control does not require redesign for different speeds in rotor applications.

AFC algorithms are proven to be equivalent to a LTI system with an oscillator internal model [MB95, GB10], so the AFC convergence and the feedback system stability are

equivalent. The AFC convergence rate for specific frequencies can be analyzed by the LTI frequency response of transfer functions at those frequencies as shown in [BSK94]. Modified adaptive algorithms with an extra phase advance are proposed in [MB95] to increase the algorithm's convergence. Despite AFC developments for SISO AFC, its stability is not investigated extensively in the literature for MIMO systems. Consequently, to ensure closed-loop stability, adaptation gains are usually selected significantly small to overcome the effects of multi-variable coupling and the frequency-dependent gain and phase variations. However, this often results in a slow rate of convergence and possible instability.

This chapter provides some insights based on complex variable analysis of the gradient-based AFC (GAFC), in contrast to the coordinate transformation method in most other derivations. It will show by frequency domain analysis that the gradient is the Hermitian. For delay, the gradient advances the delay in the time domain and thus can be easily absorbed in the sinusoidal regressor signals. Then by establishing and using the LTI equivalence to the AFC, this chapter will analyze and show that the GAFC for pure delay systems has salient features of uniform convergence rate for different and multiple frequencies for a fixed AFC gain. Then a new AFC method will be proposed by compensating the MIMO plant to follow a reference model that is essentially a decoupled delay system.

## 5.1 Preliminaries on Feedforward Disturbance Rejection

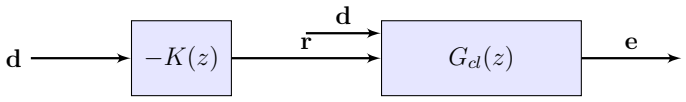


**Figure 5.1:** Feedforward input disturbance rejection scheme.

In this subsection we review some fundamental ideas on feedforward disturbance rejection (FDR) scheme that will be used later in this paper. First, consider the block diagram in Figure 5.1. There, $G_{cl}(z) = \begin{bmatrix} G_d(z) & G(z) \end{bmatrix}$ is a stable LTI system, and, the disturbance $\mathbf{d}$ is considered to be formed by a combination of sinusoidal signals with various frequencies. If the original plant system is unstable, it is assumed that it can be stabilized by LTI feedback

control.

To begin with, we describe a control scheme for FDR in which $\mathbf{d}$ is available for measurement. With the assumption that $\omega_k$ are a priori known. the natural control goal is to synthesize the stable feedforward filter K, such that frequency response of the LTI system $G_d - GK$ is zero at $\omega_k$. Using the block diagram in Figure:

$$\mathbf{e}(t) = \big(G_d(z) - G(z)K(z)\big)\mathbf{d}(t) \tag{5.1}$$

It is obvious to see that for the ideal case, $G$ is SISO minimum phase with relative degree 0, the best choice is to pick $K = \hat{G}^{-1}\hat{G}_d$, where $\hat{G}$ and $\hat{G}_d$ are estimates for the system plant $G$ and $G_d$. However, for the system with unstable zeros, two design choices are possible to obtain $K$ by directly minimizing some system norm of $\hat{G}_d - \hat{G}K$, or indirectly finding $\hat{G}^{-1}$ by solving a model-matching problem as in [Tsa94]. As illustrated, finding $K$ requires having the exact knowledge about the transfer function from disturbance to the output, which may not be known exactly for many applications.

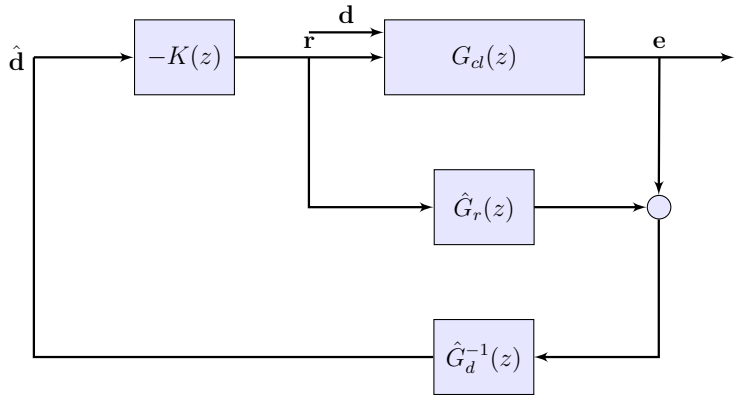


**Figure 5.2:** Estimation of $\mathbf{d}$ and FDR scheme.

The block diagram in Figure 5.1 assumes that the signal disturbance $\mathbf{d}$ is available for the measurement. However, in practice $\mathbf{d}$ has to be estimated online according the diagram in Figure 5.2, where $\hat{\mathbf{d}}$ is an estimate of $\mathbf{d}$. Clearly, when the estimation scheme shown in Figure is employed, the FDR filter $K$ becomes part of a LTI feedback controller $\nu$. Then, the closed-loop system will be stable for stable plants $G_{cl}$ and $K$ if the model $\hat{G}_{cl}$ is an exact

representation of the true plant $G_{cl}$. Otherwise, computing the LTI feedback controller $\nu$ as:

$$\nu = \frac{-K\hat{G}_d^{-1}}{1 - K\hat{G}_d^{-1}\hat{G}} \tag{5.2}$$

the small gain theorem implies a sufficient stability condition for asymptotically stability as

$$\|1 - G\nu\|_\infty < 1 \tag{5.3}$$

## 5.2 Adaptive Feedforward Compensation

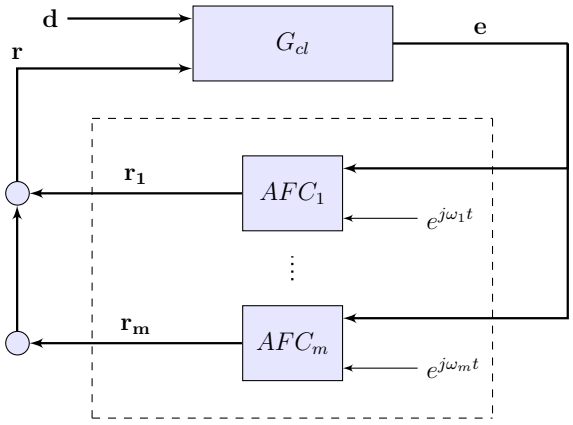


**Figure 5.3:** Block diagram of the adaptive feedforward controller with sinusoidal regressors

The adaptive feedforward control (AFC) problem in this chapter is based on the MIMO plant $G_{cl} = \begin{bmatrix} G_d & G \end{bmatrix}$, where $\mathbf{r}$ is the AFC command, $\mathbf{e}$ is the measured output vector, and $\mathbf{d}$ is the disturbance. Both $G_d$ and $G$ are assumed to be stable and square, $n \times n$, where $n$ denotes the size of $\mathbf{e}$. The purpose of the AFC presented in this paper is to minimize the output vector $\mathbf{e}$ in the presence of disturbance $\mathbf{d}$. The disturbance $\mathbf{d}$ is considered to be a complex exponential signal in the form:

$$\mathbf{d}(t) = \sum_{k=1}^{m} \mathbf{c_k}(t) e^{j\omega_k t} \tag{5.4}$$

where $t$ is continuous-time variable or discrete sample number $t = (0, 1, 2, ...)$, $\omega_k = \bar{\omega}_k T_s$, $\omega_k$ or $\bar{\omega}_k$ are disturbance frequencies, $T_s$ is the sampling time, and $\mathbf{c_k}$ are $n \times 1$ complex gain

vectors. To cancel the disturbance signal, the AFC command is also defined to be a complex exponential signal in the form:

$$\mathbf{r}(t) = \sum_{k=1}^{m} \mathbf{r_k}(t) = \sum_{k=1}^{m} \Gamma_k \mathbf{q_k}(t) e^{j\omega_k t} \tag{5.5}$$

where $\Gamma_k \in \mathcal{C}^{n\times n}$ are the regressor gains, and $\mathbf{q_k} \in \mathcal{C}^{n\times 1}$ are unknown arrays, which the adaptive algorithm attempts to identify. The block diagram in Figure 5.3 shows the AFC inside the dashed box, where a bank of adaptive controllers $AFC_k$ runs in parallel to target distinct disturbance frequencies. The AFC algorithm updates the unknown arrays by the feedback of the filtered signal $\mathbf{e}$ like an integral action:

$$\delta\mathbf{q_k}(t) = -(\mu\Phi_k e^{-j\omega_k t})\mathbf{e}(t) \tag{5.6}$$

Here, $\delta\mathbf{q_k}$ is the forward or backward different for the discrete-time or is the time derivative for the continuous-time cases, $\mu$ is a positive real number, and $\Phi_k$ are constant complex adaptation matrix gains, which specifies the degree of convergence for the AFC given the closed-loop stability of the adaptive system. The gain and phase comepnsations on $e^{j\omega_k t}$ by the complex gain $\Phi_k$ may be realized by LTI filters, which is the Filtered-X method [Bay00]. It should be noted that the AFC input $\mathbf{e}$ and output $\mathbf{r}$ may be compensated by filters, which are different from the filtering involved in the Filtered-X scheme.

The quadratic performance index used in this paper is:

$$\mathbf{J}(t) = \frac{1}{2}\mathbf{e}(t)^H\mathbf{e}(t) \tag{5.7}$$

The AFC intends to guarantee that the infinitesimal change in the performance index $\delta\mathbf{J}$ will remain non-positive. In order to find appropriate updates for the unknown coefficients in the regressor signal, first we need to find how infinitesimal changes in the coefficients change the performance index. To find $\delta\mathbf{q}$, first we need to find the complex gradient of the performance index $\mathbf{J}$ with respect to $\mathbf{q_k}$.

**Definition 1**. For a column vector $q = \begin{bmatrix} q^1 & q^2 & \cdots & q^n \end{bmatrix}^T$ where $q^l \in \mathbb{C}$, $l \in \{1, 2, ..., n\}$, the complex gradient operator is defined as

$$\nabla_q = \begin{bmatrix} \partial/\partial q^1 & \partial/\partial q^2 & \cdots & \partial/\partial q^n \end{bmatrix}^T \tag{5.8}$$

**Corollary 1**. *Given the complex gradient operator in* (5.8)*, and using* $\partial q^j/\partial q^l = \partial q^j/\partial q^{*l} = 0$ *for* $j \neq l$ *and* $\partial q^l/\partial q^l = 1$, $\partial q^l/\partial q^{*l} = 0$,

$$\begin{aligned} \nabla_{q^*} V^* q^* &= V^H \qquad \nabla_{q^*} q^H V^H = V^H \\ \nabla_{q^*} V q &= 0 \qquad\quad \nabla_{q^*} q^T V^T = 0 \end{aligned} \tag{5.9}$$

*where* $V$ *is a complex matrix with the appropriate dimension.*

**Assumption 1**. The output $\mathbf{e}$ has the following form in the steady states:

$$\mathbf{e}(t) = \sum_{k=1}^{m} \mathcal{G}_k \Gamma_k e^{j\omega_k t} \mathbf{q_k}(t) + \sum_{k=1}^{m} \mathcal{D}_k e^{j\omega_k t} \mathbf{c_k}(t) \tag{5.10}$$

where $\mathcal{G}_k = G(e^{j\omega_k}), \mathcal{D}_k = G_d(e^{j\omega_k})$ or $\mathcal{G}_k = G(j\omega_k), \mathcal{D}_k = G_d(j\omega_k)$ for discrete-time continuous-time cases respectively.

**Theorem 1**. [Bra83] *The complex gradient of the performance index* $\mathbf{J}$ *with respect to the complex coefficient* $\mathbf{q_k}$ *in the steady-states has the form*:

$$\nabla_{\mathbf{q_k}(t)} \mathbf{J}(t) = \frac{1}{2} \Gamma_k^T \mathcal{G}_k^T e^{j\omega_k t} \mathbf{e}^*(t) \tag{5.11}$$

**Proof** : Using results in [Bra83], $\nabla_{\mathbf{q_k}} \mathbf{J}$ can be simplified as following:

$$\nabla_{\mathbf{q_k}(t)} \mathbf{J}(t) = \frac{1}{2} (\nabla_{\mathbf{q_k}(t)} \mathbf{e}(t)) \mathbf{e}^*(t) \tag{5.12}$$

then, (5.10) can be used to find $\nabla_{\mathbf{q_k}} \mathbf{e}$:

$$\nabla_{\mathbf{q_k}(t)} \mathbf{e}(t) = \Gamma_k^T \mathcal{G}_k^T e^{j\omega_k t} \tag{5.13}$$

The result follows by substituting (5.13) in (5.12).

Furthermore, applying the results in [Bra83], the first order Taylor expansion of $\mathbf{J}$ can be obtained using the complex gradient of the performance index with respect to the unknown coefficients.

$$\begin{aligned} \delta \mathbf{J}(t) &= \sum_{k=1}^{m} (\nabla_{\mathbf{q_k}(t)} \mathbf{J}(t))^T \delta \mathbf{q_k}(t) + \sum_{k=1}^{m} (\nabla_{\mathbf{q_k}^*(t)} \mathbf{J}(t))^T \delta \mathbf{q_k}^*(t) \\ &= 2Re[\sum_{k=1}^{m} (\nabla_{\mathbf{q_k}(t)} \mathbf{J}(t))^T \delta \mathbf{q_k}(t)] \\ &= 2Re[\sum_{k=1}^{m} (\nabla_{\mathbf{q_k}(t)^*} \mathbf{J}(t))^H \delta \mathbf{q_k}(t)] \end{aligned} \tag{5.14}$$

**Remark 1**. It is important to remark that we have used $\nabla_{\mathbf{q_k}^*}\mathbf{J} = (\nabla_{\mathbf{q_k}}\mathbf{J})^*$.

**Theorem 2**. *The steady state quadratic performance index* $\mathbf{J}$*, given the adaptive update in* (5.6)*, is a non-increasing function of time if and only if*:

$$\sum_{k=1}^{m} \mathcal{G}_k \Gamma_k \Phi_k + \sum_{k=1}^{m} (\mathcal{G}_k \Gamma_k \Phi_k)^H > 0 \tag{5.15}$$

**Proof**: Substituting (5.6) in (5.14), the infinitesimal change in $\mathbf{J}$ is negative in the steady states if and only if

$$\mathrm{Re}(\mathbf{e}^H (\sum_{k=1}^{m} \mathcal{G}_k \Gamma_k \Phi_k)\mathbf{e}) > 0 \tag{5.16}$$

This can be also expanded to:

$$\mathbf{e}^H (\sum_{k=1}^{m} \mathcal{G}_k \Gamma_k \Phi_k)\mathbf{e} + \mathbf{e}^H (\sum_{k=1}^{m} \mathcal{G}_k \Gamma_k \Phi_k)^H \mathbf{e} > 0 \tag{5.17}$$

which is equivalent to (5.15).

**Remark 2**. It is important to note that the necessary and sufficient condition the previous theorem is for the steady state response, and it does not ensure the stability of adaptive system.

## 5.3 Stability Analysis of MIMO AFC

AFC convergence and stability analyses have been conventionally performed by averaging method [RK85] or the LTI equivalence and analysis via transformation of real sinusoidal signals [BSK94]. In the next lemma, we will use the complex exponential representations to re-derive the well established results on the AFC's LTI equivalence in a much simpler and straightforward way.

**Lemma 1**. *Let the complex signal* $\mathbf{r}$ *be defined as in* (5.5)*, then the mapping from* $\mathbf{e}$ *to* $\mathbf{r}$ *is exactly the LTI operator* $K$*,*

$$K_{forward} = -\mu \sum_{k=1}^{m} \frac{\Gamma_k \Phi_k e^{j\omega_k}}{z - e^{j\omega_k}} \tag{5.18}$$

$$K_{backward} = -\mu \sum_{k=1}^{m} \frac{\Gamma_k \Phi_k z}{z - e^{j\omega_k}} \tag{5.19}$$

$$K_{forward} = -\mu \sum_{k=1}^{m} \frac{\Gamma_k \Phi_k}{s - j\omega_k} \tag{5.20}$$

**Proof** : The case of forward difference is shown here. The continuous-time and backward difference cases are omitted since the derivations are similar. With the use of adaptive update for unknown arrays in (5.5), the complex regressor signal for one step forward can be simplified to:

$$\begin{aligned} \mathbf{r}(t+1) &= \sum_{k=1}^{m} \mathbf{r_k}(t+1) \\ &= \sum_{k=1}^{m} \Gamma_k \delta \mathbf{q_k}(t) e^{j\omega_k(t+1)} + \sum_{k=1}^{m} \Gamma_k \mathbf{q_k}(t) e^{j\omega_k(t+1)} \end{aligned} \tag{5.21}$$

Then, using 5.5,

$$\mathbf{r_k}(t+1) = \Gamma_k \delta \mathbf{q_k}(t) e^{j\omega_k(t+1)} + \mathbf{r_k}(t) e^{j\omega_k} \tag{5.22}$$

Substituting (5.6) in (5.22), and taking the z transform,

$$z\mathbf{R_k}(z) = -\Gamma_k \Phi_k e^{j\omega_k} \mathbf{E}(z) + \mathbf{R_k}(z) e^{j\omega_k} \tag{5.23}$$

gives the desired expression (5.18). For the Filtered-X scheme, $\Phi_k$ is the frequency response of the filter, assuming the regressor filtering has reached steady state response before activating the adaptive system.

**Lemma 1**. predicts precisely the stability/ instability boundary of the adaptive system. By the Internal Model Principle [FW76], the asymptotic stability and convergence of the AFC as an LTI controller is equivalent to asymptotic regulation of the output signal **e**. The necessary and sufficient stability condition for the MIMO feedback system with AFC as an LTI controller is each of the transfer functions from **d** to **r**, $(I - KG)^{-1}KG_d$, and from **d** to **e**, $(I - GK)^{-1}G_d$ to be stable. In particular, if no unstable pole-zero cancellation exists between $G$, and $K$, the stability of MIMO AFC will be determined by finding roots of the following characteristic equation:

$$det(I - KG) = det(I - GK) = 0 \tag{5.24}$$

Since $G$ is stable, the above equality holds if $G$ does not have zeros at $e^{j\omega_k}$. The conventional AFC results for SISO systems based on small adaptation gains are readily obvious. The stability analyses include root locus analysis of the loop gain $L = GK$ at $z = e^{j\omega_k}$ [Bay00, RRT20] or the averaging analysis [Bod88a], which yields identical results. In the next theorem, the AFC's stability is revisited again in the complex domain.

**Theorem 3** (**MIMO AFC**). *Consider the adaptive system* (5.6) *with regressor* (5.5) *for a square MIMO stable LTI plant $G$, where $\mathcal{G}_k$ is non-singular or $det(\mathcal{G}_k) \neq 0$. Then, there exists $\gamma > \mu$ such that the MIMO multi-frequency AFC is asymptotically stable if and only if:*

$$\mathrm{Re}(\lambda_{k,l}) > 0, (l = 1, 2, \ldots, n) \tag{5.25}$$

*where $\lambda_{k,l} \in \lambda(\mathcal{G}_k\Gamma_k\Phi_k)$, and $\lambda$ yields all eigenvalues of the complex matrix.*

**Proof** : The case of forward difference is shown here. The continuous-time and backward difference cases are not presented since the derivations are similar. With the assumption that $\mathcal{G}_k$ is non-singular, stability of $(I_n - GK)^{-1}$ gives the sufficient and necessary condition for the MIMO adaptive system's asymptotic stability, which is determined by obtaining the roots of the characteristic equation

$$det(I_n - GK) = det(I_n - \mu G \sum_{k=1}^{m} \frac{\Gamma_k\Phi_k e^{j\omega_k}}{z - e^{j\omega_k}}) = 0 \tag{5.26}$$

Since the closed-loop poles are continuous function of $\mu$, they are near the poles of $GK$ for $\mu \approx 0$. These closed-loop poles have two groups. The first group of poles emerges from the stable poles of $G$ and has a upper bound $\gamma_G > 0$, such that the poles are stable for $0 < \mu < \gamma_G$. The other group emerge from the poles of $K$, which are on the stability boundary. The closed-loop poles of this latter group are determined as follows:

For $\mu \approx 0$, and the specific pole of the second group near $\bar{z}_k = e^{j\omega_k}$, the closed-loop pole may be determined from the roots of the following:

$$det((\bar{z}_k - e^{j\omega_k})I_n - \mu e^{j\omega_k}\lambda(\mathcal{G}_k\Gamma_k\Phi_k)) = 0 \tag{5.27}$$

which can be further simplified to:

$$\bar{z}_k = e^{j\omega_k}(1 - \mu\lambda_{k,l}) \tag{5.28}$$

By continuity of pole locations with respect to the global gain, there exists $0 < \gamma < \gamma_G$ such that, for $0 < \mu < \gamma$ the adaptive system is stable if and only if (5.25) holds.

**Corollary 2** (**SISO AFC**). *Consider the adaptive system* (5.6) *with regressor* (5.5) *for a SISO stable LTI plant G, where* $\mathcal{G}_k \neq 0$. *Then, the necessary condition for the closed-loop stability is*

$$\mathrm{Re}(\mathcal{G}_k \Gamma_k \Phi_k) > 0 \tag{5.29}$$

**Remark 3**. The asymptotic stability of AFC system ensures that the performance index is monotonically decreasing in steady states for SISO plants; however, this is not true for MIMO ones.

**Theorem 3** for the MIMO AFC is an original result. The corollary for the SISO case is consistent with the well known SISO AFC stability conditions derived by the averaging method [Bod88a] or from the root-loci analyses of the real signal based LTI equivalence [Bay00, RRT20]. While these stability conditions for SISO AFCs are quite straightforward, they are not quite so for the MIMO case. The selection of the matrix $\Phi_k$ to satisfy (5.25) is not obvious. Furthermore, it is desirable to optimize the convergence rate besides establishing the stability and asymptotic convergence. Toward more transparent stability conditions and convergence rate for MIMO systems, next section proposes a gradient based AFC (GAFC) for the steepest decent of quadratic objective functions, and inversion based AFC (IAFC) as a special case of GAFC with unique features in the convergence rate of multiple frequencies. To the best of our knowledge, there exists SISO GAFC [Bay00] in the Filtered-X form. All derivations and analyses of the MIMO GAFC and SISO/MIMO IAFC facilitated by the complex exponential signal representations are original.

## 5.4 Gradient-Based AFC

The exact LTI form in the previous section enables the design and analysis of the AFC using standard LTI theory in contrast with the most other adaptive control designs involving nonlinear and/ or time varying behavior.

**Theorem 3** suggests that the complex gains $\Gamma_k$ and $\Phi_k$ must be designed to compensate for the phase within $\pm\pi/2$ for the frequency $\omega_k$ given a SISO plant. However, the designs of $\Gamma_k$ and $\Phi_k$ involve considerable complexities for MIMO AFC systems since regressor and adaptation gains are complex matrices. To overcome the difficulties in tuning regressor and adaptation gains, we propose the gradient-based AFC (GAFC) which ensures the performance index to be monotonically decreasing in steady states given the closed-loop stability.

From (5.15), it seems obvious that the performance index will be a monotonically decreasing function if:

$$\Gamma_k \Phi_k = \mathcal{G}_k^H \tag{5.30}$$

Furthermore, since $\mathcal{G}_k \mathcal{G}_k^H$ is a positive definite matrix, the MIMO GAFC is asymptotically stable given sufficiently small $\mu$. However, since only the plant model $\hat{G}$ is available for the computation, eigenvalues of $\mathcal{G}_k \hat{\mathcal{G}}_k^H$ should be positive-real for asymptotic stability of MIMO GAFC, where $\hat{\mathcal{G}}_k = \hat{G}(e^{j\omega_k})$ or $\hat{\mathcal{G}}_k = \hat{G}(j\omega_k)$ in discrete-time or continuous-time respectively. In contrast, **Corollary** 2 shows that the stability of SISO GAFC is ensured given the sufficiently small adaptation gain $\mu$ and,

$$|\theta_k| < 90 \tag{5.31}$$

where $\theta_k$ is the phase uncertainty at $\omega_k$.

To realize the MIMO GAFC, two obvious solutions can be proposed to make $\delta \mathbf{J}(t) < 0$, including $\Gamma_k = \hat{\mathcal{G}}_k^H$ and $\Phi_k = I_n$, or $\Gamma_k = I_n$ and $\Phi_k = \hat{\mathcal{G}}_k^H$.

Both proposed solutions for MIMO GAFC can be realized by multiplying the complex matrix with the complex exponential signal. However, the second solution can be also realized by applying the filter $G^T$ element-wise on the complex exponential signal to render the steady state response. Of course, $G^T = G$ for the SISO GAFC is a well-established result [MB95, GB10]. This will be explained in more details in Section 6.2.

**Remark 4**. Instead of minimizing the norm of measured output $\mathbf{e}$, some applications may require minimizing the norm of $\mathbf{e}$ filtered by a frequency weighing filer $F_L$. The adaptive

update will have the following form:

$$\delta \mathbf{q_k}(t) = -(\mu \hat{\mathcal{G}}_k^H F_L (e^{j\omega_k})^H e^{-j\omega_k t}) \mathbf{e_f}(t) \tag{5.32}$$

where $\mathbf{e_f}$ is the output of weighting filter.

The GAFC design is shown to be efficient in comparison with the original AFC since only a positive scalar number needs to be tuned for both SISO and MIMO cases. Furthermore, its stability for MIMO GAFC systems can be confirmed by incorporating the accurate plant model in the adaptive update. However, like the original AFC, fast convergence of the algorithm requires considerable tuning exercises specially for multiple-frequency cancellations and MIMO systems since the optimal gains cannot be obtained analytically. The slow and non-uniform convergence can also hugely decrease the performance of GAFC for time-varying frequency cases, which makes the knowledge of the optimal gains vital. Next corollary gives a condition in which the GAFC design synthesis has uniform convergence for different frequencies.

**Corollary 3**. *Consider the GAFC for a square MIMO stable LTI plant $G$, where $\mathcal{G}_k$ is non-singular. Assume $G = \hat{G}$. Then, there exists $\gamma > \mu$ such that the MIMO multi-frequency GAFC converges uniformly if and only if:*

$$\sigma_{k,l} = constant, (l = 1, 2, \ldots, n) \tag{5.33}$$

*where $\sigma_{k,l} \in \sigma(\mathcal{G}_k)$, and $\sigma$ yields all singular values of the complex matrix.*

**Proof** : Using results in **Theorem 3**, for $\mu \approx 0$, the closed-loop pole emerging from poles of $K$ near $\bar{z}_k = e^{j\omega_k}$ can be obtained by:

$$\bar{z}_k = e^{j\omega_k}(1 - \mu\lambda(\mathcal{G}_k \mathcal{G}_k^H)) \tag{5.34}$$

This can be further simplified to:

$$\bar{z}_k = e^{j\omega_k}(1 - \mu\sigma_{k,l}^2) \tag{5.35}$$

, and subsequently $|\bar{z}_k| = |1 - \mu\sigma_{k,l}^2|$. By continuity of pole locations with respect to the global gain, there exists $0 < \mu < \gamma$ such that the closed-loop poles near $\bar{z}_k = e^{j\omega_k}$ for

$(k = 1, 2, \ldots, m)$ move to the origin with the rate, i.e, $\frac{d|\bar{z}_k|}{d\mu} = -\sigma_{k,l}^2$. Consequently, the adaptive system will converge uniformly if and only if (5.33) holds.

**Corollary 3** shows if there is no mismatch between plant and its model, and it has constant and identical singular values at each targeted frequency, a single sufficiently small adaptation gain will result into the uniform convergence rate for all unknown coefficients in the GAFC independent of number of frequencies and their values.

## 5.5 Proposed Inversion-Based AFC

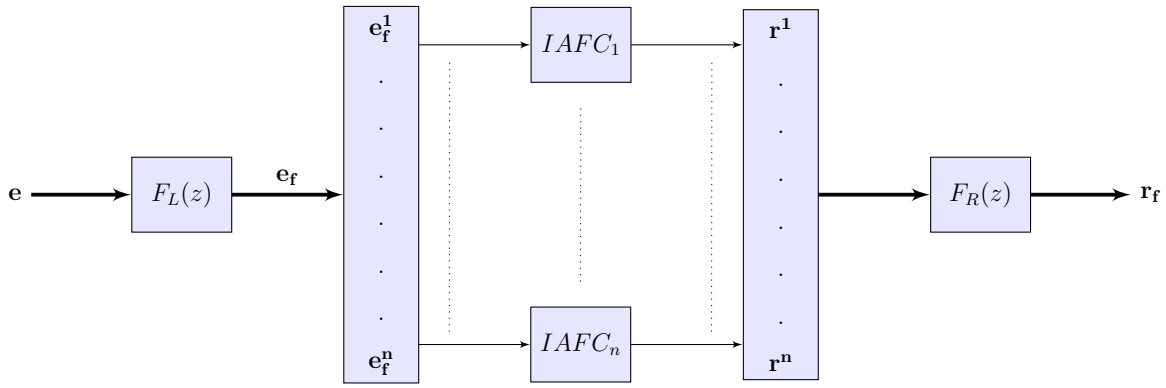


**Figure 5.4:** Block diagram of the proposed IAFC

To utilize the uniform convergence property discussed in **Corollary 3**, a feedforward filter $F_R$, which filters the AFC control command $\mathbf{r}$ and generates the control input $\mathbf{r_f}$ taken by the closed-loop system $G$, is proposed in discrete-time domain. The proposed filter is designed by solving the plant inversion problem. Exact inversion is often impossible for non-minimum phase or strictly proper systems; hence, $H_2$ or $H_\infty$ model matching can be applied to find $F_R(z)$:

$$F_R(z) = \underset{F_R(z) \in RH_\infty}{\arg\min} \|M(z)I_n - G(z)F_R(z)\|_{(\infty,2)} \tag{5.36}$$

where the reference model $M$ is any proper or strictly-proper SISO stable filter with unity gain, i.e, $|M(z)|_{z=e^{j\omega}} = 1$. The most obvious choice for the reference model is $M = 1$. However, in applications like unbalance compensation, the all-band inverse filter obtained

from the optimization problem in (5.36) may create high-gain feedforward inputs at the high frequency range because of the low-pass nature of the controlled plant $G$. This may lead to the current saturation at high rotational speeds. To address this issue, the plant inversion problem is revised as

$$F_R(z) = \underset{F_R(z)\in RH_\infty}{\arg\min} \|M(z)z^{-d}I_n - \hat{G}(z)F_R(z)\|_{(\infty,2)} \tag{5.37}$$

where $M$ is a improper zero-phase low-pass filter; $M(z)_{z=e^{j\omega}}$ equals to one at low frequencies, which is higher than the maximum frequency for cancellation, and approximates 0 at the frequencies beyond its bandwidth. Furthermore, since the improper filter $M$ in (5.36) results in a improper filter $F_R$, the delay operator is cascaded with $M$. The delay length $d$ is selected such that $Mz^{-d}$ be proper or strictly proper, so the resulting filter $F_R$ will be implementable.

**Remark 5**. The zero-phase low-pass filter $M$ may be created by $M(z) = N(z)N(z^{-1})$, where $N(z)$ is an FIR low-pass filter. The bandwidth of $N$ is selected based on the disturbance bandwidth.

**Definition 2**. For the plant inversion problem in (5.37), the error transfer function is defined as:

$$E(z) = M(z)z^{-d}I_n - G(z)F_R(z) \tag{5.38}$$

With the feedforward filter $F_R$, the adaptive algorithm sees the closed-loop plant $G$ cascaded with $F_R$ from right which can be treated as the virtual plant in the adaptive algorithm. Furthermore, increasing the delay length in (5.37) decreases $\|E\|_\infty$ allowing the virtual plant observed by the adaptive algorithm to be approximated as $Mz^{-d}I_n$ [Tsa94], which can be utilized in the gradient-based framework. In this case, both regressor and adaptation gains should be selected such that:

$$\Gamma_k\Phi_k = e^{j\omega_k d}I_n \tag{5.39}$$

Here, we use the fact that $M(e^{j\omega_k}) = 1$. The next corollary states the necessary and sufficient condition such that the proposed MIMO IAFC is asymptotically stable.

**Corollary 4** (**MIMO IAFC**). *Consider the IAFC for a square MIMO stable LTI plant $G$, where $\mathcal{G}_k$ is non-singular or* $\det(\mathcal{G}_k) \neq 0$. *Then, there exists $\gamma > \mu$ such that the MIMO*

*multi-frequency IAFC is asymptotically stable if and only if:*

$$|\bar{\lambda}_{k,l}| \cos(\omega_k d + \angle\bar{\lambda}_{k,l}) < 1, l(= 1, 2, \ldots, n) \tag{5.40}$$

*where* $\bar{\lambda}_{k,l} \in \lambda(\mathcal{E}_k)$.

**Proof** : Extending the results in **Theorem 3**, asymptotic stability of MIMO IAFC is ensured with sufficiently small choice of $\mu$ if and only if:

$$\mathrm{Re}(\lambda(I_n - \mathcal{E}_k e^{j\omega_k d})) > 0 \tag{5.41}$$

where $\mathcal{E}_k = E(e^{j\omega_k d})$. This can be further simplified to:

$$\mathrm{Re}(1 - e^{j\omega_k d}\bar{\lambda}_{k,l}) > 0 \tag{5.42}$$

which yields the result in (5.40).

**Remark 6**. Since $\lambda(\mathcal{E}_k) \leq \sigma_{max}(\mathcal{E}_k)$, $||E||_\infty < 1$ ensures the closed-loop stability of MIMO IAFC in rejecting multiple time-varying frequencies.

The MIMO IAFC can be realized by $\Gamma_k = e^{j\omega_k d_1} I_n$ and $\Phi_k = e^{j\omega_k d_2} I_n$, where $d = d_1 + d_2$. It is obvious to notice that the proposed IAFC simplifies the implementation in comparison with the GAFC for MIMO plants by decoupling the adaptive algorithm into a bank of SISO independent algorithms. This is also shown in Figure 5.4 where $IAFC_l$ $l(= 1, 2, \ldots, n)$ representing the following SISO LTI equations:

$$\begin{aligned} \delta\mathbf{q_k^l}(t) &= -(\mu e^{-j\omega_k(t-d_2)})\mathbf{e^l}(t) \\ \mathbf{r^l}(t) &= \sum_{k=1}^{m} \mathbf{q_k^l}(t) e^{j\omega_k(t+d_1)} \end{aligned} \tag{5.43}$$

## 5.6 Convergence Analysis of MIMO IAFC

The asymptotic stability conditions derived for MIMO AFCs are based on sufficiently small choice for $\mu$. Besides establishing the stability, it is desirable to optimize the convergence rate. In general, the convergence rate of adaptive algorithms is improved by choosing larger gains.

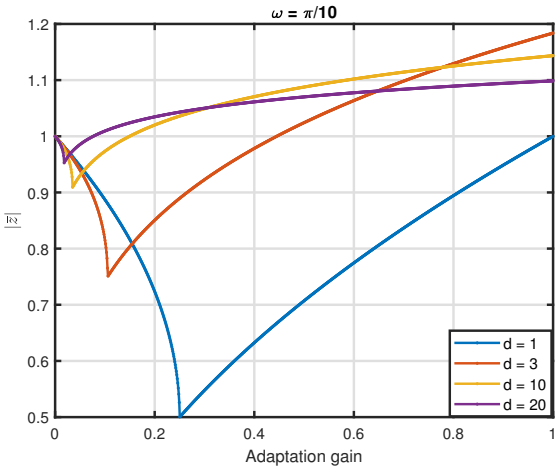


**Figure 5.5:** Dominant closed-loop pole magnitude for single complex frequency cancellation

However, LTI analysis shows that increasing the gains may push closed-loop poles into the unstable region, right half plane or outside of unite circle for continuous-time or discrete-time. Although GAFC provides a more transparent stability condition, the selection of optimal gains, which result in the quickest convergence of the adaptive system, may not be possible specially for multiple frequency cases. For the IAFC in contrast, a more uniform method may be used to approximate the allowable range and optimal value by simply assuming the ideal inversion from model-matching problem as illustrated for single frequency cancellation in Figure 5.5. Although this method can be generalized for different plants, the effect of number of frequency components and their corresponding values, and the delay length may not be obvious by simply obtaining dominant poles for various gain. The next theorem will provide an analytical framework for the MIMO single-frequency IAFC to obtain not only the maximum allowable gain $\bar{\mu}$ in which the stability is ensured, but also the optimal gain $\mu_o$ in which the adaptive system has the highest convergence rate.

**Remark 7**. For discrete-time LTI systems, the dominant pole is the furthest pole from the center of unit circle in the complex plane.

**Theorem 4**. *Consider the IAFC for a square MIMO stable LTI plant $G$ , where $\mathcal{G}_k$ is non-singular. Assume $E = 0$, or equivalently $M(z)z^{-d}I_n = G(z)F_R(z)$. Then, the following statements are true if $M(z) = 1$.*

(a) *The necessary and sufficient condition of the asymptotic stability for the MIMO single-frequency IAFC is:*

$$0 < \mu < \bar{\mu} = 2sin\big(\frac{\pi}{4d+2}\big) \tag{5.44}$$

(b)

$$\mu_o = \frac{d^d}{(d+1)^{d+1}} \tag{5.45}$$

$$p_o = \frac{d}{d+1} \tag{5.46}$$

*where $p_o$ refers to the dominant pole magnitude specifying the highest convergence rate.*

**Proof** : (a) Using (5.24), the stability of MIMO IAFC can be investigated by obtaining the roots of $det(I - GF_RK) = 0$ where $K$ has the following LTI form for the IAFC:

$$K = -\mu \frac{e^{j\omega_1(d+1)}}{z - e^{j\omega_1}} I_n \tag{5.47}$$

Then, the characteristic equation can be further simplified to:

$$det(I - GF_RK) = (1 + \mu \frac{e^{j\omega_1(d+1)} z^{-d}}{z - e^{j\omega_1}})^n = 0 \tag{5.48}$$

which can be further simplified to:

$$1 + \mu \frac{e^{j\omega_1(d+1)} z^{-d}}{z - e^{j\omega_1}} = 0 \tag{5.49}$$

Defining $\hat{z} = ze^{-j\omega_1}$, then,

$$1 + \mu \frac{\hat{z}^{-d}}{\hat{z} - 1} = 0 \tag{5.50}$$

The phase cross over frequency $\bar{\omega}_c$ in the new complex domain is found to be:

$$\bar{\omega}_c d + \frac{\bar{\omega}_c + \pi}{2} = \pi \tag{5.51}$$

the bound for $\mu$ is then obtained:

$$0 < \mu < \frac{1}{\frac{1}{|e^{j\bar{\omega}_c} - 1|}} \tag{5.52}$$

Simplifying above gives the results in (5.44).

(b) The problem of finding the optimal gain can be classified as a min-max problem, where it is desired to minimize the magnitude of dominant closed-loop pole by adjusting $\mu$. Performing the simple root-locus analysis for the characteristic equation in (5.50), it is obvious to see that the dominant pole with smallest magnitude $p_o$ will be on the real axis. Therefore, given $\mu_o$, (5.50) can be simplified to the following:

$$\hat{z} - 1 + \mu_o \hat{z}^{-d} = (\hat{z} - p_o)^2 g \tag{5.53}$$

where $g$ is a function of $\hat{z}$. Since derivative of (5.53) with respect to $\hat{z}$ is also equal to zero at $p_o$, both $p_o$ and $\mu_o$ are obtained by solving the system of equations:

$$\begin{aligned} d\mu_o p_o^{-d-1} &= 1 \\ p_o + \mu_o p_o^{-d} &= 1 \end{aligned} \tag{5.54}$$

which give the results in (5.45) and (5.46).

The gain's range in (5.44) solves the tuning complexity that exists in original AFC and GAFC designs. Furthermore, the optimal gain in (5.45) is proven to maximize the convergence rate of the adaptive system based on the assumption that $M = 1$. Both maximum allowable range and the optimal value are proven to be independent of frequency value in canceling single-tone complex exponential disturbances. For multiple frequencies, the critical and optimal gains can be obtained by numerically. In the next, we show a simple but useful approximation by the single frequency results when the frequencies are small.

**Remark 8**. For multiple frequency cancellation, the characteristic equation in (5.50) has the form:

$$1 + \mu \sum_{k=1}^{m} \frac{\hat{z}_k^{-d}}{\hat{z}_k - 1} = 0 \tag{5.55}$$

where $\hat{z}_k = ze^{-j\omega_k}$. With the assumption that all frequencies are small, i.e, $\hat{z} = \hat{z}_k$:

$$1 + \mu m \frac{\hat{z}^{-d}}{\hat{z} - 1} = 0 \tag{5.56}$$

Using (5.44), the following approximation can be made.

$$0 < \mu < \bar{\mu} = \frac{2sin(\frac{\pi}{4d+2})}{m} \tag{5.57}$$

| $d$ | $\mu_{max}$ | $\mu_{opt}$ | $\lvert p_{opt}\rvert$ |
|---|---|---|---|
| 1 | 1.000 | 0.250 | 0.500 |
| 3 | 0.445 | 0.101 | 0.750 |
| 10 | 0.149 | 0.035 | 0.909 |
| 20 | 0.0.077 | 0.018 | 0.952 |

**Table 5.1:** Design approximations for a single-tone IAFC.

Using small angle approximation, the gain's range in (5.57) can be further simplified given large values for the delay length, i.e, $d > 5$, $\bar{\mu} = \frac{\pi}{2dm+m}$.

Furthermore, the optimal gain and pole magnitude can be found by solving the following system of equation:

$$\begin{aligned} d\mu_o m p_o^{-d-1} &= 1 \\ p_o + \mu_o m p_o^{-d} &= 1 \end{aligned} \tag{5.58}$$

which gives the same optimal dominant pole magnitude as the single frequency, and the optimal gain as:

$$\mu_o = \frac{d^d}{m(d+1)^{d+1}} \tag{5.59}$$

It is clear to see that increasing the delay length for reducing the inversion error will decrease the maximum allowable range and the optimal value for the adaptation gain, and consequently reducing the potential highest convergence rate. This illustrates the trade-off between inversion error and convergence rate, which is also shown in Table 5.1.

**Corollary 5**. *Consider the IAFC for a square SISO LTI plant $G$ , where $\mathcal{G}_k$ is non-singular. Then, the necessary condition for the closed-loop stability is*

$$-\frac{\pi}{2} < \angle \mathcal{G}_k F_R(e^{j\omega_k}) e^{j\omega_k d} < \frac{\pi}{2} \tag{5.60}$$

**Proof** : The result can be obtained from **Corollary 2**.

## 5.7 Application to Time-Varying Frequency Disturbance Rejection

The uniform convergence property of the inversion based AFC also fits well in considering a class of problem where disturbance frequency is varying linearly. To reject the sinusoidal disturbance in (5.4) with $\omega_k(t) = \eta_k t$, the following inversion based adaptive update is utilized,

$$\delta\mathbf{q_k}(t) = -\mu e^{-j\eta_k t(t-d)}\mathbf{e}(t) \tag{5.61}$$

where $\eta_k$ is a constant one step frequency difference, and

$$\mathbf{r_k}(t) = \mathbf{q_k}(t)e^{j\eta_k t^2} \tag{5.62}$$

In this subsection we show that IAFC with the proposed adaptive is a linear-periodically-time-varying (LPTV) system. The notable property of LPTV controllers is that they can be represented with time-invariant dynamics by applying the Floquet-Lyapunov transformation, while the time-varying part is described by the static input or output gains. [VS94, BC00, BC09]. Introducing Fourier-series expansions of the periodically time-varying static input and output gains, the optimal LTI approximation of the LPTV controller can be obtained [TH15]. Thus, in order to find the optimal LTI form of the inversion based AFC, first we need to define some concepts to be used later.

**Definition 3**. For a SISO stable periodic system $H$ with the impulse response $h(.,.)$, and the period $T$, the Hilbert-Schmidt norm is defined as [CQ97]:

$$\|H\|_{HS} = \left(\frac{1}{T}\sum_{t=0}^{\infty}\sum_{l=0}^{T-1}|h(t,l)|_2^2\right)^{1/2} \tag{5.63}$$

The next results characterize the optimal approximate LTI operator that maps the measured output $\mathbf{e}$ to the complex signal $\mathbf{r_k}$ as defined in (5.62) by minimizing the squared Hilbert-Schmidt norm of the error between the LPTV operator $H_{k,LPTV}$ and its LTI approximation $H_{k,LTI}$.

$$K_{k,LTI} = \arg\min \|K_{k,LPTV} - K_{k,LTI}\|_{(HS)}^2 \tag{5.64}$$

**Theorem 5**. *Consider the IAFC with regressor in* (5.62)*, and the adaptive update in* (5.61) *for a stable plant* $G$*. Then we have the following.*

(a) *The IAFC is a parallel connection of LPTV controllers.*

(b) *The solution to the optimization problem in* (5.64) *is given by*

$$K_k(z) = -\frac{\mu\eta_k}{\pi} e^{j\eta_k(\frac{d}{2})^2} \sum_{l=-L}^{L} \frac{e^{j\eta_k l(d+2)}}{z - e^{j2\eta_k l}} \tag{5.65}$$

**Proof**. (a) It is sufficient to prove that the mapping from $\mathbf{e}$ to $\mathbf{r_k}$ is a LPTV operator. Extending results in (5.21), and applying $\bar{\omega}_k(t+1) = \eta_k t + \eta_k$:

$$\mathbf{r_k}(t+1) = \delta\mathbf{q_k}(t) e^{j\eta_k(t+1)^2} + \mathbf{q_k}(t) e^{j\eta_k(t+1)^2} \tag{5.66}$$

then, substituting (5.61) for $\delta\mathbf{q_k}(t)$ and factoring out $e^{j\eta_k(2t+1)}$ gives

$$\mathbf{r_k}(t+1) = e^{j\eta_k(2t+1)}(-\mu e^{j\eta_k td}\mathbf{e}(t) + \mathbf{r_k}(t)) \tag{5.67}$$

which its dynamic and input gain have a period of $\frac{\pi}{\eta_k}$ and $\frac{2\pi}{\eta_k(2+d)}$ respectively. Therefore, (5.67) is LPTV with $T_k = \frac{\pi}{\eta_k}$ if $d$ is even, or $T_k = \frac{2\pi}{\eta_k}$ if $d$ is odd.

**Proof**. (b) Applying the Floquet-Lyapunov transformation to the LPTV in (5.67):

$$\mathbf{x_k}(t+1) = \mathbf{x_k}(t) - \mu e^{j\eta_k t(d-t)}\mathbf{e}(t) \tag{5.68}$$

where $\mathbf{x_k}(t) = e^{-j\eta_k t^2}\mathbf{r_k}(t)$, the resulting LPTV has time-invariant dynamics. The time periodic static input gain in (5.68) can be expanded in terms of its frequency components by introducing the symmetric Fourier expansion

$$b_k(t) = \sum_{l=-L}^{L} \hat{b}_{kl} e^{\frac{j2\pi lt}{T_k}} \tag{5.69}$$

where $b_k(t) = e^{j\eta_k t(d-t)}$ and $\hat{b}_k$ is its Fourier transform, and $T_k = \frac{\pi}{\eta_k}$ if $d$ is even, or $T_k = \frac{2\pi}{\eta_k}$ if $d$ is odd.

Using the Fourier-series expansion, the mapping from $\mathbf{e}$ to $\mathbf{r_k}$ can be represented as a

LPTV system with the presence of time-varying part as a static output gain only [TH15]

$$\begin{aligned}\mathbf{s_{kl}}(t+1) &= e^{-\frac{j2\pi l}{T_k}}\mathbf{s_{kl}}(t) - \mu\hat{b}_{kl}\mathbf{e}(t)\\ \mathbf{r_{kl}}(t) &= c_k(t)e^{\frac{j2\pi l(t-1)}{T_k}}\mathbf{s_{kl}}(t)\\ \mathbf{r_k}(t) &= \sum_{l=-L}^{L}\mathbf{r_{kl}}(t)\end{aligned} \tag{5.70}$$

where $c_k(t) = e^{j\eta_k t^2}$, and $\mathbf{x_k}(t) = \sum_{l=-L}^{L} e^{\frac{j2\pi l(t-1)}{T_k}}\mathbf{s_{kl}}(t)$. The impulse response of (5.70) for $t > 0$, which describes $\mathbf{r_k}$ in terms of $\mathbf{e}$, is then given by

$$h_{k,LPTV}(t, T_k) = \sum_{l=-L}^{L} h_{kl,LPTV}(t, T) \tag{5.71}$$

$$h_{kl,LPTV}(t, T_k) = -\mu c_k(t)\hat{b}_{kl} \tag{5.72}$$

Given the decoupled LTI dynamic equation in, the optimization problem in (5.64) can be reformulated as

$$c_{kl} = \arg\min \sum_{t=1}^{\infty} |h_{kl,LPTV}(t) - h_{kl,LTI}(t)|_2^2 \tag{5.73}$$

where $c_{kl}$ is an optimal time-invariant scalar that can substitute the time-varying static output gain in (5.70), and

$$h_{kl,LTI}(t) = -\mu c_{kl}\hat{b}_{kl}e^{-\frac{j2\pi l(t-1)}{T_k}} \tag{5.74}$$

Using the periodicity of impulse responses and expanding the objective function in (5.73)

$$\begin{aligned}c_{kl} = \arg\min \mu^2\hat{b}_{kl}^*\hat{b}_{kl}\Bigg(&\sum_{t=1}^{T_k} c_k^*(t)c_k(t) - c_k^*(t)c_{kl}e^{-\frac{j2\pi l(t-1)}{T_k}}\\ &- c_k(t)c_{kl}^*e^{\frac{j2\pi l(t-1)}{T_k}} + c_{kl}^*c_{kl}\Bigg)\end{aligned} \tag{5.75}$$

, and applying the results in **Corollary 1**, $c_{kl}$ is solved by making the complex gradient of the objective function in (5.75) with respect to $c_{kl}^*$ equal to zero:

$$c_{kl} = \frac{1}{T_k}\sum_{t=0}^{T_k-1} c_k(t+1)e^{\frac{j2\pi lt}{T_k}} \tag{5.76}$$

Then, to find $c_{kl}\hat{b}_{kl}$, the convolution theorem can be applied for $\tilde{c}_k$ and $b_k(t)$, where $\tilde{c}_{kl}(t) = c_k(t+1)e^{\frac{j4\pi lt}{T_k}}$:

$$c_{kl}\hat{b}_{kl} = \frac{1}{T_k^2}\sum_{t=0}^{T_k-1}\tilde{c}_k(t) \circledast b_k(t)e^{-\frac{j2\pi lt}{T_k}} \tag{5.77}$$

, and

$$\begin{aligned}\tilde{c}_{kl}(t) \circledast b_k(t) &= \sum_{n=0}^{T_k-1} e^{j\eta_k(n+1)^2} e^{\frac{j4\pi ln}{T_k}} e^{j\eta_k(t-n)(d-t+n)} \\ &= e^{j\eta_k(td-t^2+1)}\sum_{n=0}^{T_k-1}\left(e^{j\eta_k(2t-d+2+\frac{4\pi l}{T_k\eta_k})}\right)^n \\ &= T_k e^{j\eta_k(td-t^2+1)}, \qquad t = \frac{d}{2}-1-\frac{2\pi l}{T_k\eta_k}\end{aligned} \tag{5.78}$$

Then, if $d$ is even,

$$\begin{aligned}c_{kl}\hat{b}_{kl} &= \frac{\eta_k}{\pi}e^{j\eta_k(td-t^2+1)}e^{-j2\eta_k lt}, \qquad t = \frac{d}{2}-1-2l \\ &= \frac{\eta_k}{\pi}e^{j\eta_k(\frac{d^2}{4}-ld-2l)}\end{aligned} \tag{5.79}$$

The result follows by substituting (5.79) into the z transform of (5.74).

## 5.8 Summary

By using complex exponential than the usual real sinuosidal signal representations and analyses, we have made transparent AFC stability analysis and added insights to the existing results in the literature:

- The LTI equivalence of the AFC is exact when the AFC involves frequency dependent complex gain compensations; therefore, LTI stability analysis may be applied to the seemingly nonlinear AFC.
- The LTI equivalence of the AFC is approximate when the AFC involves filtering on the regressors, i.e. Filtered-X implementation.
- AFC is stable with sufficiently small gains when it adapts in the greatest decent direction (GAFC), i.e. the Hermitian matrix of the plant's frequency response. For the Filtered-X implementation, the regressors would be filtered by the plant's transpose.

- Filtering of the error signal is equivalent to the left compensation of the plant dynamics and placing frequency weighting on the error's quadratic cost.

- Filtering of the AFC control signal is equivalent to the right compensation of the plant dynamics. By the delay inversion within the bandwidth of the disturbance frequency (IAFC), the gradient becomes simple phase compensation. For Filtered-X implementation, this is fixed time step shift and is finite step settling. Therefore, the IAFC, inheriting the GAFC, is stable for sufficiently small gains. Furthermore, the convergence rate is identical for all channels and frequencies for IAFC and the optimal gains (for minimizing the closed loop pole spectral radius) have been derived with respect to the number of the steps in the delay inversion.

# CHAPTER 6

# Automation Balancing in AMB Rotor-Systems

Periodic disturbances occur in various control engineering applications. For example, synchronous vibrations caused by mass unbalance are common problems in all rotating machinery, including AMBS. Unbalance occurs when the rotor's geometrical axis is not aligned with the inertia axis. The AMBS provides both the contact-less support for the rotor without any mechanical friction and the possibility of minimizing such vibrations by controlling the electromagnetic forces applied to the rotor. Furthermore, the AMBS's control objective is for the rotor to either spin about its inertial or geometrical center axis. The former is generally called automation balancing, the latter imbalance compensation [KCL15]. In either case, the control must suspend the rotor and suppress a periodic dynamic disturbance synchronized with the spindle rotation frequency and dominated by the sinusoidal waves of the first harmonic frequency.

The closed-loop plant with the stabilizing LQGi controller is illustrated in Figure 6.1 where $O_0(z)$ is a full-order Luenberger state observer, and $L_0$, $K_0$ and $K_i$ are state observer, state feedback and integrator gains with appropriate dimension. To analyze the dynamic response of an unbalance rotor, two factors should be considered, including the force disturbance $\mathbf{d_{in}}$ and measuring disturbance $\mathbf{d_{out}}$.

The radial unbalance force is due to the rotor's mass eccentricity leading to the rotor's synchronous vibration. In steady state, the unbalance force can be modeled as:

$$\mathbf{d_{in}}(t) = em\omega^2 sin(\omega t + \theta) \tag{6.1}$$

where $m$ is the rotor mass, $\omega$ in the spin frequency, $e$ is the distance between the rotating and mass mass center as shown in Figure 6.2. Furthermore, since the no-contact sensor measures

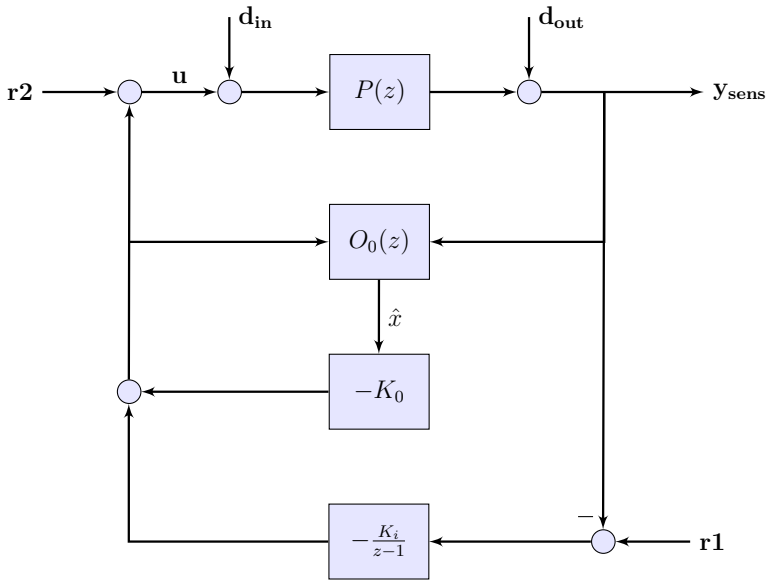


**Figure 6.1:** Block diagram of the proposed IAFC

the rotor's geometric center position, the output signal of the sensor can be denoted by $\mathbf{y_{sens}} = \mathbf{y} + \mathbf{d_{out}}$, and

$$\mathbf{d_{out}}(t) = e_0 sin(\omega t + \theta) \tag{6.2}$$

where $e_0$ is the geometric eccentricity which is the distance between the geometrical center and the mass center. The force disturbance and the measuring disturbance have the same frequency and simultaneously exist in the control loop.

## 6.1 Rotor Unbalance Control

Given the sufficient gap between the housing and the rotor, and under the closed-loop operation, the automation balancing makes the rotor spins about its inertial center; however, this requires obtaining the rotor mass center position. The rotor mass sensor position can be obtained by eliminating the measuring disturbance from $\mathbf{y_{sens}}$ which intuitively can be achieved by placing the notch filter to filter out the measuring disturbance from $\mathbf{y_{sens}}$. Under the closed-loop control of mass center position, the rotor inertial center position will gradually tend to be steady, and the mass and rotating centers will be aligned. Consequently, the

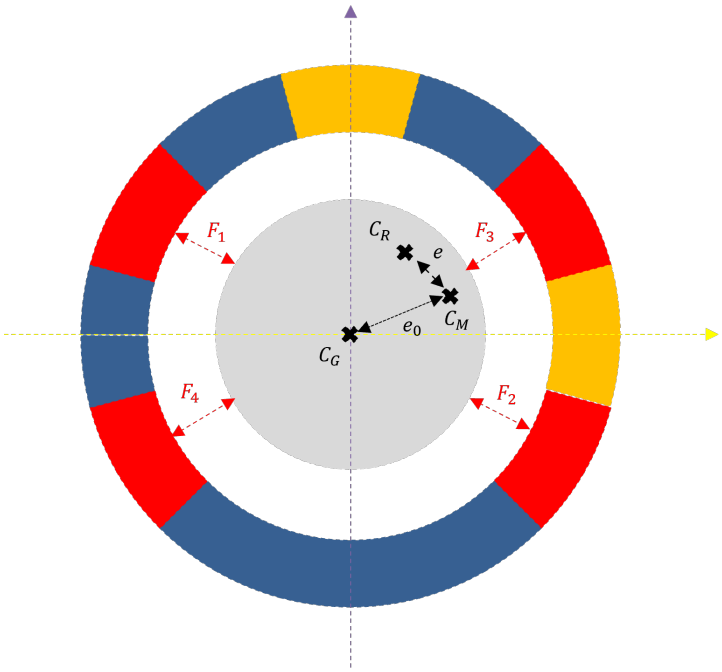


**Figure 6.2:** Unbalance planar rotor

force disturbance will vanish spontaneously.

For imbalance compensation, the rotor is forced to spin about its geometrical center. Since the rotor's position of geometrical center is requited, the measuring disturbance is not treated as a disturbance. The imbalance compensation is achieved by counteracting the force disturbance completely. Under the closed-loop control of the geometrical center, the rotor will gradually spin about its geometrical center once the disturbance force is counteracted. It is shown that imbalance compensation and automation balancing can be realized by minimizing displacement and current respectively [SZQ04].

The proposed IAFC in this dissertation can be used for automation balancing or imbalance compensation by minimizing the current $\mathbf{u}$ or the sensor measurement $\mathbf{y}_{\mathbf{sens}}$ respectively. It is obvious that minimizing the sensor measurement can lead to imbalance compensation. For automation balancing in contrast, minimizing the current reduces the electromagnetic forces from the AMB to the rotor, and essentially reduces the reaction vibration forces from the rotor to the housing which makes the disturbance force vanish. Furthermore, the proposed IAFC can realize the automation balancing, or the imbalance compensation, by the

different control junction junction positions as shown in Figure (6.1). Consequently, one of the four closed-loop transfer functions with inputs $[\mathbf{r1}, \mathbf{r2}]$ and outputs $[\mathbf{u}, \mathbf{y}]$ shall be used for the inversion design based on the junction position or the application. The closed-loop transfer functions have the following form:

$$\begin{bmatrix} G_{\mathbf{ur1}}(z) \\ G_{\mathbf{yr1}}(z) \end{bmatrix} = \left[\begin{array}{cc|c} A - BK_0 & -BK_i & 0 \\ -C & I_n & I_n \\ \hline -K_0 & -K_i & 0 \\ C & 0 & 0 \end{array}\right] \tag{6.3}$$

$$\begin{bmatrix} G_{\mathbf{ur2}}(z) \\ G_{\mathbf{yr2}}(z) \end{bmatrix} = \left[\begin{array}{ccc|c} A - BK_0 & -BK_i & BK_0 & B \\ -C & I_n & 0 & 0 \\ 0 & 0 & A - LC & B \\ \hline -K_0 & -K_i & K_0 & I_n \\ C & 0 & 0 & 0 \end{array}\right] \tag{6.4}$$

where the plant model has the state space representation $P_n(z) = (A, B, C, D)$.

## 6.2 AFC Application to Real Sine Wave Cancellations

Many applications, including rotary systems require considering the problem of rejecting real sinusoidal disturbances. However, real sine wave cancellations can be considered as a special type of complex exponential cancellation. Hence, the AFC formulation and analysis in the previous chapter can be applied to real sinusoidal disturbances as well. In this case, the regressor signal has the following form:

$$\begin{aligned} \mathbf{r}_{real} &= \frac{1}{2}\mathbf{r} + \frac{1}{2}\mathbf{r}^* \\ &= \sum_{k=1}^{m} \bar{\mathbf{a}}_{\mathbf{k}}(t)\sin(\omega_k t) + \sum_{k=1}^{m} \bar{\mathbf{b}}_{\mathbf{k}}(t)\cos(\omega_k t) \end{aligned} \tag{6.5}$$

where $\bar{\mathbf{a}}_{\mathbf{k}} \in \mathcal{R}^{n\times 1}$ and $\bar{\mathbf{b}}_{\mathbf{k}} \in \mathcal{R}^{n\times 1}$ are unknown Fourier coefficients for the regressor signal. In this case, the unknown coefficient $\mathbf{q}_{\mathbf{k}}$ from the complex AFC formulation can be

parameterized as:

$$\mathbf{q_k}(t) = \mathbf{b_k}(t) - j\mathbf{a_k}(t) \tag{6.6}$$

With this proposed formulation, and the general form of the adaptive update in (5.6), the unknown coefficients $\mathbf{a_k}$ and $\mathbf{b_k}$ will have the following update form.

$$\begin{aligned} \delta\mathbf{a_k}(t) &= -\mu(\mathrm{Re}(\Phi_k)\sin(\omega_k t) - \mathrm{Im}(\Phi_k)\cos(\omega_k t))\mathbf{e}(t) \\ \delta\mathbf{b_k}(t) &= -\mu(\mathrm{Re}(\Phi_k)\cos(\omega_k t) + \mathrm{Im}(\Phi_k)\sin(\omega_k t))\mathbf{e}(t) \end{aligned} \tag{6.7}$$

Also, the Fourier coefficients $\bar{\mathbf{a}}_\mathbf{k}$ and $\bar{\mathbf{b}}_\mathbf{k}$ can be found in terms of the unknown coefficients $\mathbf{a_k}$ and $\mathbf{b_k}$.

$$\begin{aligned} \bar{\mathbf{a}}_\mathbf{k}(t) &= \mathrm{Re}(\Gamma_k)\mathbf{a_k}(t) - \mathrm{Im}(\Gamma_k)\mathbf{b_k}(t) \\ \bar{\mathbf{b}}_\mathbf{k}(t) &= \mathrm{Re}(\Gamma_k)\mathbf{b_k}(t) + \mathrm{Im}(\Gamma_k)\mathbf{a_k}(t) \end{aligned} \tag{6.8}$$

Extending results in **Lemma 1**, the exact form of AFC controller based on the adaptive update in the matrix multiplication form can be derived in both forward and backward differences:

$$\begin{aligned} K_{forward} &= -\mu \sum_{k=1}^{m} \frac{(\mathrm{Re}(\Gamma_k\Phi_k)\cos(\omega_k) - \mathrm{Im}(\Gamma_k\Phi_k)\sin(\omega_k))z - \mathrm{Re}(\Gamma_k\Phi_k)}{z^2 - 2\cos(\omega_k)z + 1} \\ K_{backward} &= -\mu \sum_{k=1}^{m} \frac{\mathrm{Re}(\Gamma_k\Phi_k)z^2 - (\mathrm{Re}(\Gamma_k\Phi_k)\cos(\omega_k) + \mathrm{Im}(\Gamma_k\Phi_k)\sin(\omega_k))z}{z^2 - 2\cos(\omega_k)z + 1} \end{aligned} \tag{6.9}$$

### 6.2.1 Pseudo-Gradient Algorithm

The realization of algorithm is simply achieved by assuming the plant transfer function to be identity, hence the name is pseudo-gradient algorithm. Consequently, both adaptive updates and regressors can be realized as following:

$$\begin{aligned} \delta\mathbf{a_k}(t) &= -\mu\sin(\omega_k t)\mathbf{e}(t) \\ \delta\mathbf{b_k}(t) &= -\mu\cos(\omega_k t)\mathbf{e}(t) \end{aligned} \tag{6.10}$$

$$\begin{aligned} \bar{\mathbf{a}}_\mathbf{k}(t) &= \mathbf{a_k}(t) \\ \bar{\mathbf{b}}_\mathbf{k}(t) &= \mathbf{b_k}(t) \end{aligned} \tag{6.11}$$

The Lyapunov stability of overall adaptive system with pseudo-gradient algorithm and convergence of the output $\mathbf{e}$ to zero is ensured if the plant transfer function is SPR for SISO plants [SB89]. However, the SPR condition barely exists for physical plants. In contrast, **Corollary 2** predicts that the SISO adaptive system can be stabilized with a sufficiently small gain if the plant transfer function is positive-real at the disturbance frequency. The decoupled pseudo-gradient can be shown to have the following LTI exact form:

$$\begin{aligned} K_{forward} &= -\mu \sum_{k=1}^{m} \frac{\cos(\omega_k)z - 1}{z^2 - 2\cos(\omega_k)z + 1} I_n \\ K_{backward} &= -\mu \sum_{k=1}^{m} \frac{z^2 - \cos(\omega_k)z}{z^2 - 2\cos(\omega_k)z + 1} I_n \end{aligned} \tag{6.12}$$

### 6.2.2 GAFC

For GAFC discussed in Section 5.4, there are two distinct ways of realization depending on the choice for $\Gamma_k$ and $\Phi_k$. The first realization assigns $\Gamma_k = \hat{\mathcal{G}}_k^H$ and $\Phi_k = I_n$. For this form, the adaptation can be achieved like the pseudo-gradient algorithm. However, the Fourier coefficients for the regressor signal have the following forms:

$$\begin{aligned} \bar{\mathbf{a}}_\mathbf{k}(t) &= \mathrm{Re}(\hat{\mathcal{G}}_k^T)\mathbf{a}_\mathbf{k}(t) + \mathrm{Im}(\hat{\mathcal{G}}_k^T)\mathbf{b}_\mathbf{k}(t) \\ \bar{\mathbf{b}}_\mathbf{k}(t) &= \mathrm{Re}(\hat{\mathcal{G}}_k^T)\mathbf{b}_\mathbf{k}(t) - \mathrm{Im}(\hat{\mathcal{G}}_k^T)\mathbf{a}_\mathbf{k}(t) \end{aligned} \tag{6.13}$$

The second realization assigns $\Gamma_k = I_n$ and $\Phi_k = \hat{\mathcal{G}}_k^H$. For this realization the regressor signal has the same form as pseudo-gradient algorithm. However, the adaptation can be achieved in matrix-multiplication form as following:

$$\begin{aligned} \delta\mathbf{a}_\mathbf{k}(t) &= -\mu(\mathrm{Re}(\hat{\mathcal{G}}_k)\sin(\omega_k t) + \mathrm{Im}(\hat{\mathcal{G}}_k)\cos(\omega_k t))\mathbf{e}(t) \\ \delta\mathbf{b}_\mathbf{k}(t) &= -\mu(\mathrm{Re}(\hat{\mathcal{G}}_k)\cos(\omega_k t) - \mathrm{Im}(\hat{\mathcal{G}}_k)\sin(\omega_k t))\mathbf{e}(t) \end{aligned} \tag{6.14}$$

Extending results in **Lemma 1**, both realizations of GAFC based on selection of regressor and adaptation gains have the exact LTI form.

$$\begin{aligned} K_{forward} &= -\mu \sum_{k=1}^{m} \frac{(\mathrm{Re}(\hat{\mathcal{G}}_k)\cos(\omega_k) + \mathrm{Im}(\hat{\mathcal{G}}_k)\sin(\omega_k))z - \mathrm{Re}(\hat{\mathcal{G}}_k)}{z^2 - 2\cos(\omega_k)z + 1} \\ K_{backward} &= -\mu \sum_{k=1}^{m} \frac{\mathrm{Re}(\hat{\mathcal{G}}_k)z^2 - (\mathrm{Re}(\hat{\mathcal{G}}_k)\cos(\omega_k) - \mathrm{Im}(\hat{\mathcal{G}}_k)\sin(\omega_k))z}{z^2 - 2\cos(\omega_k)z + 1} \end{aligned} \tag{6.15}$$

For $\Phi_k = \mathcal{G}_k^H$, it can be shown that the adaptive update in (6.14) can be realized by applying the filter $G^T$ element-wise on sin and cos:

$$\begin{aligned} \delta \mathbf{a_k}(t) &= -\mu \hat{G}^T(z)[\sin(\omega_k t)]\mathbf{e}(t) \\ \delta \mathbf{b_k}(t) &= -\mu \hat{G}^T(z)[\cos(\omega_k t)]\mathbf{e}(t) \end{aligned} \tag{6.16}$$

where $G(z)[.]$ denotes the MIMO transfer function acting on scalar sin or cos signals in time-domain element-wise. Since the filter realization is equivalent to (6.14) in the steady states, the LTI form in (6.15) is only an approximation for the filter realization. However, the LTI approximation can be used for stability analysis under the condition of persistent excitation (PE) [Bay00]. For sine waves with time-varying frequency, the matrix-multiplication is cumbersome since it requires the burden of implementing look-up tables based on linear interpolations of the plant's frequency response. Therefore, the filter realization of GAFC is popular for SISO plants, which is called Filtered-X method [Bay00]. However, for MIMO high order plants like AMBS, the Filtered-X method is also cumbersome since it requires implementing $n \times n$ high order filters for element-wise filtering of sin and cos. Consequently, the proposed IAFC is found superb not only because of its stability and convergence properties but also its practically simple implementations for MIMO plants.

### 6.2.3 IAFC

For the proposed IAFC discussed in Section 5.5, the realization of adaptive update and regressor signals are simply achieved by time-delay and time-advance respectively as following:

$$\begin{aligned} \delta \mathbf{a_k}(t) &= -\mu \sin(\omega_k(t - d_2))\mathbf{e}(t) \\ \delta \mathbf{b_k}(t) &= -\mu \cos(\omega_k(t - d_2))\mathbf{e}(t) \end{aligned} \tag{6.17}$$

$$\mathbf{r}_{real} = \sum_{k=1}^{m} \mathbf{a_k}(t) \sin(\omega_k(t + d_1)) + \sum_{k=1}^{m} \mathbf{b_k}(t) \cos(\omega_k(t + d_1)) \tag{6.18}$$

It can be easily shown that the IAFC for multiple frequency real sine cancellation also has the exact LTI form:

$$\begin{aligned} K_{forward} &= -\mu \sum_{k=1}^{m} \frac{\cos(\omega_k(d+1))z - \cos(\omega_k d)}{z^2 - 2\cos(\omega_k)z + 1} I_n \\ K_{backward} &= -\mu \sum_{k=1}^{m} \frac{\cos(\omega_k d)z^2 - \cos(\omega_k(d-1))z}{z^2 - 2\cos(\omega_k)z + 1} I_n \end{aligned} \tag{6.19}$$

Furthermore, in contrast with the GAFC, the filter realization of the adaptive update is exactly equivalent to the matrix multiplication form for the proposed IAFC:

$$\begin{aligned} \delta \mathbf{a_k}(t) &= -\mu z^{-d_2}[\sin(\omega_k t)]\mathbf{e}(t) \\ \delta \mathbf{b_k}(t) &= -\mu z^{-d_2}[\cos(\omega_k t)]\mathbf{e}(t) \end{aligned} \tag{6.20}$$

Consequently, for the case that $d_2 = d$, the stability analysis based on LTI equivalence in the previous chapter predicts exactly the stability of adaptive system with the filter realization. For example, given ideal inversion, i.e, $E = 0$, **Corollary** 3 shows that all poles from the IAFC controller will move to the origin of unit circle with the equal rate, $\frac{d|\bar{z}_k|}{d\mu} = \frac{-1}{2}$, which is independent of number of frequency components and their corresponding values as shown in Figure 6.3 when the delay length is considered to be zero.

As discussed before, increasing the delay length reduces the norm of model-matching error transfer function $E(z)$ which is necessary to ensure the stability of IAFC. Previously, an analytical framework was developed to exactly obtain the maximum allowable $\bar{\mu}$ and optimal adaptation $\mu_o$ gains for single-tone complex exponential cancellations given the ideal inversion of the plant transfer function. Furthermore, an approximation was made to find both $\mu_o$ and $\bar{\mu}$ for multi-tone complex cancellations. Since the single-tone real sine cancellation can be classified as double-tone complex exponential cancellations $\pm\omega$, the analytical framework in Section 5.6 can be utilized to estimate $\mu_o$ and $\bar{\mu}$. To see how precise the estimates are, both values are computed numerically for different delay lengths as shown in Figure 6.4. The numerical computation shows that increasing the delay length for single-tone IAFC reduces both $\bar{\mu}$ and $\mu_o$ which is as expected from the analytical framework. Furthermore, $\bar{\mu}$ turns out to be uniform across the frequency for small delay lengths while it has a peak for larger delays. In contrast, $\mu_o$ turns out to have more uniform behavior for larger delays compared

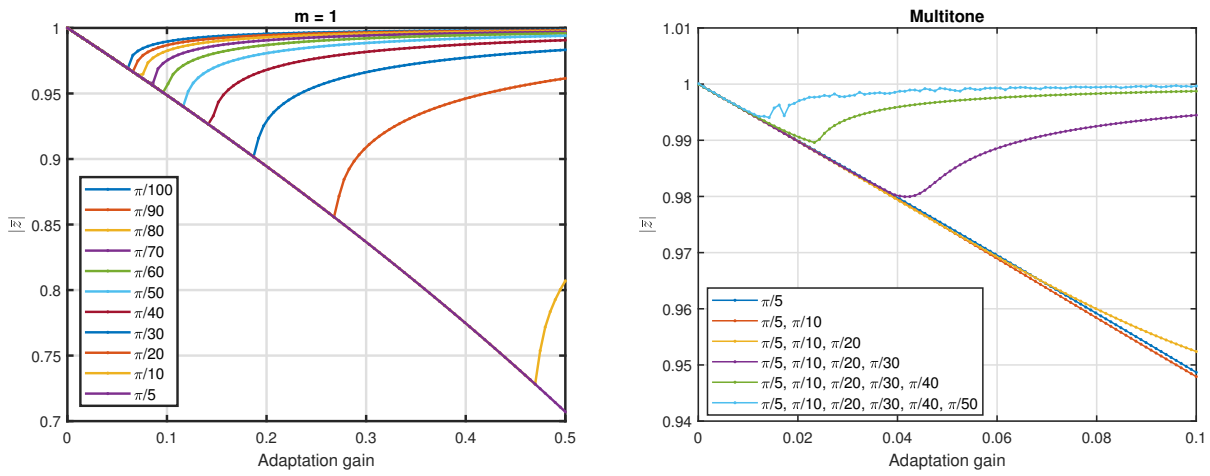


**(a)** **(b)**

**Figure 6.3:** Dominant closed-loop magnitude for $G = 1$. (a) Single-Tone IAFC (b) Multi-Tone IAFC

to the small ones. Using the result from numerical computation and considering the trade-off between inversion error and highest convergence rate, 10 step delays is selected as a suitable preliminary candidate for the IAFC design.

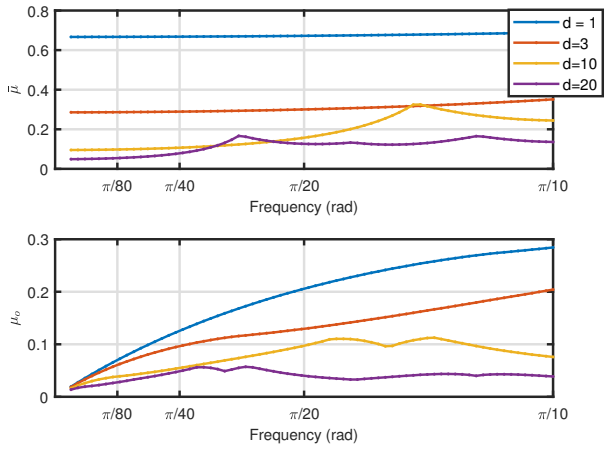


**Figure 6.4:** Maximum allowable gain and optimal gain for single-tone cancellation

In the application presented later in Section 6.5, a single-tone IAFC, $m = 1$, is used to reject the real sinusoidal disturbance at spin frequency, and a double-tone IAFC, $m = 2$ is

further used to reject the spin frequency and its first harmonic. To investigate the maximum allowable and the optimal adaptation gains, the dominant closed-loop pole magnitude is shown for various frequencies in Figure 6.5. In single-tone IAFC, it can be shown that for $d = 10$ at small frequencies $\bar{\mu} = 0.11$ which is close to $\bar{\mu} = 0.149$ obtained from the analytical framework, and $\mu_o = 0.04$ at $\omega = \pi/100$ which is close the analytical value $\mu_o = 0.035$. Critical values shown to be approximately halved for double-tone IAFC as expected.

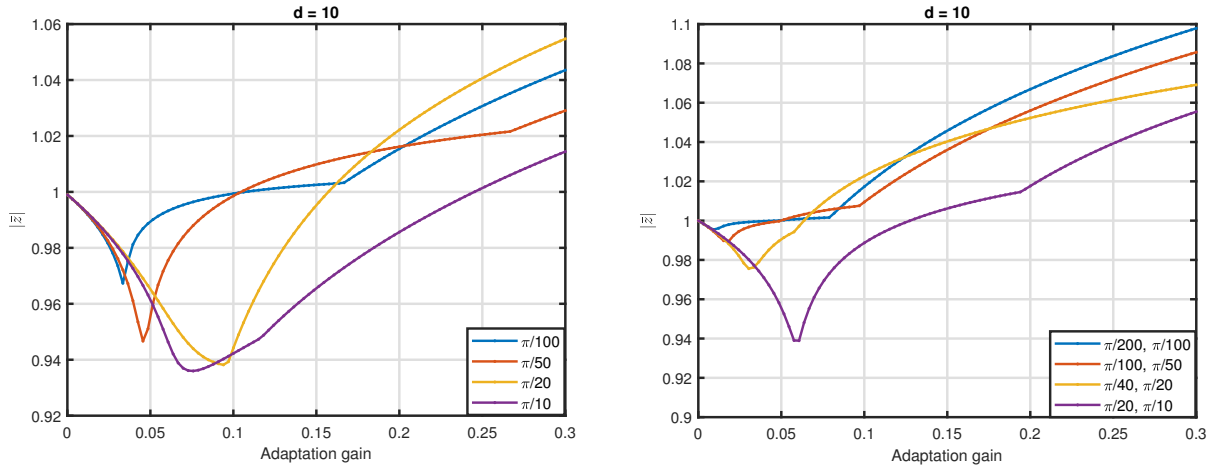


**(a)** **(b)**

**Figure 6.5:** Dominant closed-loop pole magnitude. (a) Single-Tone IAFC (b) Double-Tone IAFC.

Furthermore, both single-tone and double-tone IAFC will be used during the spinning-up and down as well as the constant speed operation. The ramping process can be considered as a chirp disturbance which its fundamental frequency is synchronized with the rotor's speed. For the automation balancing, the rotor is spun up to 500 Hz, $0 \leq \bar{\omega} \leq \frac{\pi}{10}$. To investigate the possibility of IAFC transient behavior and the possibility of rejecting the chrip disturbance, the convergence rate is investigated in Figure 6.6 and 6.7 for single and double tone IAFCs respectively. It can be confirmed that the possible choice of $\mu = 0.04$ for single-tone IAFC and $\mu = 0.04$ for double-tone IAFC can ensure both stability and fast convergence which is required for the transient performance.

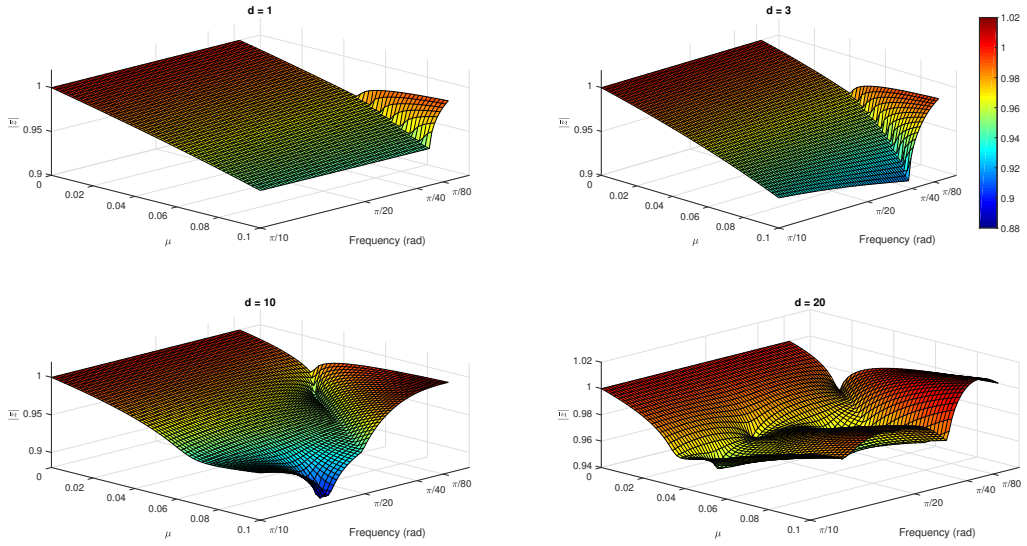


**Figure 6.6:** Dominant closed-loop pole magnitude for single-tone IAFC

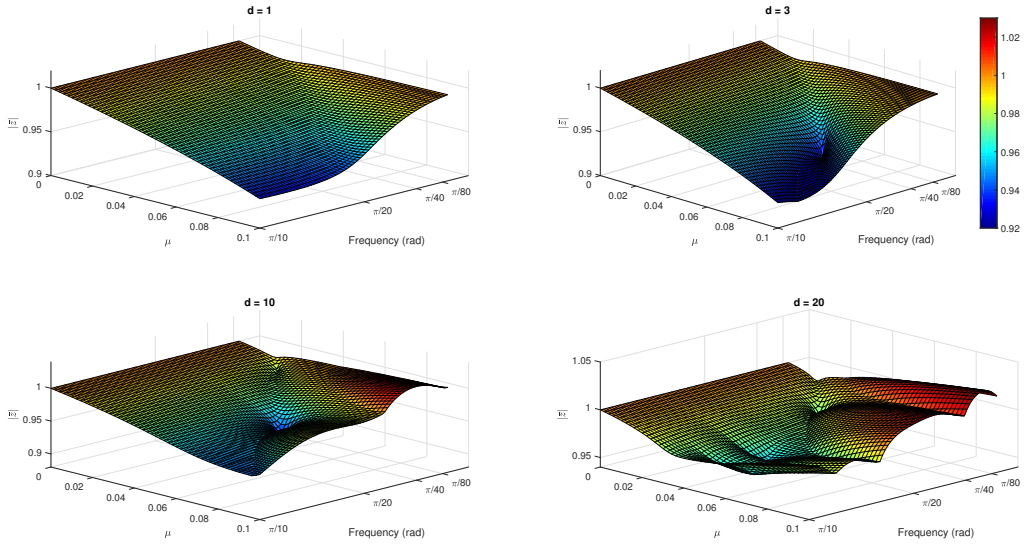


**Figure 6.7:** Dominant closed-loop pole magnitude for double-tone IAFC

## 6.3 MIMO IAFC Design and Performance

To justify the proposed method, first a MIMO IAFC is investigated for automation balancing application by using $\mathbf{u}$ in 5.7, $F_L(z) = I_n$, and the optimal inversion filer $F_R$ is obtained

by using $M = 1$. The inversion filter design is also dependent on the junction position. Furthermore, the inversion filter can be obtained by solving the plant inversion problem in (5.37) in $H_2$ or $H_\infty$. For Configuration 1, there exist optimal inversion filters in both $H_2$ and $H_\infty$ sense. However, the optimal filter from $H_\infty$ design results in smaller error as shown in Figure 6.9. Since the application later discussed in Section (6.5) requires rejecting a chirp disturbance ranging from 0 to 500 Hz for the single-tone IAFC, **Corollary 4** ensures the stability of MIMO IAFC for $d > 1$ given the $H_\infty$ design. The $H_2$ design only ensures stability for larger delay lengths. Given the trade-off between delay length and convergence rate, the $H_\infty$ design looks more promising for the first configuration. In contrast, there exists no optimal $F_R$ for $H_\infty$ design when Configuration 2 is placed. Moreover, the $H_2$ design fails to stabilize the closed-loop plant for $d < 10$ as shown in Figure 6.8.

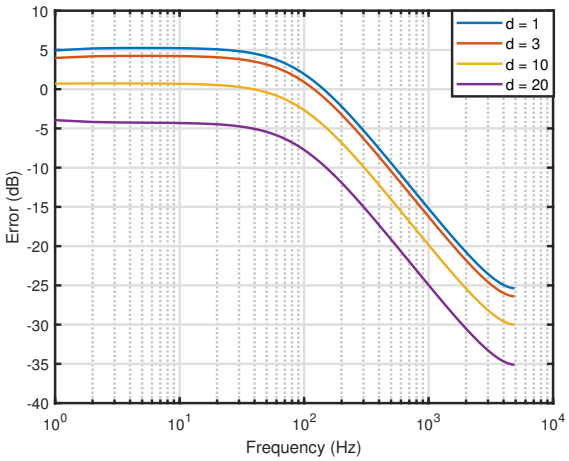


**Figure 6.8:** Configuration 2, maximum singular value of model-matching error transfer function $E$

Given above discussions above the control junctions and plant-inversion design technique, Configuration 1 is selected for implementation of the proposed IAFC, $G = G_{\mathbf{ur1}}$ and the $H_\infty$ design is selected to obtain the optimal $F_R$. Since $\hat{G}$ is used instead of $G$ in finding $E$, $d > 3$ can be considered as a more robust choice. The optimal analyses carried in the previous section are based on the assumption that $E = 0$. However, it is clear that increasing the delay length decreases both $\bar{\mu}$ and $\mu_o$, and the highest potential convergence rate. To that

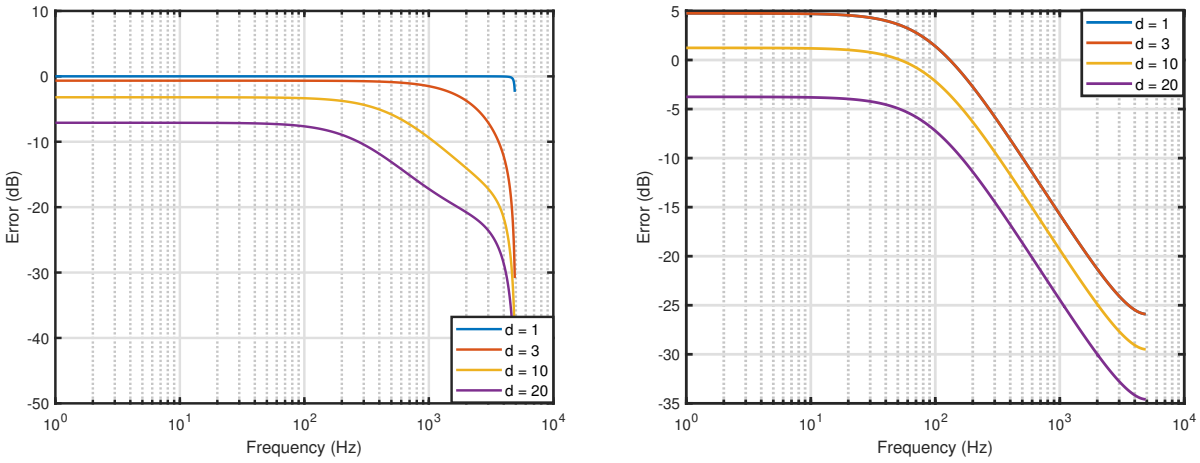


**(a)** **(b)**

**Figure 6.9:** Configuration 1, maximum singular value of model-matching error transfer function $E$. (a) $H_\infty$ (b) $H_2$

end, we choose $d = 10$ as a trade-off between the inversion error and convergence rate.

To illustrate the superior performance of IAFC in comparison with GAFC in creating a uniform and fast convergence, Figure 6.10 and 6.11 are presented. It can be shown that at $\omega = \pi/100$ and $\omega = \pi/50$, the single-tone IAFC has $\bar{\mu} = 0.11$ which is identical to the case with ideal inversion. The existence of model-matching error is pushing the optimal gain further for this particular plant. However, the GAFC is shown to have non-uniform and slow convergence as expected, which makes the implementation impractical for spin-up application. The double-tone IAFC is shown to have the critical values almost half of the single-tone as predicted. Consequently, using the analytical framework, and including the possible model-matching error, the adaptation gain was selected to be 0.04 for the single-tone and 0.02 for the double-tone IAFC.

To utilize the SISO framework developed in **Corollary 5**, the maximum singular value of model-matching error transfer function is decomposed into diagonal and off-diagonal elements as presented in Figure 6.12. It can be observed that increasing delay lengths decrease the maximum singular values of diagonal elements while increasing the non-diagonal sides.

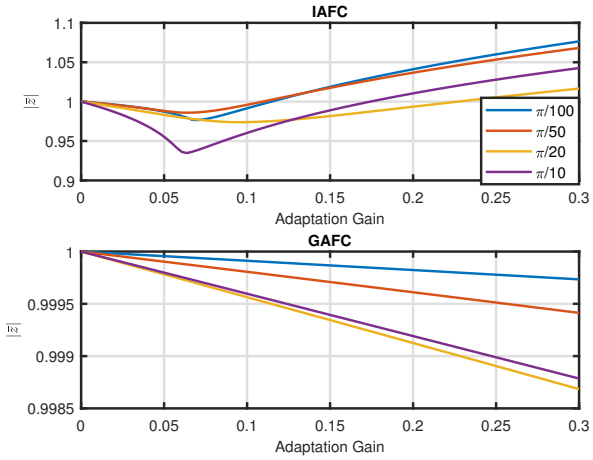


**Figure 6.10:** Dominant closed-loop pole magnitude for Single-Tone AFC. Top: IAFC with non-zero model-matching error. Bottom: GAFC

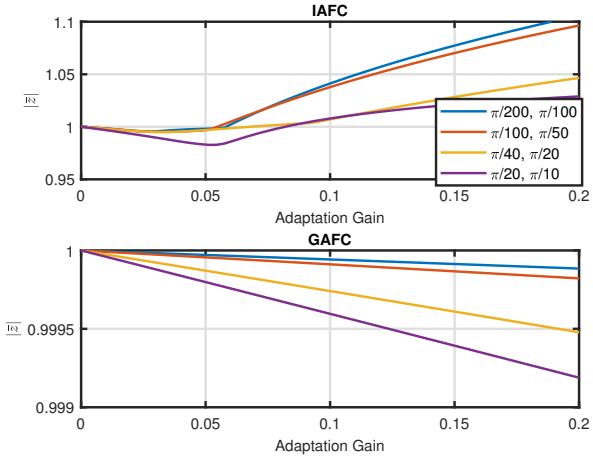


**Figure 6.11:** Dominant closed-loop pole magnitude for Double-Tone AFC. Top: IAFC with non-zero model-matching error. Bottom: GAFC

SISO analysis may be found more suitable form $d < 10$. However, since $\|E(z)\|_\infty < -17dB$, the stability of proposed IAFC is also investigated using the SISO framework by looking at diagonal elements of $G(z)F_R(z)z^d$. The SISO analysis also confirms the result that the closed-loop system is stable for $d > 1$, but to ensure the robustness $d$ may be selected higher as illustrated in Figure 6.13. Lastly, the SISO analysis can be verified for all channels as shown for the selected delay length $d = 10$ in Figure 6.14.

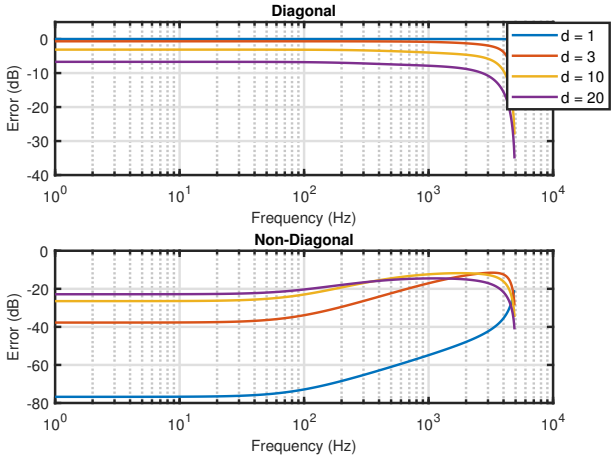


**Figure 6.12:** Maximum singular value of model-matching error transfer function

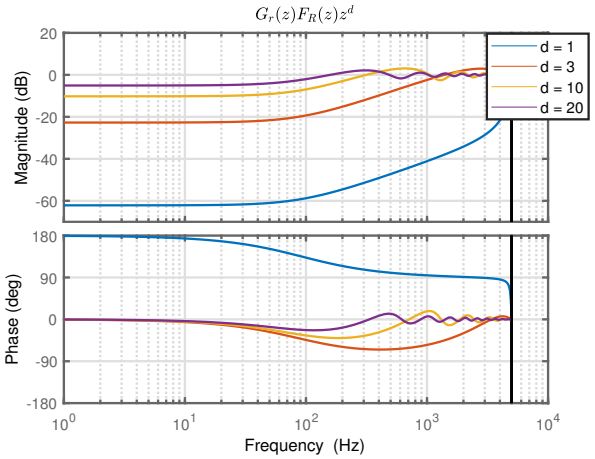


**Figure 6.13:** Bode plot of $G_r(z)F_R(z)z^d$ for one diagonal element

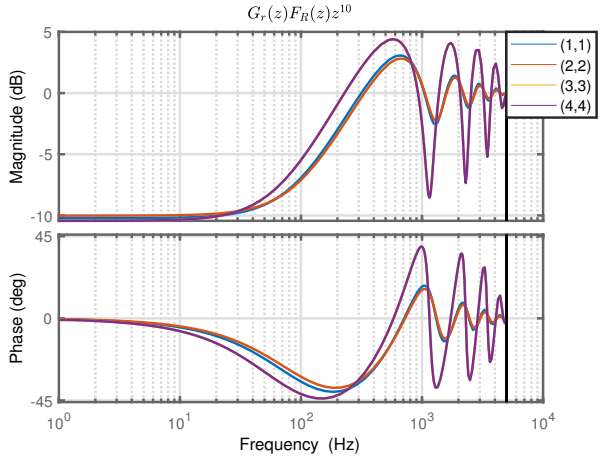


**Figure 6.14:** Bode plot of $G_r(z)F_R(z)z^d$ for all diagonal element, $d = 10$

## 6.4 Simulation Validation

In Section 6.2, it is shown that given $\Phi_k = \mathcal{G}_k^H$, the adaptive update can be realized by applying the filter $G^T$ element-wise on sin and cos. Under the PE conditions, the filter form is equivalent to the matrix-multiplication form obtained by using the Hermitian of plant's transfer function. However, if the PE condition does not hold, two forms of GAFC realization will have different behaviors in transient response. The Matrix-multiplication form turns out to have a faster convergence rate in comparison with the filter form as shown in the simulation where two forms of realization are tested to reject 500 Hz as shown in Figure 6.15 .

To investigate the performance of proposed IAFC in comparison with the existing GAFC, both algorithms are tested in identical simulations to reject a chirp disturbance ramping up and down linearly from stationary to 500 Hz as shown in Figure 6.16. In all simulations, a normally distributed random signal is added to the output to show the possible measurement noises. The noise is zero mean and 0.5 standard deviation. Furthermore, a 100th order model is used as a plant model to simulate the algorithm while the 20th order one is used for LQGi, GAFC and IAFC design. For both AFC algorithms, a constant adaptation gain $\mu = 0.04$ is used as discussed in the previous section. Effectiveness of the proposed IAFC in comparison

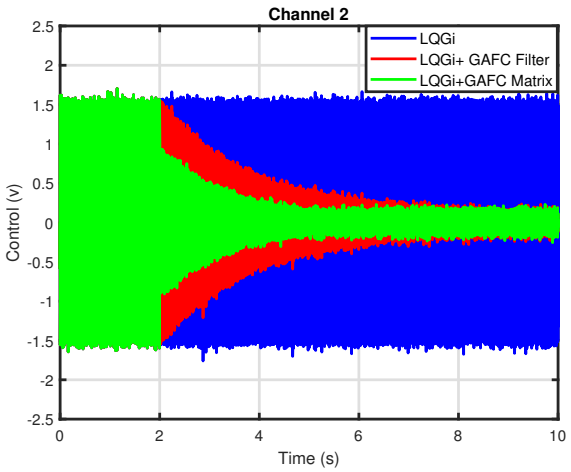


**Figure 6.15:** Simulation comparison showing faster convergence rate achieved by the matrix-multiplication form in comparison with the filter realization for MIMO GAFC. The baseline LQGi controller stabilizes the plant while GAFCs are activated at $t = 2$ s. The sin and cos filtering starts right after the activation.

with GAFC can be seen in both rejecting the time-varying frequency disturbance, and having faster convergence in rejecting the constant frequency disturbance.

## 6.5 Experimental Results

This section presents the experimental validation of the proposed IAFC in the automation balancing application. Two distinct sets of experimental results are illustrated where in the first experiment the single-tone IAFC were implemented to reduce the control effort during both the transient, spin-up and spin-down, and the steady state, constant spin at 500 Hz. On the other hand, in the next set of experiments, the single-tone and double-tone IAFC were implemented separately to compare their performances in reducing the control effort during both spin-up and spin-down, and also constant spin at 250 Hz.

The experiments in this section were performed by Dr. Sandeep Rai and some of the results for GAFC implementation in matrix-multiplication form through applying look-up tables were reported in dissertation of Dr. Rai [Rai18]. In all experiments, the precise

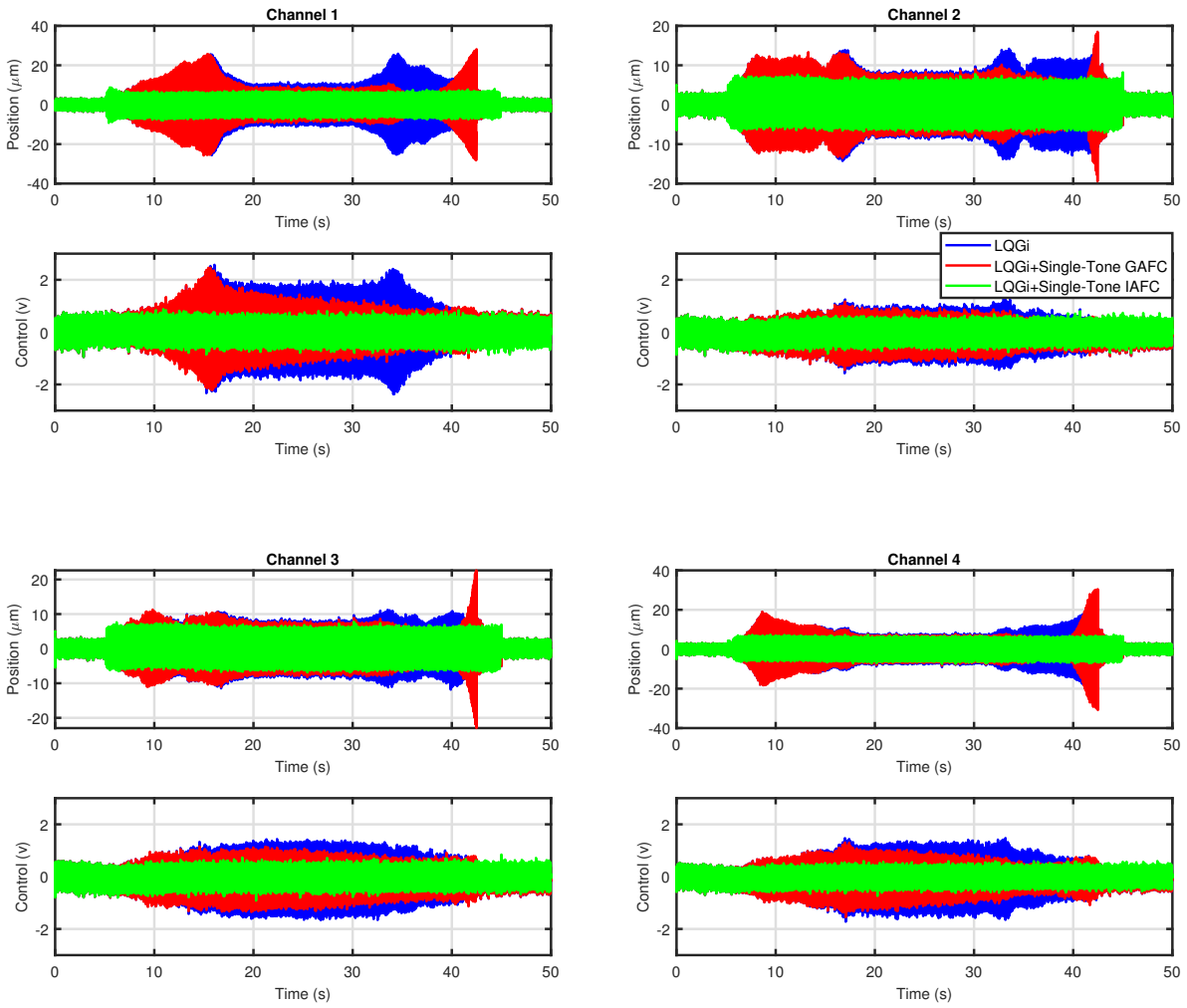


**Figure 6.16:** Simulation comparison showing both improved disturbance rejection and reduced control effort achieved by the single-tone IAFC. The baseline LQGi controller stabilizes the open-loop plant for the first five seconds, and then the $\mathbf{d_{out}}$ is introduced while its frequency changes linearly to 500 Hz. From $t = 20$ s to $t = 30$ s, the disturbance frequency is constant, 500 Hz, then it goes down linearly to stationary. The rotor's geometric position $\mathbf{y}$ from each sensor is in micro-meter, and the control command $\mathbf{u}$ is in volt.

regressors were generated in FPGA by reading the spindle encoder signals. Furthermore, the baseline LQGi controller was used initially to levitate the rotor. To help the transient behavior of the closed-loop system, the adaptive controllers were activated in about two seconds after the spin-up. Lastly, an accelerometer was mounted on the housing to monitor

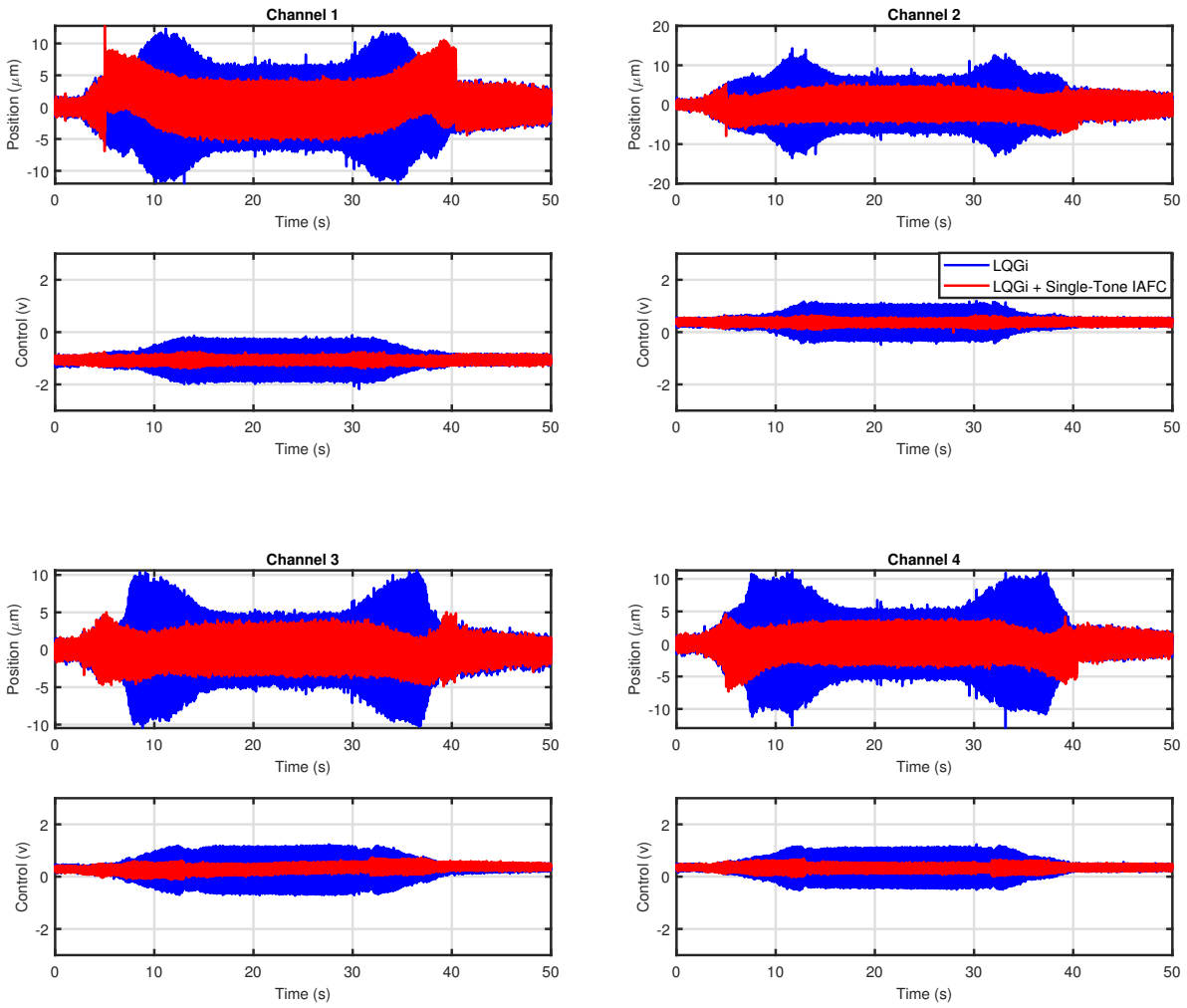


**Figure 6.17:** Experimental comparison showing both improved disturbance rejection and reduced control effort achieved by the single-tone IAFC. The rotor was lifted for the first three seconds, and then it was spun up linearly to 500 Hz. From $t = 17$ s to $t = 28.5$ s, the rotor was spun constantly at 500 Hz, and from $t = 28.5$ s to $t = 40.5$ s it was spun down to stationary. The rotor's geometric position $\mathbf{y}$ from each sensor is in micro-meter, and the control command $\mathbf{u}$ is in volt.

the housing vibrations during each experiment.

Although the LTI controller in (6.19) could have been implemented, the AFC form in (6.17, 6.18) was preferred for the following reason. The AFC implementation requires the spindle angles from the encoder readings whereas the LTI control implementation requires the rotational frequency in the filter parameters. When rotational frequencies varies, AFC

regressors are updated based on the rotational angles and are otherwise blind to the speed changes. The LTI controller must determine the frequency in every time step and change the controller parameters accordingly, so the implementation of the time varying internal model is much more tedious than that for the external regressor signals in the AFC. As an example, time varying internal models for a different AMB based on unity-magnitude or zero-phase compensations for SISO plant model is presented in [KT16].

### 6.5.1 Set I: Single-Tone IAFC

In the first set of experiments shown in Figure 6.17, the rotor was spun-up from stationary to 500 Hz, and then spun constantly at 500 Hz for 11.5 seconds, and finally spun-down to stationary. For all channels, the proposed single-tone IAFC reduced the control effort and improved the disturbance rejection more significantly during the transient spin-up and spin-down. Furthermore, the Power Spectral Density (PSD) plot of the control input in Figure 6.18 shows the proposed single-tone IAFC reduced the control effort by 100 dB at the spin frequency, and effectively notched out the control effort. Also, it can be shown that the housing vibration was attenuated 35 dB at the spin frequency.

To highlight the effectiveness of the proposed IAFC in rejecting disturbances with time-varying frequencies, the short-time Fast-Fourier-Transform (FFT) of the control signal with and without the adaptive controller is illustrated in Figure 6.19. The spin-up and spin-down are similar to a chirp input disturbance, and the single-tone IAFC is shown to be capable of rejecting the chirp disturbance as well as a constant 500 Hz disturbance. It is also worth to point out the existence of the first harmonic of spin frequency that can be modeled as another disturbance with the time-varying frequency. This signifies the importance of implementing multi-tone IAFCs which can target not only the spin frequencies but also the higher harmonics.

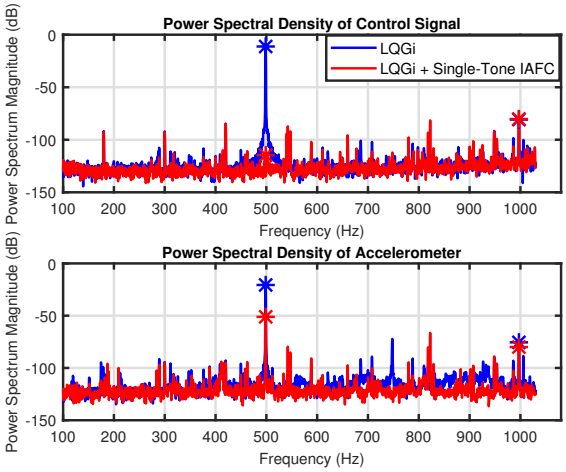


**Figure 6.18:** Power Spectral Density during the constant spin at 500. Top: Channel 3 control command **u**. Bottom: the external accelerometer signal.

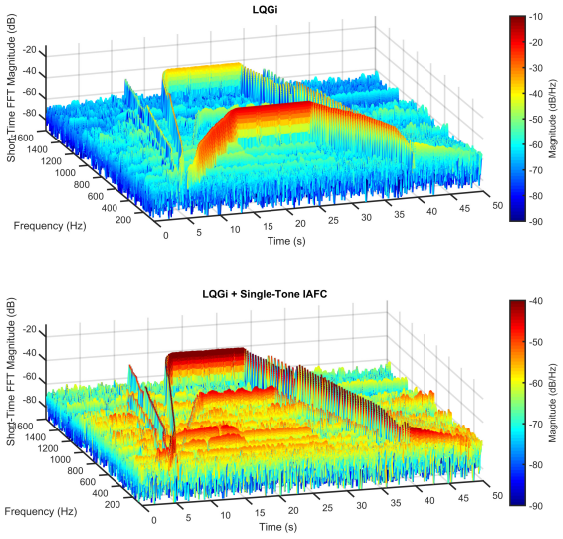


**Figure 6.19:** Short-time Fast Fourier of the Channel 3 control command with and without the adaptive controller. Top: LQGi only. Bottom: LQGi + Single-Tone IAFC.

### 6.5.2 Set II: Single-Tone VS Double-Tone IAFC

The existence of spin frequency harmonics in the disturbance model motivates the next set of experiments in which three representative experiments were performed to compare the performance of baseline LTI controller alone and the LTI controller augmented with the

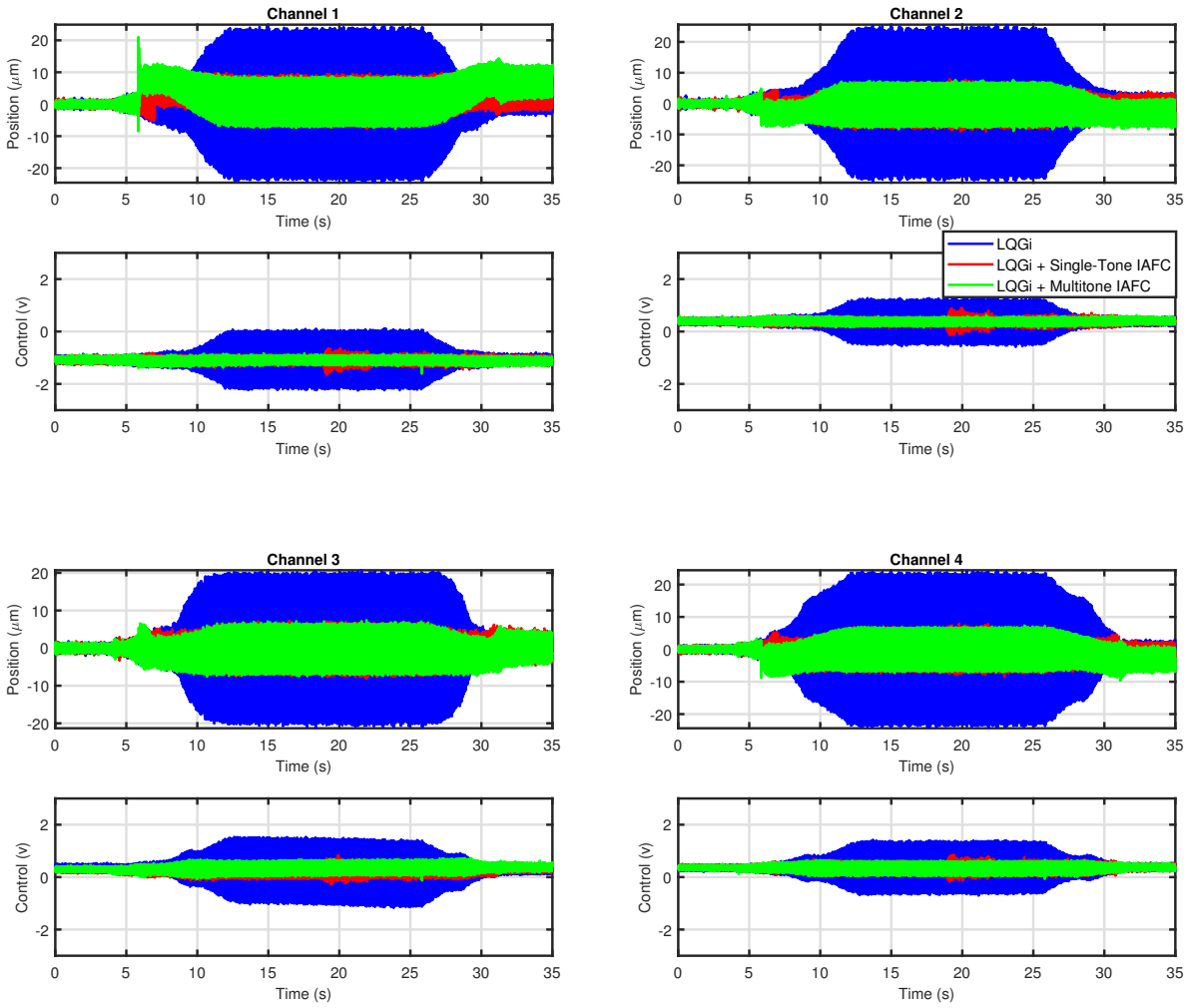


**Figure 6.20:** Experimental comparison showing improved disturbance rejection and reduced control effort achieved by the single-tone and double-tone IAFC. The rotor was lifted for the first four and half seconds, and then it was spun up linearly to 500 Hz. From $t = 13$ s to $t = 26$ s, the rotor was spun constantly at 500 Hz, and from $t = 26$ s to $t = 33$ s it was spun down to stationary. The rotor's geometric position $\mathbf{y}$ from each sensor is in micro-meter, and the control command $\mathbf{u}$ is in volt.

single-tone and double-tone IAFCs as shown in Figure 6.17. In all experiments, the rotor was spun-up from stationary to 250 Hz, and then spun constantly at 250 Hz until $t = 26s$, and finally spun-down to stationary. Although both adaptive algorithms reduced the control effort significantly, the single-tone IAFC resulted in better disturbance rejection during the transient with the cost of more required control effort during the constant spin.

The steady state behavior of adaptive algorithms is also investigated in Figure 6.21 with the PSD plots of the control signal for Channel 3. The double-tone IAFC was able to minimize the control input at spin frequency as well as the single-tone IAFC while rejecting the first harmonic at 500 Hz. From the PSD plot of the accelerometer signal, both algorithms reduced the housing vibration at the spin frequency. To highlight the fast convergence of both adaptive controllers, the short-time FFT plots of the control signal also shows that both adaptive approaches were successful in reducing the control signals at the spin frequency during the transient spin-up and spin-down while the double-tone IAFC also reduced the signal at the first harmonic of the spin frequency.

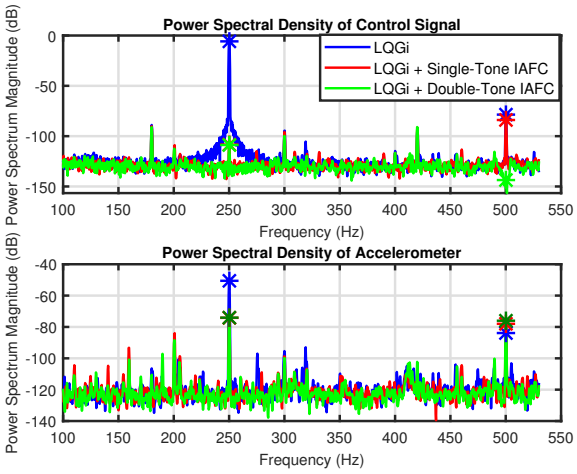


**Figure 6.21:** Power Spectral Density during the constant spin at 250. Top: Channel 3 control command **u**. Bottom: the external accelerometer signal.

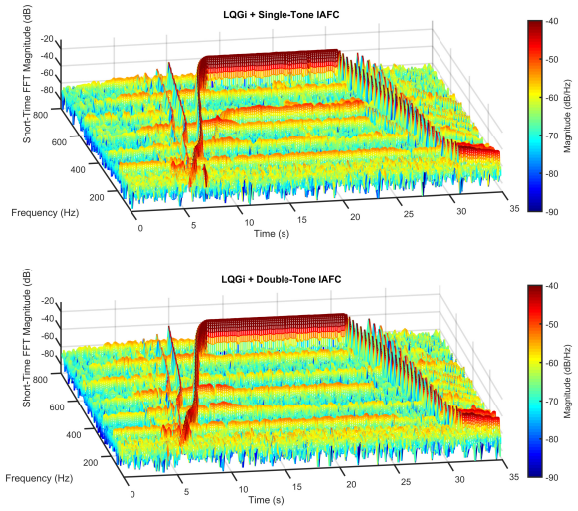


**Figure 6.22:** Short-time Fast Fourier of the Channel 3 control command with single and double tone adaptive controllers. Top: LQGi + Single-Tone IAFC. Bottom: LQGi + Double-Tone IAFC.

## 6.6 Summary

In this chapter, It is shown that the filter realization of the proposed IAFC in the previous chapter is exactly equivalent to the matrix-multiplication form obtained from the gradient algorithm. Consequently, the LTI equivalence obtained from the matrix-multiplication form enables the precise closed-loop stability and convergence analysis without requiring the further assumption of the steady-states or persistent excitation (PE) conditions. Also, a IAFC design synthesis is discussed for the automation balancing based on the trade-off between the inversion error and convergence rate.

When applied to the MIMO AMBS, where the vibrations are synchronous to the spindle rotational speed, the AFC implementation using external regressor signals has a significant advantage over the LTI controller implementation of the internal model, where the former only uses the rotation angles from the encoder readings while the latter must infer rotational speeds and update the internal model parameters when they are varying. Experimental results show that the IAFC has achieved suppressions for the entire speed profile that includes both ramping and constant speed sections. The IAFC's synchronous vibration suppressions

over a speed range and with varying speeds would otherwise not be achievable by the GAFC.

# CHAPTER 7

# Conclusion

This dissertation presented the use of linear estimators for FDI on an AMBS-rotor system. Due to the coupled-axis MIMO nature of the AMBS, the Riccati-based detection filters obtained from the application of game theory to the disturbance attenuation problem are an appropriate candidate to decouple the multi-variable component faults into the single scalar faults for detection, isolation. To further add the fault estimation into the FDI scheme, a bank of UIOs based on the decoupled error dynamics of each GTDF was proposed in this work. In comparison with the direct UIO approach in fault estimations, the inherited uncertainty consideration in the disturbance attenuation formulation ensures the robustness of the proposed method.

Motivated by the bank of GTDFs for the FDI scheme, this dissertation further proposed a general MIMO DOBC design based on extending the Youla parameterization of stabilizing controller with a FOSO feedback compensation, which includes multiple observers. This extension has facilitated the observer design for FDI and state estimation, and has utilized the inversion filters for disturbance estimation and rejection. This integrated control system has been proven stable since the observer residuals are used for the disturbance observer feedback compensation. The application to the AMBS demonstrated the several features of the proposed method and its practical usefulness and effectiveness in monitoring and control of the MIMO unstable open-loop system.

The second half of this dissertation presented a novel multi-variable adaptive feedforward compensation with an original stability and convergence analysis for MIMO systems and its use in suppressing the synchronous vibration in rotating machinery. The proposed inversion-

based adaptive feedforward control (IAFC) was based on the delay-inversion of the MIMO plant and its phase compensations by simple time shifts in AFC signals. In contrast with the original gradient-based algorithm, the filter realization of the proposed algorithm was shown to be exactly equivalent to the matrix multiplication form directly obtained from the gradient descent algorithm. Consequently, the exact LTI form of the proposed IAFC enables the exact stability and convergence analysis of the adaptive closed-loop system using the LTI framework.

The proposed IAFC was shown to be suitable for the automation balancing application on the MIMO AMBS not only because of its stability and fast convergence but also due to its practically simple implementations requiring implementing the inversion filter as opposed to implementing $n \times n$ high order filters for element-wise filtering of sin and cos in the original gradient-based algorithm. The effectiveness of IAFC in reducing the control effort during both the transient spin-up and spin-down and steady-state constant spinning was highlighted in the experiments.

From the results of this study, the following recommendations can be made going forward:

- Identifying and utilizing the cutting dynamics in the GTDF and inversion filter's design, the proposed integrated FDI and DOBC scheme can be implemented for chatter compensation to predict and prevent chatter instability in the cutting application.

- To further reduce the housing vibration, the performance index in the proposed IAFC formulation can include both the control effort and the measured position signal with appropriate weights, and the optimal inversion filter can be designed based on the non-square closed-loop plant. Consequently, by adjusting the weights, the AMBS's control allows the rotor to switch spinning about its inertial or geometrical center.

# BIBLIOGRAPHY


[ACL04] Sébastien Auchet, Pierre Chevrier, Michel Lacour, and Paul Lipinski. "A new method of cutting force measurement based on command voltages of active electro-magnetic bearings." *International Journal of Machine Tools and Manufacture*, **44**(14):1441–1449, 2004.

[Bay00] David S Bayard. "A general theory of linear time-invariant adaptive feedforward systems with harmonic regressors." *IEEE Transactions on Automatic Control*, **45**(11):1983–1996, 2000.

[BC00] Sergio Bittanti and Patrizio Colaneri. "Invariant representations of discrete-time periodic systems." *Automatica*, **36**(12):1777–1793, 2000.

[BC09] Sergio Bittanti and Patrizio Colaneri. *Periodic systems: filtering and control*, volume 5108985. Springer Science & Business Media, 2009.

[Bea71] Richard Vernon Beard. *Failure accomodation in linear systems through self-reorganization.* PhD thesis, Massachusetts Institute of Technology, 1971.

[BKU99] Foued Ben Amara, Pierre T Kabamba, and A Galip Ulsoy. "Adaptive sinusoidal disturbance rejection in linear discrete-time systems—Part I: Theory." *Journal of Dynamic Systems, Measurement, and Control*, **121**(4):648–654, 1999.

[BOA02] Tilman Bünte, Dirk Odenthal, Bilin Aksun-Güvenç, and Levent Güvenç. "Robust vehicle steering control design based on the disturbance observer." *Annual reviews in control*, **26**(1):139–149, 2002.

[Bod88a] M. Bodson. "Effect of the choice of error equation on the robustness properties of adaptive control systems." *International Journal of Adaptive Control and Signal Processing*, **2**:249–257, 1988.

[Bod88b] Marc Bodson. "Effect of the choice of error equation on the robustness properties of adaptive control systems." *International Journal of Adaptive Control and Signal Processing*, **2**(4):249–257, 1988.

[Bra83] DH Brandwood. "A complex gradient operator and its application in adaptive array theory." In *IEE Proceedings H-Microwaves, Optics and Antennas*, volume 130, pp. 11–16. IET, 1983.

[BSK94] Marc Bodson, Alexei Sacks, and Pradeep Khosla. "Harmonic generation in adaptive feedforward cancellation schemes." *IEEE Transactions on Automatic control*, **39**(9):1939–1944, 1994.

[BT99] Robert Bickel and Masayoshi Tomizuka. "Passivity-based versus disturbance observer based robot control: equivalence and stability." 1999.

[Che00] H Ming Chen. "A self-healing magnetic bearing." In *NASA CONFERENCE PUBLICATION*, pp. 25–34. NASA; 1998, 2000.

[Che04] Wen-Hua Chen. "Disturbance observer based control for nonlinear systems." *IEEE/ASME transactions on mechatronics*, **9**(4):706–710, 2004.

[CK07a] Min Chen and Carl R Knospe. "Control approaches to the suppression of machining chatter using active magnetic bearings." *Control Systems Technology, IEEE Transactions on*, **15**(2):220–232, 2007.

[CK07b] Min Chen and Carl R. Knospe. "Control Approaches to the Suppression of Machining Chatter Using Active Magnetic Bearings." *IEEE Transactions on Control Systems Technology*, **15**(2):220–232, 2007.

[CKS04] Matthew OT Cole, Patrick S Keogh, Mehmet N Sahinkaya, and Clifford R Burrows. "Towards fault-tolerant active control of rotor–magnetic bearing systems." *Control Engineering Practice*, **12**(4):491–501, 2004.

[CLW16] Peiling Cui, Sheng Li, Qirui Wang, Qian Gao, Jian Cui, and Huijuan Zhang. "Harmonic current suppression of an AMB rotor system at variable rotation speed based on multiple phase-shift notch filters." *IEEE Transactions on Industrial Electronics*, **63**(11):6962–6969, 2016.

[CP12] Jie Chen and Ron J Patton. *Robust model-based fault diagnosis for dynamic systems*, volume 3. Springer Science & Business Media, 2012.

[CPZ96] Jie Chen, Ron J Patton, and Hong-Yue Zhang. "Design of unknown input observers and robust fault detection filters." *International Journal of control*, **63**(1):85–105, 1996.

[CQ97] Tongwen Chen and Li Qiu. "Linear periodically time-varying discrete-time systems: Aliasing and LTI approximations." *Systems & control letters*, **30**(5):225–235, 1997.

[CS98] Walter H Chung and Jason L Speyer. "A game theoretic fault detection filter." *IEEE Transactions on Automatic Control*, **43**(2):143–161, 1998.

[CT98] Martin Corless and JAY Tu. "State and input estimation for a class of uncertain systems." *Automatica*, **34**(6):757–764, 1998.

[CYG15] Wen-Hua Chen, Jun Yang, Lei Guo, and Shihua Li. "Disturbance-observer-based control and related methods—An overview." *IEEE Transactions on Industrial Electronics*, **63**(2):1083–1095, 2015.

[DI01] Claudio De Persis and Alberto Isidori. "A geometric approach to nonlinear fault detection and isolation." *IEEE transactions on automatic control*, **46**(6):853–865, 2001.

[FB06] Thierry Floquet and Jean-Pierre Barbot. "State and unknown input estimation for linear discrete-time systems." *Automatica*, **42**(11):1883–1889, 2006.

[FT10] Xuan Fan and Masayoshi Tomizuka. "Robust disturbance observer design for a power-assist electric bicycle." In *American Control Conference (ACC), 2010*, pp. 1166–1171. IEEE, 2010.

[FW76] Bruce A Francis and W Murray Wonham. "The internal model principle of control theory." *Automatica*, **12**(5):457–465, 1976.

[Gao14] Zhiqiang Gao. "On the centrality of disturbance rejection in automatic control." *ISA transactions*, **53**(4):850–857, 2014.

[GB10] Xiuyan Guo and Marc Bodson. "Equivalence between adaptive feedforward cancellation and disturbance rejection using the internal model principle." *International journal of adaptive control and signal processing*, **24**(3):211–218, 2010.

[GK65] Gene Golub and William Kahan. "Calculating the singular values and pseudo-inverse of a matrix." *Journal of the Society for Industrial and Applied Mathematics, Series B: Numerical Analysis*, **2**(2):205–224, 1965.

[GLC15] Zhiwei Gao, Xiaoxu Liu, and Michael ZQ Chen. "Unknown input observer-based robust fault estimation for systems corrupted by partially decoupled disturbances." *IEEE Transactions on Industrial Electronics*, **63**(4):2537–2547, 2015.

[GM82] Carlos E Garcia and Manfred Morari. "Internal model control. A unifying review and some new results." *Industrial & Engineering Chemistry Process Design and Development*, **21**(2):308–323, 1982.

[GR71] Gene H Golub and Christian Reinsch. "Singular value decomposition and least squares solutions." In *Linear Algebra*, pp. 134–151. Springer, 1971.

[Han09] Jingqing Han. "From PID to active disturbance rejection control." *IEEE transactions on Industrial Electronics*, **56**(3):900–906, 2009.

[HBG96] Raoul Herzog, Philipp Buhler, Conrad Gahler, and Rene Larsonneur. "Unbalance compensation using generalized notch filters in the multivariable feedback of mag-

netic bearings." *IEEE Transactions on Control Systems Technology*, **4**(5):580–586, 1996.

[Hub13] M Huba. "Comparing 2DOF PI and predictive disturbance observer based filtered PI control." *Journal of Process Control*, **23**(10):1379–1400, 2013.

[IJG07] Lars Imsland, Tor Arne Johansen, Håvard Fjær Grip, and Thor I Fossen. "On non-linear unknown input observers–applied to lateral vehicle velocity estimation on banked roads." *International Journal of Control*, **80**(11):1741–1750, 2007.

[Jon73] Harold Lee Jones. *Failure detection in linear systems.* PhD thesis, Massachusetts Institute of Technology, 1973.

[JSS10] Nam Hoon Jo, Hyungbo Shim, and Young Ik Son. "Disturbance observer for non-minimum phase linear systems." *International Journal of Control, Automation and Systems*, **8**(5):994–1002, 2010.

[KC03] Bong Keun Kim and Wan Kyun Chung. "Advanced disturbance observer design for mechanical positioning systems." *IEEE Transactions on Industrial Electronics*, **50**(6):1207–1216, 2003.

[KCL15] Jiang Kejian, Zhu Changsheng, and Chen Liangliang. "Unbalance compensation by recursive seeking unbalance mass position in active magnetic bearing-rotor system." *IEEE Transactions on Industrial Electronics*, **62**(9):5655–5664, 2015.

[KHF95] Carl R Knospe, R Winston Hope, Stephen J Fedigan, and Ronald D Williams. "Experiments in the control of unbalance response using magnetic bearings." *Mechatronics*, **5**(4):385–400, 1995.

[Kin13] Robert King. *Handbook of high-speed machining technology.* Springer Science & Business Media, 2013.

[KIO91] Satoshi Komada, Muneaki Ishida, Kouhei Ohnishi, and Takamasa Hori. "Disturbance observer-based motion control of direct drive motors." *IEEE Transactions on Energy Conversion*, **6**(3):553–559, 1991.

[KT16] Christopher Kang and Tsu-Chin Tsao. "Control of Magnetic Bearings for Rotor Unbalance With Plug-In Time-Varying Resonators." *Journal of Dynamic Systems, Measurement, and Control*, **138**(1):011001, 2016.

[LKJ16] Seung Jae Lee, Suseong Kim, Karl Henrik Johansson, and H Jin Kim. "Robust acceleration control of a hexarotor UAV with a disturbance observer." In *Decision and Control (CDC), 2016 IEEE 55th Conference on*, pp. 4166–4171. IEEE, 2016.

[LLW18] Zhijie Liu, Jinkun Liu, and Lijun Wang. "Disturbance observer based attitude control for flexible spacecraft with input magnitude and rate constraints." *Aerospace Science and Technology*, **72**:486–492, 2018.

[LP08] Shuliang Lei and Alan Palazzolo. "Control of flexible rotor systems with active magnetic bearings." *Journal of Sound and Vibration*, **314**(1-2):19–38, 2008.

[LYC16] Shihua Li, Jun Yang, Wen-Hua Chen, and Xisong Chen. *Disturbance observer-based control: methods and applications*. CRC press, 2016.

[Mas86] M-A Massoumnia. "A geometric approach to the synthesis of failure detection filters." *IEEE Transactions on automatic control*, **31**(9):839–846, 1986.

[MB95] William Messner and Marc Bodson. "Design of adaptive feedforward algorithms using internal model equivalence." *International Journal of Adaptive Control and Signal Processing*, **9**(2):199–212, 1995.

[MM95] Eric H Maslen and David C Meeker. "Fault tolerance of magnetic bearings by generalized bias current linearization." *IEEE Transactions on Magnetics*, **31**(3):2304–2314, 1995.

[MNH96] Fumio Matsumura, Toru Namerikawa, Kazuhiko Hagiwara, and Masayuki Fujita. "Application of gain scheduled H/sub/spl infin//robust controllers to a magnetic bearing." *IEEE Transactions on Control Systems Technology*, **4**(5):484–493, 1996.

[MS00] Laurence H Mutuel and Jason L Speyer. "A discrete-time game-theoretic fault detection filter." In *American Control Conference, 2000. Proceedings of the 2000*, volume 5, pp. 3388–3392. IEEE, 2000.

[MS14] Emmanuell A Murray and Jason L Speyer. "A discrete-time game theoretic multiple-fault detection filter." In *Decision and Control (CDC), 2014 IEEE 53rd Annual Conference on*, pp. 5750–5757. IEEE, 2014.

[MVW89] M-A Massoumnia, George C Verghese, and Alan S Willsky. "Failure detection and identification." *IEEE transactions on automatic control*, **34**(3):316–321, 1989.

[NH09] Jianbin Nie and Roberto Horowitz. "Design and implementation of dual-stage track-following control for hard disk drives." In *ASME 2009 Dynamic Systems and Control Conference*, pp. 565–572. American Society of Mechanical Engineers, 2009.

[NO08] Kenji Natori and Kouhei Ohnishi. "A design method of communication disturbance observer for time-delay compensation, taking the dynamic property of network disturbance into account." *IEEE Transactions on Industrial Electronics*, **55**(5):2152–2168, 2008.

[NSL15] Amin Noshadi, Juan Shi, Wee Sit Lee, Peng Shi, and Akhtar Kalam. "System Identification and Robust Control of Multi-Input Multi-Output Active Magnetic Bearing Systems." 2015.

[ONO87] Kiyoshi Ohishi, Masato Nakao, Kouhei Ohnishi, and Kunio Miyachi. "Microprocessor-controlled DC motor for load-insensitive position servo system." *IEEE Transactions on Industrial Electronics*, (1):44–49, 1987.

[PC00] Ron J Patton and Jie Chen. "On eigenstructure assignment for robust fault diagnosis." *International Journal of Robust and Nonlinear Control: IFAC-Affiliated Journal*, **10**(14):1193–1208, 2000.

[Rai18] Sandeep Singh Rai. *Identification and Control of a Magnetic Bearing System for Boring Application*. University of California, Los Angeles, 2018.

[RCS16] Sandeep Rai, Grant Cavalier, James Simonelli, and Tsu-Chin Tsao. "MIMO Repetitive Control of an Active Magnetic Bearing Spindle." *IFAC-PapersOnLine*, **49**(21):192–199, 2016.

[RK85] Bradley Riedle and P Kokotovic. "A stability-instability boundary for disturbance-free slow adaptation with unmodeled dynamics." *IEEE transactions on automatic control*, **30**(10):1027–1030, 1985.

[RRT20] Shahin Rouhani, Sandeep Rai, and Tsu-Chin Tsao. "Inversion Based Adaptive Feedforward Control for Multivariable Systems." *IFAC-PapersOnLine*, **53**(2):3791–3796, 2020.

[RTS19] Shahin Rouhani, Tsu-Chin Tsao, and Jason L Speyer. "Robust Disturbance Estimation-An Integrated Game Theoretic and Unknown Input Observer Approach." In *2019 American Control Conference (ACC)*, pp. 5077–5082. IEEE, 2019.

[RTS21] Shahin Rouhani, Tsu-Chin Tsao, and Jason L Speyer. "Integrated MIMO fault detection and disturbance observer-based control." *Mechatronics*, **73**:102482, 2021.

[SB89] Shankar Sastry and Marc Bodson. "Adaptive control: stability, convergence, and robustness.", 1989.

[SBL94] Beale Shafai, S Beale, P LaRocca, and E Cusson. "Magnetic bearing control systems and adaptive forced balancing." *IEEE Control Systems*, **14**(2):4–13, 1994.

[Sch05] Gerhard Schweitzer. "Safety and reliability aspects for active magnetic bearing applications-a survey." *Proceedings of the Institution of Mechanical Engineers, Part I: Journal of Systems and Control Engineering*, **219**(6):383–392, 2005.

[SHW11] Thomas Schuhmann, Wilfried Hofmann, and Ralf Werner. "Improving operational performance of active magnetic bearings using Kalman filter and state feedback control." *IEEE Transactions on Industrial Electronics*, **59**(2):821–829, 2011.

[SM09] Gerhard Schweitzer and Eric H Maslen. "Magnetic bearings. Theory, design, and application to rotating machinery." 2009.

[SO02] Jin-Hua She and Yasuhiro Ohyama. "Estimation and rejection of disturbances in servo systems." *IFAC Proceedings Volumes*, **35**(1):67–72, 2002.

[SO14] Emre Sariyildiz and Kouhei Ohnishi. "A guide to design disturbance observer." *Journal of Dynamic Systems, Measurement, and Control*, **136**(2), 2014.

[SS15] Bahram Shafai and Mehrdad Saif. "Proportional-Integral observer in robust control, fault detection, and decentralized control of dynamic systems." In *Control and Systems Engineering*, pp. 13–43. Springer, 2015.

[SZQ04] Juan Shi, R Zmood, and L Qin. "Synchronous disturbance attenuation in magnetic bearing systems using adaptive compensating signals." *Control Engineering Practice*, **12**(3):283–290, 2004.

[TH15] Hannu T Toivonen and Lassi Hietarinta. "Fourier state-space analysis of linear discrete-time periodic systems." *Automatica*, **53**:136–140, 2015.

[THD07] Kari Tammi, Jari Hätönen, and Steve Daley. "Novel adaptive repetitive algorithm for active vibration control of a variable-speed rotor." *Journal of Mechanical Science and Technology*, **21**(6):855, 2007.

[Tsa94] Tsu-Chin Tsao. "Optimal feed-forward digital tracking controller design." *Journal of dynamic systems, measurement, and control*, **116**(4):583–592, 1994.

[TT94] Tsu-Chin Tsao and Masayoshi Tomizuka. "Robust adaptive and repetitive digital tracking control and application to a hydraulic servo for noncircular machining." 1994.

[TTC89] Masayoshi Tomizuka, Tsu-Chin Tsao, and Kok-Kia Chew. "Analysis and synthesis of discrete-time repetitive controllers." 1989.

[UKH93] Takaji Umeno, Tomoaki Kaneko, and Yoichi Hori. "Robust servosystem design with two degrees of freedom and its application to novel motion control of robot manipulators." *IEEE Transactions on Industrial Electronics*, **40**(5):473–485, 1993.

[VS94] Paul Van Dooren and J Sreedhar. "When is a periodic discrete-time system equivalent to a time-invariant one?" *Linear Algebra and its Applications*, **212**:131–151, 1994.

[WS87] JOHNE White and JASONL Speyer. "Detection filter design: Spectral theory and algorithms." *IEEE Transactions on Automatic Control*, **32**(7):593–603, 1987.

[WS15] Lu Wang and Jianbo Su. "Disturbance rejection control for non-minimum phase systems with optimal disturbance observer." *ISA transactions*, **57**:1–9, 2015.

[XS03] Yi Xiong and Mehrdad Saif. "Unknown disturbance inputs estimation based on a state functional observer design." *Automatica*, **39**(8):1389–1398, 2003.

[YCS09] Jingang Yi, Steven Chang, and Yantao Shen. "Disturbance-observer-based hysteresis compensation for piezoelectric actuators." *IEEE/Asme transactions on mechatronics*, **14**(4):456–464, 2009.

[YH01] Shiang-Hwua Yu and Jwu-Sheng Hu. "Asymptotic rejection of periodic disturbances with fixed or varying period." *J. Dyn. Sys., Meas., Control*, **123**(3):324–329, 2001.

[YJB76] Dante Youla, Hamid Jabr, and Jr Bongiorno. "Modern Wiener-Hopf design of optimal controllers–Part II: The multivariable case." *IEEE Transactions on Automatic Control*, **21**(3):319–338, 1976.

[YK94] Tomoki Yokoyama and Atsuo Kawamura. "Disturbance observer based fully digital controlled PWM inverter for CVCF operation." *IEEE Transactions on Power Electronics*, **9**(5):473–480, 1994.

[YS14] Jong Nam Yun and Jian-Bo Su. "Design of a disturbance observer for a two-link manipulator with flexible joints." *IEEE Transactions on Control Systems Technology*, **22**(2):809–815, 2014.

[ZDG96] Kemin Zhou, John Comstock Doyle, Keith Glover, et al. *Robust and optimal control*, volume 40. Prentice hall New Jersey, 1996.

[ZJS10] Ke Zhang, Bin Jiang, and Peng Shi. "Observer-based integrated robust fault estimation and accommodation design for discrete-time systems." *International Journal of Control*, **83**(6):1167–1181, 2010.

[ZZT17] Minghui Zheng, Shiying Zhou, and Masayoshi Tomizuka. "A design methodology for disturbance observer with application to precision motion control: an H-infinity based approach." In *American Control Conference (ACC), 2017*, pp. 3524–3529. IEEE, 2017.